Mass Balance of Arsenic in Microelectrolysis Treatment of Arsenic-Containing Landfill Gas Condensate and Initial Study of Formation of Volatile Arsenic Species

Aminda Cheney-Irgens

A thesis

Submitted in partial fulfillment of the

Requirements for the degree of

Master of Environmental Engineering

University of Washington

2022

Committee:

Gregory Korshin

Jessica Ray

Program Authorized to Offer Degree:

Civil and Environmental Engineering

University of Washington

Abstract

Mass Balance of Arsenic in Microelectrolysis Treatment of Arsenic-Containing Landfill Gas Condensate and Initial Study of Formation of Volatile Arsenic Species

Aminda Cheney-Irgens

Chair of the Supervisory Committee:

Gregory Korshin

Department of Civil and Environmental Engineering

The behavior of arsenic in treated landfill gas condensate from the BioEnergy Washington facility at the Cedar Hills Regional Landfill in King County, WA was studied with the goal to quantify the mass balance of arsenic typical for microelectrolysis (ME) treatment and identify the extent of volatilization and speciation of arsenic species that may be formed in ME treatment. Microelectrolysis treatment successfully removes arsenic at >90% from the condensate, but mass balance experiments demonstrate little to no arsenic retained by ME solid reaction media. Therefore, an analytical method based on the formation of colored complexes between arsines and silver diethyldithiocarbamate (AgDDC) was tested to examine the generation of arsines and, to a lesser extent, stibines. These gases are formed in highly reducing conditions induced by sodium borohydride and milder reduction occurring in the ME treatment, converting the dissolved arsenic. AgDDC absorbance data that comprise the spectra of individual arsine/AgDDC complexes, their characteristic maxima and kinetic profiles of concentration-dependent absorbance development and, in some important cases, fading strongly indicate that the arsenic volatiles formed upon the borohydride reduction of the condensate are dominated by methylated arsines. These results need to be confirmed and expanded for ME treatment of BEW process water. Further work is needed to determine the extent of As volatiles' removal by oxidative and reductive processes, adsorption, and thermal treatment.

Contents

List of Figures

List of Tables

List of Abbreviations

AgDDC	Silver Diethyldithiocarbamate
BEW	Bio Energy Washington
BPW	BEW Process Water
CHRLF	Cedar Hills Regional Landfill
DMA	Dimethylarsinic Acid
LFG	Landfill Gas
ME	Microelectrolysis
PAC	Powdered Activated Carbon
SR	Sampling Round
TMA	Trimethyl Arsine
TMAO	Trimethylarsine Oxide
ZVI	Zero Valence Iron

Chapter 1: Introduction

Arsenic exists in the environment as a result of its release from anthropogenic, geogenic, and biogenic sources (Sahoo et al. (2013), Kumar et al. (2015)). Municipal solid waste is an important anthropogenic source of arsenic, and the focus of this research is ultimately on its removal from landfill leachate and, more specifically, from landfill gas condensate (Sahoo et al. 2013). In the environment, arsenic is found in many forms and most often is inorganic As (III) or As (V), but methylated and thiolated forms also are common (Korshin (2021) Arsenic in the environment, redox effects. CEE 445 lecture notes). In the solid state, arsenic oxide, orpiment, realgar, elemental arsenic, and arsenic pentoxide are typical (Korshin (2022) Redox transitions. Pe, pH predominance diagrams for $Fe^{3+/}Fe^{2+}$ and As^{5+}/As^{3+} transitions. CEWA 543 lecture notes.) In the context of the presentation of the experiments described herein, it is important to note that while the environmental chemistry of arsenic is immensely complex, suffice it to say here that most of the arsenic species relevant to this study contain iron, sulfur, or oxygen, as well as varying numbers of methyl groups. In the case of inorganic As species, As and Fe mobility in particular are closely related in environmental systems, as evidenced in Pourbaix diagrams for the two elements, shown in the Appendix (Korshin (2022) Redox transitions. pe, pH predominance diagrams for $Fe^{3+/}Fe^{2+}$ and As^{5+}/As^{3+} transitions. CEWA 543 lecture notes.).

A salient feature of this study is its focus on the formation of volatile arsenic species, notably those formed in municipal landfill and released to landfill gas (LFG) that is frequently referred to as biogas. Biogas is a very important emerging energy carrier that can be a substitute for natural gas and fossil fuels. However, the utilization of biogas has been shown to have an unexpected challenge because of the presence of volatile contaminants, notably trace levels of AsH_3 and more dominant levels of methylated forms of arsines (Weithmann et al. (2019)). The presence of

arsenic in municipal solid waste has also been proposed as a dose-dependent inhibitor for acetoclastic methanogenesis, which could limit the overall biogas production possible (Weithmann et al. (2019)). Feldmann (2003) reported that landfill environments can induce the formation of organometallic compounds, notably those of arsenic and antimony, a process that may impact the landfill gas production at our study site of Bio Energy Washington (BEW) at the Cedar Hills Regional Landfill (CHRLF).

In many compartments of the environment, higher arsenic concentrations tend to be observed at decreased oxygen saturation and ultimately in anoxic conditions (Korshin (2021) Arsenic occurrence and sources. CEE 445 lecture notes). Given this observation, it is not necessarily surprising that the landfill leachate generated at a landfill in which anaerobic processes are involved in the degradation of anthropogenic waste generate landfill gas that can have measurable amounts of arsenic, may have increasing arsenic concentrations. While the exact source of arsenic at CHRLF remains to be elucidated further, the interception of arsenic volatiles by LFG treatment solids used at the collocated LFG refinery (BioEnergy Washington) and the disposal of these solids in the landfill characterized by anaerobic conditions is likely to be the major mechanism (Korshin (2021) Arsenic occurrence and sources. CEE 445 lecture notes). It is known that redox potentials exhibit pronounced variations throughout a landfill (Arora et al., Naudet et al.) reaching in some conditions very low levels that enhance arsenic mobility and formation of As volatiles (Korshin (2021) Arsenic occurrence and sources. CEE 445 lecture notes).

The municipal waste deposited at CHRLF undergoes anaerobic digestion, which produces methane that is sent to the BEW plant on-site for refinement. As mentioned above, the focus of this research is defined by the presence of arsenic found both in the landfill leachate released

from the CHRLF facility and the gas condensate formed at BEW and then returned to the CHRLF leachate where it is mixed with the other leachate streams (Figures 1, 2). Arsenic concentration has generally increased over the study period of the last decade in both the landfill leachate and gas condensate albeit recent measurements of As concentrations may indicate some decrease of its levels; further observations are necessary to confirm this trend.

The difference in As concentration between these streams is noteworthy, with up to 0.5 mg/L in leachate and 25 mg/L in condensate (Figures 1,2), or BEW process water which tends to contribute only to ca. 2% of the overall discharge flow from the CHRLF site. The ongoing research carried out by Prof. Korshin's group has shown that LFG treatment solids deposited in the landfill contain arsenic, which release arsenic that may become partially volatilized and transferred to the BEW facility, and partially directly discharged to the leachate.

Due to the need to remove arsenic from the CHRLF leachate, as necessitated by the environmental and human health concern associated with the well known As toxicity, our group has been developing appropriate treatment methods. This research has shown that while none of the traditional treatment methods (e.g., coagulation, permanganate oxidation, advanced oxidation processes, adsorption on activated carbon, use of zero valence iron per se, others) are successful in As removal from the leachate or LFG condensate, the novel microelectrolysis (ME) approach is capable to efficiently removing arsenic from these solutions.

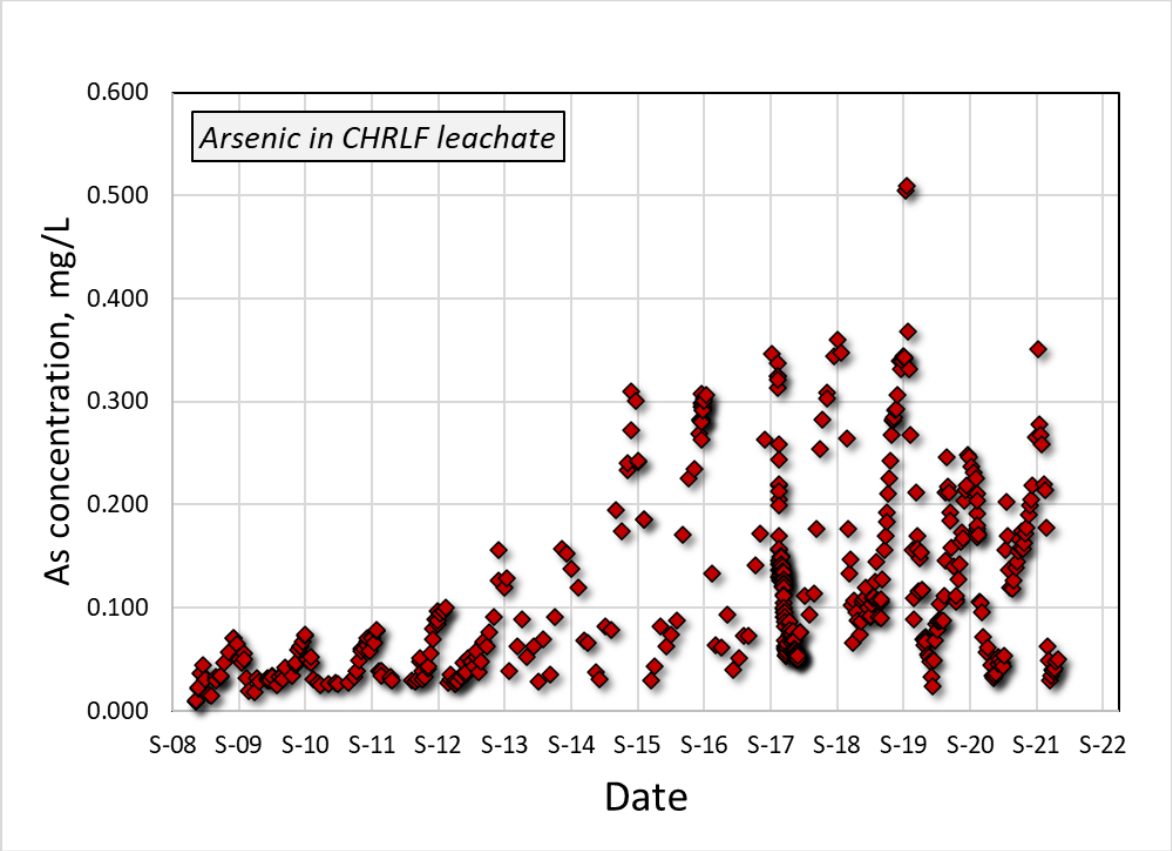

Figure 1. Arsenic concentration in CHRLF leachate from 2008 to 2022. The analytical results presented in this figure were provided by Kris McArthur, PE (KC SWD) and processed by Prof. Korshin.

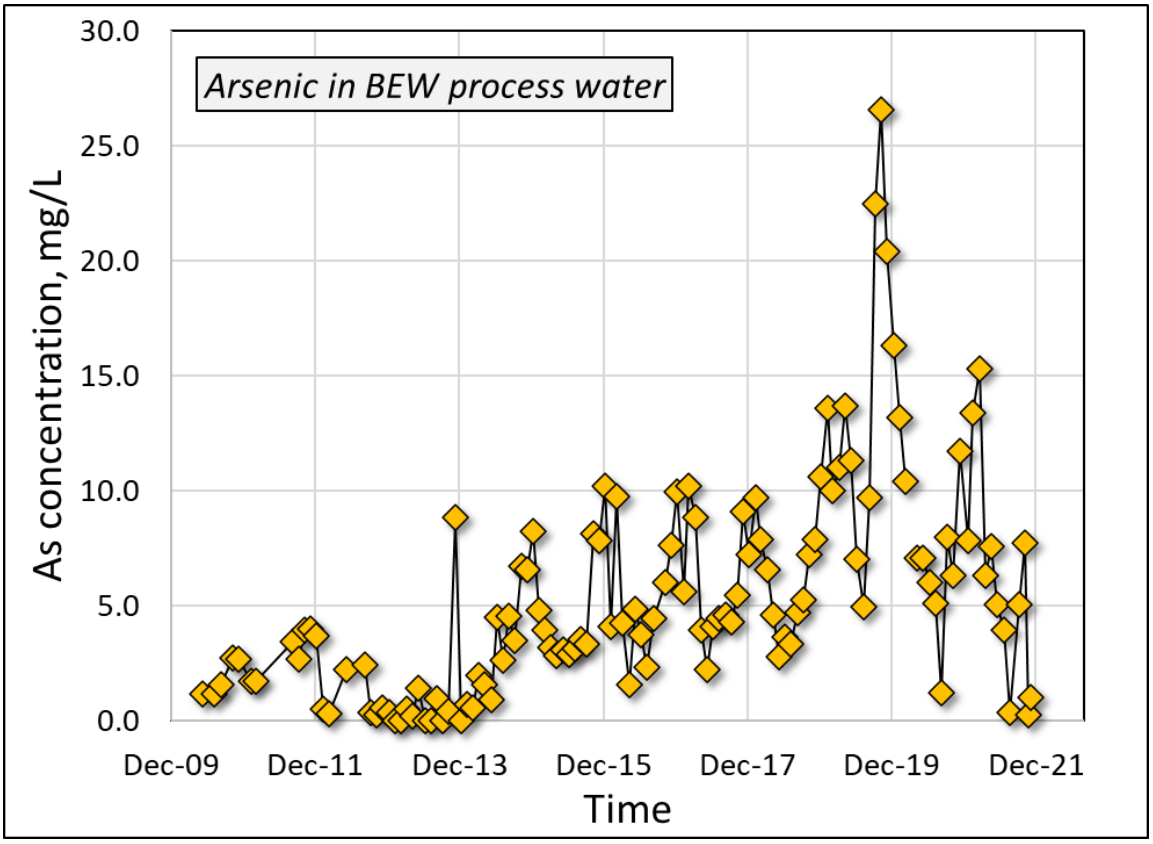

Figure 2. Arsenic concentration in BEW process water from 2009-2021. The analytical results presented in this figure were provided by Kris McArthur, PE (KC SWD) and processed by Prof. Korshin.

The microelectrolysis approach relies on a combination of adsorptive and reductive treatment to remove arsenic from the BEW process water (Korshin et al. 2019, Liu et al. 2022). ME treatment employs a mixture of solids, namely powdered activated carbon (PAC) and zero valence iron (ZVI). ZVI is thought to assist and accelerate the reduction of the arsenic species found in BEW process water (BPW) to arsine, most likely to a methylated form of arsine gas (Korshin et al. 2019, Liu et al. 2022). A sequence of specific reductive reactions that result in the formation of methylated arsines is presented later in this thesis.

The interactions of ZVI and PAC via complex, yet to be ascertained mechanisms that are likely to include formation of complexes of arsenic species with Fe^{2+} ions, promote the volatilization of

As (Korshin et al. 2019, Liu et al. 2022). This process is called microelectrolysis because of electrochemical reactions which occur at the numerous microscopic-size contacts between the particles of ZVI and carbon particles, which are suspended together in solution (Korshin et al 2019, Liu et al. 2022). The group found this approach to be remarkably successful at removing arsenic from the BPW, with varying doses of PAC and ZVI, and in a pH range of 3-5, although the required contact time may range from below 4 to 24 hours, depending on the PAC/ZVI dose (Korshin et al. 2021). With these conditions and a typically used 2:1 weight ratio of ZVI/PAC, >90% of arsenic can be removed from BPW over a concentration range of 4-12 mg/L (Korshin et al. 2019). Additionally, the gas flow component was an important part of the ME protocol development, with the group concluding that CO_2 carrier flow is essential for successful arsenic removal (Korshin et al. 2020).

A major challenge encountered in both determining an appropriate treatment method and providing environmental recommendations is the unknown speciation of arsenic in BPW. The initial CHRLF arsenic source might be geogenic but the cycling of As associated with the presence in CHRLF of the used LFG treatment solids that originate from BEW operations is also likely to play a very important (Korshin, CEE 445 Notes, Arsenic in the environment, redox effects).

Microelectrolysis Treatment and Arsenic Volatilization

Experiments described in this document focus on the examination of the formation of As volatiles in ME treatment, using absorbance spectra of arsine complexes with a sensitive reagent (silver diethyldithiocarbamate, AgDDC) as a tool for discerning the form of arsenic present in BPW. The group is also pursuing methods such as Extended X-Ray Absorbance Spectroscopy

(EXAFS) to elucidate the chemical structure found in our samples. Results of the ongoing EXAFS studies are beyond the scope of this thesis and will be discussed elsewhere.

As volatilization is of great concern for both understanding for As mobilization processes at the CHRLF site and optimization of BPW treatment using the ME approach. The arsenic concentration in landfill gas (LFG) equates to 0.07-0.25 ug As/ g CH_4 (Korshin, CEE 445, Environmental chemistry of arsenic: volatilization, interception, and mobilization). With an annual LFG volume of 50,000 tons/year at CHRLF, this translates to 3500-12,500 g/year of As (Korshin, CEE 445, Environmental chemistry of arsenic: volatilization, interception, and mobilization).

In the volatilized As species, varying degrees of methylation are seen and arsenic exists in the form of mono-, di- or trimethyl arsine (Korshin, CEWA 543 Notes, Redox transitions. Pe, pH predominance diagrams for Fe^{3+}/Fe^{2+} and As^{5+}/As^{3+} transitions). Trimethyl arsine $(CH_3)_3As$ (TMA), which has a trigonal pyramidal structure, has been reported to be the dominant arsine species in landfill gas (Korshin, CEE 445, Environmental chemistry of arsenic: volatilization, interception, and mobilization). It is expected that, in agreement with the data of prior research, trimethylated solutes are the dominant form of arsenic in the CHRLF leachate and in BPW. Given the success of the ME treatment of BPW, it appears that arsenic species in this matrix are reduced to form trimethylarsine. Specific mechanisms of the reduction-adsorption reactions typical for ME remain to be ascertained.

The arsines have varying boiling points that range from -62.5 °C for arsine AsH_3, 2.0°C for methylarsine CH_3AsH_2, 35.6°C for dimethylarsine, DMA $(CH_3)_2AsH$ to 56 °C for trimethyl arsine, TMA $(CH_3)_3As$. These compounds, particularly AsH_3, are volatile albeit their volatility decreases with the degree of methylation (Wang et al. (2014)). Arsine, and its mono, di, and

trimethylated forms can be generated in landfill gas, of which arsine is the least stable (Feldman (2003), Wang et al. (2014)). Feldmann (2003) found that trimethyl arsine oxide (TMAO), which is likely to act as the precursor of TMA in sufficiently reducing conditions, contribute to ca. 50.1% of the total arsenic in the landfill water samples and trimethyl arsine TMA accounted for 67.8% of the volatile arsenic compounds created after hydride generation, demonstrating that TMA represents a greater portion of the arsenic-related volatile compounds than lesser methylated forms. It has also been reported that 80% of volatile arsenic species in a biogas digester was TMA. TMA is thought to be less toxic than the most volatile and reactive inorganic arsine AsH_3, which causes immediate death at a 150 ug/m^3 concentration (Weithmann et al. (2019), Wang et al. (2014)). Similarly, trimethyl stibine $(CH_3)_3Sb$ comprised a higher percentage of volatile antimony compounds (Feldmann (2003)). This trend can be attributed to the decrease in half life with an increase in methylation for these compounds, which is also associated with a decrease in toxicity as compared with inorganic forms (Feldmann (2003), Weithmann et al. (2019)). Wang et al. (2014) reported that a pH of 5-6 is optimal for the evolution of volatile arsines, and that methylation increases with a decrease in redox potential which supports the idea that arsenic volatilization would be more favorable in anaerobic conditions.

Feldmann (2003) explained that both oxidation and methylation of the volatile arsenic and antimony compounds occur when they percolate through the water column, and recommended a greater column reaction time to limit the release of these compounds into the atmosphere. Because these volatile compounds can diffuse through both solid and liquid media, they present a serious health concern and need for appropriate capture measures (Feldmann (2003)). Feldmann (2003) confirmed that there is limited toxicological information known for these compounds relating to mammalian and human health. Because of the high sulfur content of BPW

samples, the possibility of arsenic-sulfur compounds is of particular interest. Sulfur-containing As volatiles species have indeed been in natural systems such as geothermal vents and information concerning their toxicologic effects is similarly lacking (Wang et al. (2014)).

It is estimated that approximately 2.1 x 10^7 kg arsenic are volatilized annually worldwide. A large part of the volatilized As originates from biological sources, which are reported to be the largest contributor of arsenic to the atmosphere (Mestrot et al. (2011), Wang et al. (2014)). Microorganisms like fungi, bacteria, and archaea can cause arsenic salts to volatilize through a metabolic process to protect these organisms and remove arsenic from their environment (Mestrot et al. (2011), Weithmann et al. (2019), Wang et al. (2014)). This is particularly likely in soils with reducing conditions, where TMA again is the dominant volatile form of arsenic generated, and dependent on the soil DOC content which fuels microbial reduction processes that favor mobile arsenic species (Mestrot et al. (2011)).

The generation and capture of volatile arsines (AsH_3 and its methylated derivatives mono-, di- and trimethylarsine) is of great interest to the BEW process water treatment. Considering the mass balance results and understanding of reduction chemistry, it is likely that volatile arsines are generated during the microelectrolysis treatment developed thus far. As such, the arsines represent a likely hazard of BPW treatment. As mentioned above, the nature of the dominant arsine solutes found in BPW and As volatiles formed as a result of its treatment is yet unclear, and could comprise both methylated and/or sulfur-containing As species. It is suspected that dimethyl and trimethyl arsines, DMA and TMA along with lower concentrations of inorganic arsine AsH_3 are generated in ME treatment. These arsines have different reactivities and stabilities, which may influence the protocol for capture and treatment based on the differences of properties of these forms. Because of the considerable toxicity of arsine gas, it is imperative

that gas capture methods accompany BPW treatment. While inorganic arsine gas AsH_3 is more reactive than its methylated analogues, it is still relatively stable in the air and has been reported to be immediately dangerous to life or health (IDLH) level at 3ppm and has a permissible exposure level (PEL) of 50 ppb (Lin et al. (2017), Guo et al. (2020), Virji et al. (2009), Levy et al. (2012), Wang et al. (2018)). There is substantial concern for lung damage, kidney damage, and risk of cancer with prolonged exposure to this volatile (, Levy et al. (2012), Wang et al. (2018)).

On the other hand, efficient interception of arsines generated during the ME treatment of BPW can simplify the disposal of the treatment media and decrease its cost. In prior research concerned with either with the intentional use of arsines (e.g., in semiconductor manufacturing) or their formation as by-products, arsine separation and control has been explored, for instance, in the context of syngas (mixture of hydrogen and carbon monoxide) generation, resulting in a variety of methods, for instance those that use alumina-supported metal- and metal oxides adsorbents containing silver, manganese, copper, and nickel that remove high arsine concentrations. The goal of this research is to explore the treatment option needed to characterize arsines and/or other volatiles (e.g., thiolated As species) generated in the ME treatment of BEW effluents, examine methods to remove them from the off-gas stream and thus address the health concerns related to treatment of arsenic-containing water sources (Seredych et al. (2010), Quinn et al. (2006)).

Materials and methods suitable for capture of arsines

Several methods have been suggested to generate and capture arsines (Table 1). Lin et al. (2017) utilized molecular sieves impregnated with transition metal oxides and found that at low oxygen concentration and a temperature range of 120-160 °C, arsine was effectively removed using a

manganese oxide catalyst. This material was thus recommended for industrial applications, as an alternative to a method using Pt (Lin et al. (2017)). Lin et al. (2017) encouraged the use of catalytic oxidation methods because of a high removal efficiency and because these materials can function at high temperatures, noting that Pb, Co, and Ce performed below Ni and Mn, both of which had a high breakthrough time. While Lin et al. (2017) noted that precious metal catalysts are very effective in promoting the oxidation of arsines, these catalysts are not practical because of their expense, limited longevity, and temperature range of operation. Lin et al. (2017) also observed that higher temperatures (above 200 °C) led to improved arsine removal as arsenic and hydrogen, speculating that these conditions may encourage chemical adsorption over physical adsorption and improve catalytic oxidation.

Guo et al. (2020) reported that adsorption on activated carbon or other porous materials is a common way to address the treatment of toxic gases, while Mestrot et al. (2011) reported the use of an arsine gas trap that utilized a silver nitrate impregnated silica gel. They noted that arsines are among a group of gases that exhibit an S-type isotherm (Guo et al. (2020), Sparks (2003)).

Table 1. Summary of Representative Materials and Adsorbent Suitable for Arsine Gas Removal

Adsorbent	Treatment	Source	Advantages	Disadvantages
Molecular sieves	catalytic oxidation, low O_2 concentration, high temp (120->200°C)	Lin et al. (2017)	Low O_2 concentration needed	Relatively high temperature requires appropriate materials and safety precautions
Potassium permanganate	High concentration $KMnO_4$ solution used to treat a gas stream containing	Lin et al. (2017)	Easily accessible materials, can be	$KMnO_4$ is a strong oxidant and appropriate safety measures need

	100 ppm arsine in N_2.		implemented with a scrubber	to be implemented
Activated carbon	Room temperature (293 K) or greater, atmospheric pressure	Lin et al. (2017), Guo et al. (2020)	Ambient environmental conditions, easily accessible materials	Unclear how often spent material needs to be exchanged for fresh carbon
Silver nitrate impregnated silica gel	Silver nitrate traps were attached to outlet ports in a flow box, pushed 2 cm into soil with negative pressure maintained by 0.2 LPM pump flow.	Mestrot et al. (2011)	Silica gel is cost-effective	Requires use of pump. Fire and health hazards associated with silver nitrate
Metal Organic Frameworks (MOFs)	Performance examined based on density functional theory modeling, high concentration of toxic gas (1 bar)	Guo et al. (2020)	Porous material can aid in adsorption, expected to work for high concentrations of arsine	Expense of MOFs, little data on the stability of these materials
Zeolite	Performance examined based on density functional theory modeling, pores of 4.9-6.7 nm, low concentration of toxic gas (100 ppmv)	Guo et al. (2020)	Porous material for adsorption, cost-effective	Expected to be effective only for low concentrations of arsine
Copper oxide and copper metal on carbon	Less than 30% humidity, arsine delivered as 4% mixture in nitrogen	Seredych et al. (2010)	Very effective for arsine treatment in syngas	Best with low humidity, may not be conducive to the treatment of high-humidity landfill gas
CuO_x/TiO_2	Successful even in absence of oxygen and at low temp, 30-120 °C, N_2 and O_2 (0-2%)	Wang et al. (2018)	Successful at low temp, does not require oxygen	Cost of materials

Adsorption treatment has proven successful in the context of syngas treatment and removal of arsines using various catalysts (Seredych et al. (2010), Levy et al. (2012), Quinn et al. (2006)). Lin et al. (2017) also discussed the possibility of arsine removal using adsorption on activated carbon or oxidation by potassium permanganate, but expressed concern for this method because of the possibility of As being reintroduced to the potassium permanganate absorption solution, producing K_2HAsO_4. While a range of metal oxides including copper, lead, chromium, nickel, silver, manganese, or zinc have been explored, Seredych et al. (2010) reported that the most effective adsorbent for syngas arsine treatment is a combination of copper oxide and metal copper on carbon, where copper arsenite or arsenic forms. Wang et al. (2018) asserted that CuO_x/TiO_2 could be a promising adsorbent, with an arsine breakthrough adsorption capacity of 534.3 mg/g. This study cited the ability of CuO to oxidize arsine even in the absence of oxygen and the use of this material at low temperatures (Wang et al. (2018)).

Quinn et al. (2006) also reported that a CuO/carbon adsorbent is very effective, but suggested the use of a $Cu/ZnO/Al_2O_3$ catalyst which has a thermodynamically favorable reaction with arsine on the surface of the copper to form Cu_3As. This article explains that reactive adsorption depends on the ability of surface groups to activate oxygen, leading to the oxidation of arsines to arsenic trioxide (Seredych et al. (2010), Zhang et al. (2019)). In addition to oxygen, nitrogen and sulfur can also be used in combination with oxidized carbons to convert arsines to either arsenic trioxide or arsenic pentoxide, with the possibility of arsenic sulfide formation as well (Seredych et al. (2010)). If water is present in the system, it is recommended that a hydrophobic surface chemistry be implemented to ensure arsine adsorption and oxidation (Seredych et al. (2010)). It was also mentioned that arsine removal was only half as effective in high humidity environments

where water filled pores and adsorption was not as successful (Seredych et al. (2010)). Fu et al. (2000) reported the use of a gallium dimer, explaining that a small portion of arsenic adsorbed to a surface will decompose to form a dimer, but at temperatures too high to be practical for our application.

Laboratory-scale generation and detection of arsines

Several methods have been proposed for arsine generation in the context of analytical determinations of concentrations of As solutes. A well-established method for interception and colorimetric identification of arsine gas involves the borohydride reduction of soluble As species to volatile arsines and use of silver diethyldithiocarbamate (AgDDC) in an organic solvent, namely pyridine or chloroform. Possible reaction schemes for this process are as follows, as suggested by Professor Korshin.

Reduction of DMA, precursor of dimethylarsine: :

Step 1. DMA is reduced to a demethylated As (IV) intermediate through electron transfer and protonation.

$$(CH_3)_2AsO(OH) + H^+ + e \rightarrow (CH_3)_2AsO(OH_2) \rightarrow (CH_3)_2AsO + H_2O$$

Step 2. The dimethylated As (IV) intermediate is converted to dimethylarsinous acid by electron transfer and protonation.

$$(CH_3)_2AsO + H^+ + e \rightarrow (CH_3)_2AsOH$$

Step 3. Dimethylarsinous acid is converted to a demethylated As (II) radical though electron transfer and protonation.

$$(CH_3)_2AsOH + H^+ + e \rightarrow (CH_3)_2As(OH_2) \rightarrow (CH_3)_2As\bullet + H_2O$$

Step 4. Electron transfer and protonation convert the demethylated As (II) radical to dimethyl arsine.

$$(CH_3)_2As \bullet + H^+ + e \rightarrow (CH_3)_2AsH$$

Reduction of trimethylarsine oxide, precursor of trimethylarsine:

Step 1. TMAO is reduced to a trimethylated As (IV) intermediate through electron Transfer and protonation.

$$(CH_3)_3AsO + H^+ + e \rightarrow (CH_3)_3AsOH$$

Step 2. The trimethylated As (IV) intermediate is converted to trimethylarsine by electron transfer and protonation.

$$(CH_3)_3AsOH + H^+ + e \rightarrow (CH_3)_3As$$

Interactions between arsines and AgDDC have been reported to result in the formation of products characterized by a broad absorbance band with a peak at 520 nm, as seen in Figure 3 (Cross (1979), Kopp (1973), Budesinksy (1979), Sandhu and Nelson (1978)). The AgDDC/solvent mixture acts as a scrubber solution for the capture of arsines and the AgDDC serves as a color-responsive reagent that reflects the presence and concentration of arsines (Cross (1979), Kopp (1973), Budesinsky (1979)). Arsine and AgDDC reportedly react at a 1:6 ratio resulting in formation of an AsDDC compound whose chemical nature remains to be ascertained. Some studies suggested that the red color that develops as a result of the interactions in the

AgDDC/arsine systems, reflect the generation of colloidal silver (Budensinsky (1979)) but other studies assume the formation of arsine-AgDDC complexes. Because pyridine has a very strong and unpleasant odor, it was suggested that chloroform paired with an organic base can be used as well (Kopp (1973)).

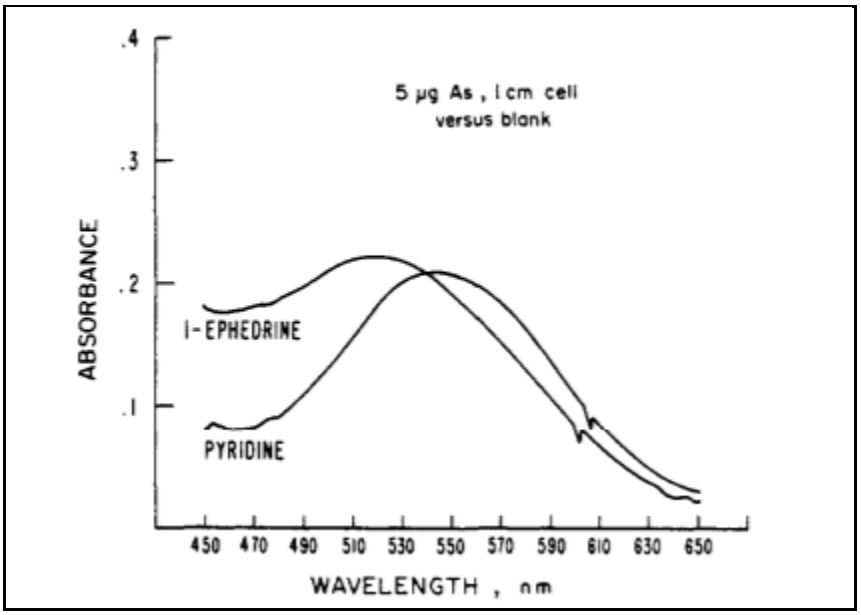

Figure 3. Absorbance spectra of arsine-AgDDC systems; the peak observed for l-ephedrine occurs at 520 nm (adapted from Kopp, 1973).

There are interferences to note regarding this method. Chromium, cobalt, copper, mercury, molybdenum, nickel, platinum, and silver interfere with arsine generation (Kopp (1973)). Antimony and phosphorus can form volatile hydrides that reduce AgDDC, aiding in color development, while the volatile sulfur species can interact with AgDDC to form an insoluble silver product (Budesinsky (1979)). However, antimony presents a concern for interference only for Sb concentrations 0.2 mg/L or higher (Sandhu and Nelson (1978)). Because many of these elements, notably sulfur species, are present in BPW samples, this may impact arsine generation measurements. It is also noteworthy that in particular, chromium interference is reported to

decrease arsine generation and show a peak absorbance at 425 nm rather than at the often reported 520 nm (Sandhu and Nelson (1978)). While chromium concentration is not high in BPW effluent, for example 3.82 ug/in in SR11, this may be a significant area of concern for similar future studies in leachate. This peak position is similar to maxima found thus far for SR8-10 in kinetics experiments described in more detail elsewhere in this document. Additionally, impurities in AgDDC (e.g., presence of silver nitrate) have been reported to cause a shift in absorbance to higher wavelengths resulting in maxima observed at wavelengths greater than 520 nm (Budesinsky (1979)).

The AgDDC method has also been shown to successfully measure stibines at concentrations much less than the 0.5 mg/m^3 limit set forth by American Conference of Government Industrial Hygienists in the 1970s (Cross (1979)). In this case, an absorbance peak is observed at 510 nm, which may be difficult to distinguish from an arsine peak at 520 nm (Kopp (1973), Sandhu and Nelson (1978)). This may be further explored after the behavior of arsines is well-established in the BPW samples.

The use of the AgDDC method for analytical purposes is predicated by the availability of methods for efficient conversion of As solutes to the corresponding arsines. Hussam et al. (1999) explored arsine generation from inorganic arsenic using field test kits and used Na_2HAsO_4 to prepare their arsenate standards. In their work, a solution trap of 6 M HCl was used to prevent arsine exposure to their workspace, while using the Merck field kit (Arsenic Quant Test Strips, Alfa-Aesar, USA) that measures a color change in silver nitrate and $HgBr_2$ components (Hussam et al. (1999)). Levy et al. (2012) further examined the issue of arsine generation through the use of photocatalytic reduction of arsenate and arsenite as a method of generating arsine. They attempted arsine detection with AgDDC capture and concluded that approximately 0.07% of

arsenic present in solutions of arsenite or arsenate was converted to arsine (Levy et al. (2012)). Sengupta et al. (2010) reported that electrochemical reduction to arsine is much more efficient with arsenite than with arsenate, and after using borohydride to reduce arsenic, it was decided to use electroreduction with gas phase chemiluminescence where generated arsine can react with ozone to produce light. Shen and Dasgupta (2014) also opted for electroreduction over a sodium borohydride approach due to the cost and instability at high humidity of this material, a concern reiterated by Sengupta and Dasgupta (2011). Sengupta and Dasgupta (2011) reported that low current densities are only successful in reducing arsenite, while higher current densities can reduce arsenate as well.

Shen and Dasgupta (2014) showed that an acidic pH is necessary for reduction of inorganic arsenic to arsine, and the greater reduction of arsenite over arsenate to arsine may be used for speciation purposes. Shen and Dasgupta (2014) also noted that adding ferric iron to arsenite causes a conversion to arsenate, a possible occurrence in the BPW samples. Uthus et al. (1981) observed that low concentrations of tin can impede arsine generation, and that EDTA was successful in reducing interferences caused by copper, iron, and nickel. They experimented with a range of sodium borohydride concentrations for arsenic reduction including 1, 5,10, and 15% solutions using atomic absorbance spectroscopy, and found the greatest atomic absorbance of the volatilized arsine when conditions of 1.0 N HCl and 10% w/v sodium borohydride solution were used, as seen in Figure 4 (Uthus et al. (1981)).

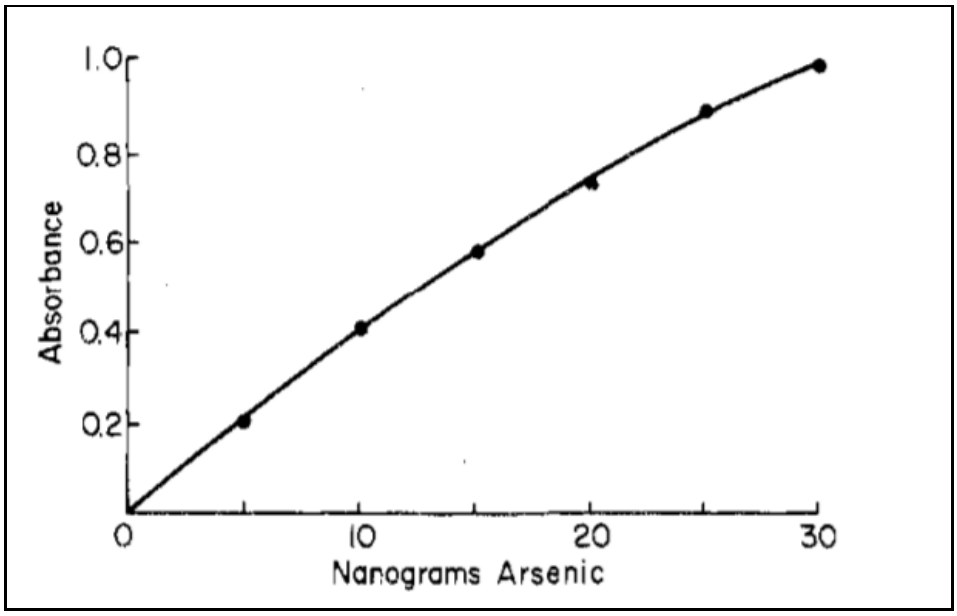

Figure 4. Standard curve for the detection of As by AgDDC method in the case of arsine generation that used 4 mL of a 10% NaBH4 solution and 1.0 N HCl with 10 mL samples of arsenic solutions (adapted form Uthus et al. 1981).

However, other groups used lower sodium borohydride solutions to generate arsines. Shaikh and Tallman (1977) utilized a 2% sodium borohydride solution, with a setup instead consisting of arsenic standard solutions in 0.1 M NaOH, and discussed the use of AgDDC solution in pyridine or chloroform/ephedrine. They recommended a combination of a large water sample and a laborious step of evaporating the solvent in the AgDDC solution to have a greater concentration for better spectroscopy measurements (Shaikh and Tallman (1977)). As a filter, they use anhydrous calcium chloride and cotton inside a glass stopper (Shaikh and Tallman (1977)). Tesfalidet and Irgum (1989) used a 4% w/v sodium borohydride solution with NaOH background, and also prepared their standard solutions with NaOH. Their method of arsine generation and capture utilized an anion-exchange resin column, and they assert that a polymer-attached tetra borohydride is more effective and stable than a borohydride solution, although this

method does not allow for speciation between arsenite and arsenate because of a decreased detection of arsenate (Tesfalidet and Irgum (1989)).

Virji et al. (2009) also mentioned the use of chemiluminescence and electrochemical reduction techniques, but offered an alternative solution because of concern for cost, durability and safety of materials used, and ease of the process. Instead, Virji et al. (2009) reported using a polyaniline nanofiber-metal salt composite that relies on changes in measured resistance as a cost-effective way to detect arsine that works at room temperature, similar to previously reported experiments in literature using modified polyaniline nanofibers to detect hydrogen sulfide. This method works through arsine reacting with the metal salt to create acid that reduces the metal and allows arsine to be oxidized (Virji et al. (2009)). They reported that a copper (II) bromide/ polyaniline nanofiber composite was most successful at indicating arsine exposure by over an order of magnitude difference in measured resistance (Virji et al. (2009)).

Reviewing these detection and generation methods, the group concluded that the AgDDC approach was most feasible, given needed equipment and materials, as well as cost. By reducing arsenic in the BPW and model solutions (e.g., arsenite, DMA) to arsines and, in the case of BPW, possibly other As volatiles, using sodium borohydride, a set of sufficiently detailed data can be created to explore the arsine generation processes that take place as a result of ZVI-driven reduction in the ME treatment. This data can be used to determine the extent of arsenic volatilization in the BPW, and further design and optimize on-site gas treatment to ensure that environmental and occupational safeguarding measures are put in place.

Goals of this study

The goals of this study therefore are twofold and will be discussed as follows:

- First, the ME method will be further explored through analysis of the treatment solids (PAC/ZVI) to determine whether arsenic is retained by these solids and close the mass balance of the reactions.
- Second, arsenic volatilization needs to be explored, notably using the AgDDC method combined with detailed absorbance spectra measurements needed to determine the nature of As volatiles formed upon the reduction of the model compounds. Based on such results, specific recommendations are needed to be developed for further work to characterize the generation and speciation of arsines in the case of the ME treatment of BPW solutions, removal of volatile As species in the off-gas generated in ME treatment.

Chapter 2: Materials and Methods

Mass Balance and As Recovery from ME Treatment Solids

Each mass balance experiment used 100 mL of BPW from Sampling Round 7 (SR7). SR7 sample was obtained in November 2020. BPW SR7 samples used in the mass balance (MB) experiments were filtered using a 0.45 micron nylon filter (WRR International) before each ME experiment. Concentrations of As and Sb in the SR7 sample were 7.49 and 0.67 mg/L, respectively. To control pH increase as a result of ME treatment, pH of 5 was maintained throughout the experiment by adding concentrated hydrochloric acid at 0, 15, 30, 45, and 60 minutes as well as 24 hours. Zero minute samples were collected after initial pH adjustment and stored in 15 mL polypropylene test tubes (Fisher Scientific, Cat. No. 05-539-12). A 2:1 ratio of LC Plus Fines zero valence iron, ZVI (Hoganas) and Powdered Activated Carbon (PAC, Fisher Scientific) was dosed as 5 g/L in the 100 mL BPW sample. ZVI was activated before dosing with 0.1 M hydrochloric acid, which begins oxidation of the iron, while the pH of the sample was adjusted. DI water was then added to the weigh boat containing ZVI to rinse and was quickly

removed. Iron and PAC were added after taking the zero minute sample. All reaction flasks were tightly sealed with parafilm to isolate contents from the atmosphere, but it must be stated that this seal is not airtight. A Lab Line orbital shaker vigorously mixed samples throughout the 24 hour experiment. Zero minute and 24 hour samples were filtered with a 0.45 micron nylon filter. Experiments were carried out with a CO_2 flux of 2.5 psi at 0.1 liters per minute, which simultaneously serves to flush environmental atmospheric components out of the flask and assist ME treatment, and without CO_2. In the case of experiments with CO_2 flux, the tubing delivering gas was also sealed in with parafilm and CO_2 was delivered to the sample throughout the 24 hours.

Two distinct types of mass balance experiments were performed. In the first experiment, percent arsenic recovery was measured without separating the PAC and ZVI active phases.

In these experiments, the 100 mL sample was transferred to two 50 mL Falcon test tubes (50 mL Polypropylene Conical Tube, REF 352070) after the 24 hour period was completed and centrifuged for 5 minutes at 4000 rpm using a Sorvall Legend RT centrifuge (Thermo Electron Corporation). Supernatant was drained using a syringe to isolate the solid treatment media, which was settled in granules in the centrifugation tube. The identical PAC/ZVI mixed media present in the two test tubes were combined after each experienced centrifugation, and the empty test tube filled with an equal mass of DI water was placed in the centrifuge to maintain the needed mass equalization and stability. This allowed for the treatment solids to be combined in one tube. Centrifugation was repeated until all supernatant could be removed and only solid contents remained in the test tube containing the sample. To mobilize the retained arsenic, 20 mL of 0.1 M nitric acid or 1 M sodium hydroxide was added. The solution was then vortexed for 5

minutes and centrifuged using the parameters described before taking a sample. Additional measurements confirmed that no arsenic was lost in these measurements due to centrifugation.

In the second type of mass balance experiments, arsenic recovery was measured from the ZVI and PAC active phases separately. After 24 hours, a strong magnet was used to separate the iron from the sample. The iron was rinsed with DI water to ensure transfer of PAC and the solution was decanted to two 50 mL Falcon test tubes, using the magnet to retain the iron. The PAC-containing separation was treated as described in the first mass balance experiment. To understand the possible impact of acid versus base extraction procedures, a volume of 20 mL of 0.1 M nitric acid or 1 M sodium hydroxide was added to the jar with iron and contents were mixed for 5 minutes. In the case of mass balance experiments performed with solutions other than BPW, the same volume and protocol was followed, and a concentration of 10 mg/L as As was used.

The XPS samples were prepared from both solid model compounds (arsenopyrite FeAsS, realgar As_4S_4, and orpiment As_2S_3) and from dried suspended solids of ME experiments with arsenate, arsenite, and DMA with concentrations of 100 mg/L as arsenic in solution. A Surface Science Instruments S-probe spectrometer at the Molecular Analysis Facility (MAF) was used to generate XPS data. The analytical chamber had a pressure of 1×10^{-8} Torr and data analysis was performed using Service Physics Hawk Analysis 7. Spectra were corrected to show the 1s C at 285 eV, and a Shirley background was used to analyze the high resolution spectra.

Analytical Measurements of Arsenic Volatilization

In this study, many experiments on arsine (and in some extent stibine) generation and detection were carried out using a Chemglass Life Sciences Arsine Generator (Fisher Scientific Catalog No. 50-872-930) in a chemical fume hood. Solutions of sodium arsenite (sodium meta-arsenite, Reagette, Baker Analyzed), dimethylarsinic acid (Cacodylic acid, 98%, Acros Organics), and sodium arsenate (Integra, powder, Certified Analytical Reagent ACS) with a range of concentrations from 50 to 200 ug/L as arsenic were utilized to create standard curves (50, 100, 150, 200, ug/L). BPW SR solutions were diluted at 10x, 25x, 50x, and 100x. As and Sb concentration values for the different SR solutions are listed in Table 2.

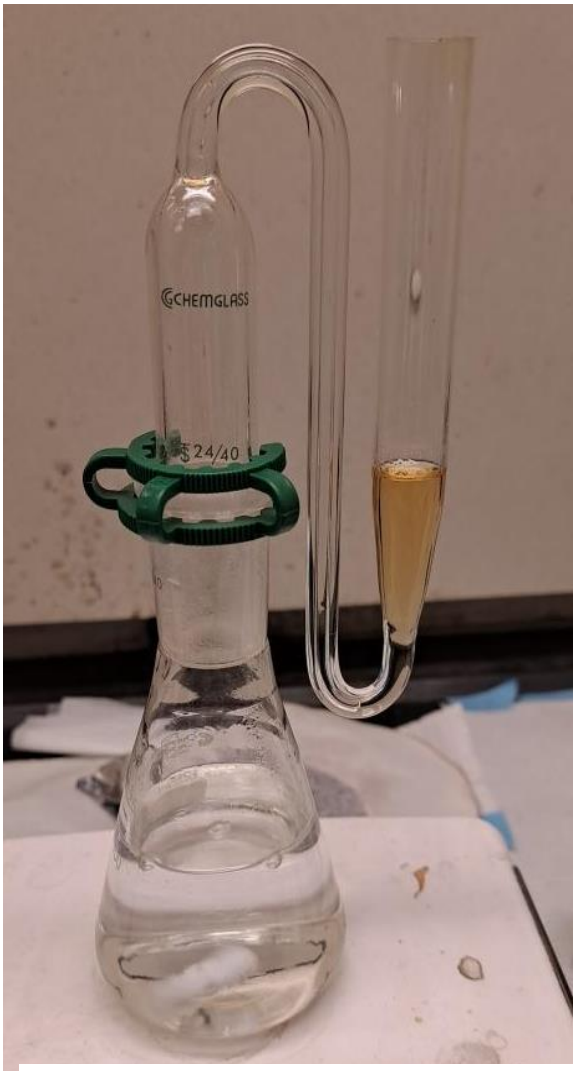

Figure 5. Standard Arsine Generator Setup.

The pH of these solutions was adjusted to 1.7 using concentrated hydrochloric acid (Millipore, ACS grade) before beginning the experiment. In the case of arsenate, 10 mL of a 2N HCl solution was added instead of adjusting the pH to 1.7, which resulted in pH values well below 1 (~0.2-0.4). Per suggestions in the standard method consulted, 3500-As C, the pH in the case of arsenate was lower to enhance mobility of arsenic. A sodium borohydride (98+%, powder, Acros Organics) 1% w/v solution was used as a reducing agent and added to the Erlenmeyer flask containing the low-pH arsenic solution in a quantity of 15 mL, along with a stir bar (Figure 5).

Immediately after these steps, the gas capture tube (otherwise referred to as the arsine scrubber) was attached to the Erlenmeyer flask. This tube contained a volume of 4 mL of a silver diethyldithiocarbamate (ACS grade, Alfa Aesar) solution in pyridine (Certified ACS, Fisher Chemical) (0.3 g AgDDC/70 mL solvent). The generation experiment ran for 20 minutes and the AgDDC/pyridine solution was spetrophotometrically monitored for the 20 minutes after the experiment was completed to identify whether color faded. During this 40 minute period, scans were taken every 2 minutes with an integration count of 30,000.

It was observed that the silver diethyldithiocarbamate does not dissolve quickly. Solutions therefore were made at least a day before experiments were carried out. The stir bar was set to spin at 360 rpm and the tubes were firmly attached using the provided Keck clip. The experiment was carried out for 15 minutes. Absorbance measurements were taken with a Perkin Elmer Lambda 456 Spectrometer using a fiber optic probe with a 1 cm pathlength.

Table 2. Arsenic and Antimony Concentrations of BPW Samples, sampling rounds SR7 to SR13.

BPW SR Solution	Sampling Date	As (mg/L)	Sb (mg/L)
SR7	11/2019	7.49	0.674
SR8	2/2021	12.10	0.484
SR9	3/2021	11.20	0.549
SR10	7/1/2021	4.45	0.172
SR11	8/17/2021	4.34	0.400
SR12	9/14/2021	6.87	0.731
SR13	3/2/2022	8.20	0.354

Chapter 3: Mass Balance of Arsenic and Antimony in Microelectrolysis Treatment of BEW Process Water

Goals

The aim of the mass balance experiments reported in this document is to understand the fate of arsenic in BEW process water (BPW). BPW SR7 contains arsenic and antimony at concentrations of 6000 to 7000 and 600 to 700 ppb, respectively. As demonstrated by these and previous experiments from the group, more than 90% of arsenic can be removed from BEW process water using microelectrolysis (ME) (Korshin et al. (2019), Korshin et al. (2020), Korshin et al. (2021)). However, the fate of the arsenic removed as a result of this treatment has yet to be determined. The fate of antimony, a contaminant co-occurring with As in BPW, is similarly incompletely understood. This set of experiments and the suggested future work seeks to explore in more detail the mass balances of As and Sb in ME operations and characterize the reactivity and behavior of arsenic and the co-occurring element antimony in BPW through a combination of ME treatment and extraction methods with HNO_3 and NaOH.

Results

Arsenic removal after a 24 hour contact time was > 90% for all experiments carried out in the presence of CO_2 flux (Figure 6). This is consistent with the results obtained using different instruments and confirms the findings of the group thus far (Korshin et al. (2019), Korshin et al. (2020), Korshin et al. (2021)). This high As removal does not hold for the experiments without CO_2 purge (Figure 7). In these experiments, arsenic removal did not exceed about 20% after the 24 hours. Comparison of the data shown in these figures demonstrates that the difference in arsenic removal in the presence and absence of CO_2 gas flow was substantial. In the case of CO_2 flux, the first mass balance experiment resulted in 98% average removal, while only 24% of arsenic was removed without CO_2 (Figure 8).

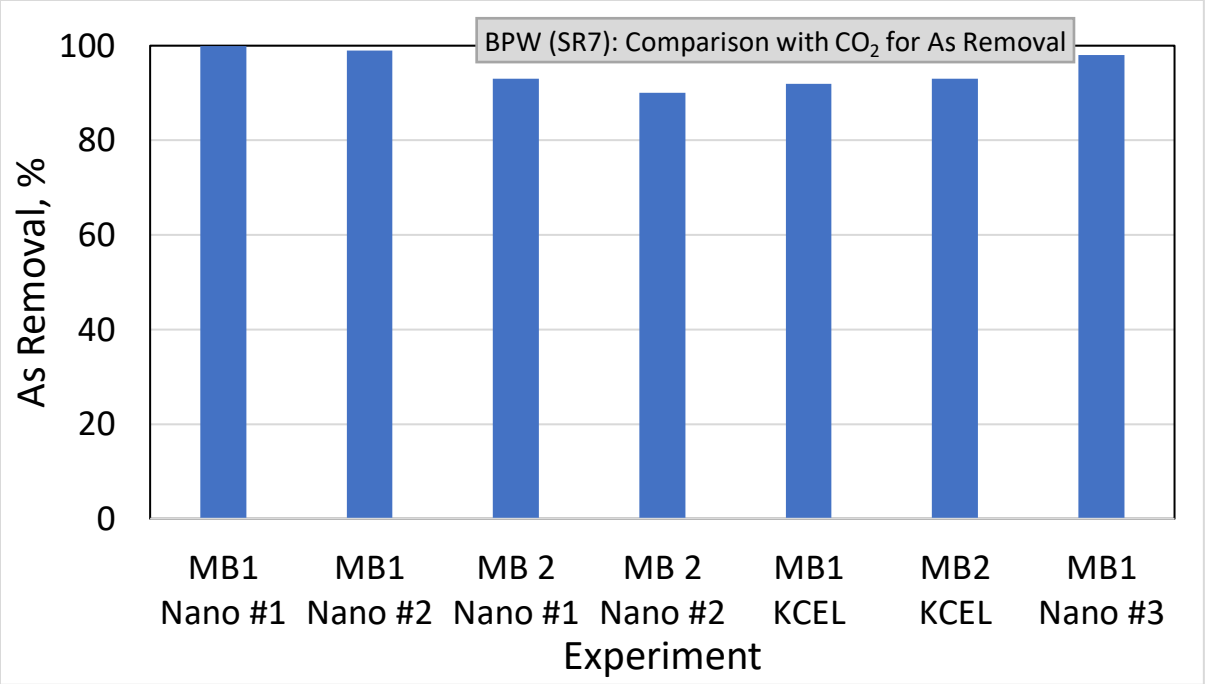

Figure 6. BPW (SR7): As removal by ME treatment of BPW (SR7) with CO_2 flux, Fe/C 2:1, LCPF|PAC, 5g/L, pH 5. ICP-MS data generated in Nanoscience 1/29/21, 2/5/21 and KCEL 1/19/21. (MB1 refers to Mass Balance Experiment Type 1, MB2 refers to Mass Balance Experiment Type 2. These differ only in the separation of Fe/PAC solid media after completion of the ME experiment. Nano refers to UW Nanoscience ICP, KCEL refers to King County Environmental Labs ICP.)

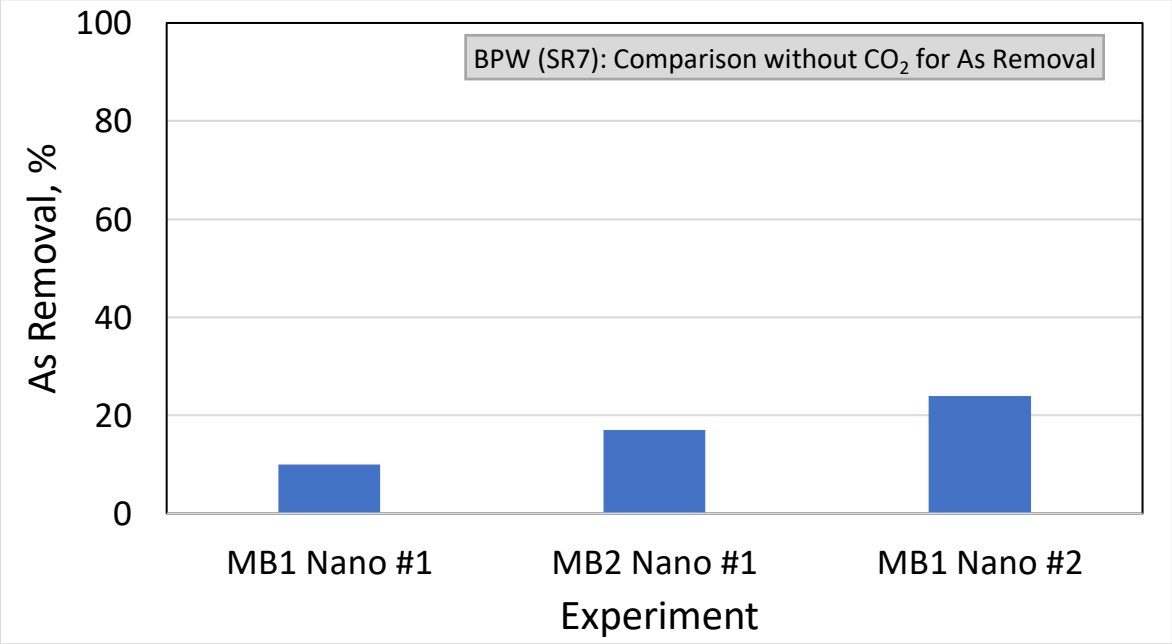

Figure 7. As removal by ME treatment of BPW (SR7) without CO_2 flux, Fe/C 2:1, LCPF|PAC, 5g/L, pH 5. (Data generated in Nanoscience 2/5/21). (MB1 refers to Mass Balance Experiment Type 1, MB2 refers to Mass Balance Experiment Type 2.)

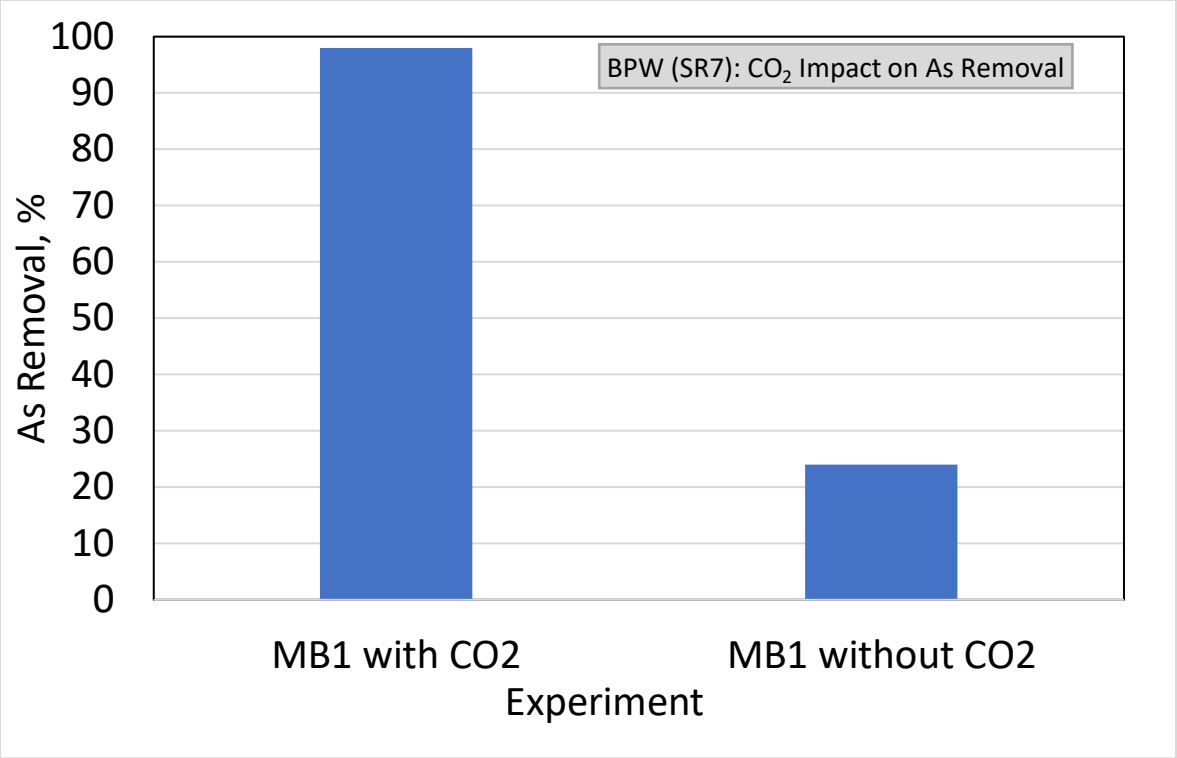

Figure 8. Comparison of average As removal results for ME treatment with CO_2 and without CO_2 carrier gas. Fe/C 2:1, LCPF|PAC, 5g/L, pH 5. (Data generated in Nanoscience 2/5/21). (MB1 refers to Mass Balance Experiment Type 1, MB2 refers to Mass Balance Experiment Type 2).

These experiments also showed differences in terms of pH changes throughout the 24 hours of BPW treatment. Experiments with CO_2 showed that pH values stayed within a range of 5 to 5.3 during the first hour and increased to between 5.7 and 6 at the 24 hour contact time. Experiments without CO_2 flux showed that pH increased more quickly from the initial pH adjustment of 5. After the first hour, pH had already increased to above 6. In all cases, pH increased throughout the experiment.

In an effort to complete the mass balance and liberate the arsenic retained by Fe/C media, Fe/C solids used to remove As from BPW were exposed after the 24 hour period to either 0.1 M nitric acid or 1.0 M sodium hydroxide solutions. The use of the strongly acidic or basic eluents was to examine whether cationic or anionic forms of arsenic species that typically desorb and become mobile at low and high pHs, respectively, were present in the Fe/C media used for ME treatment.

Results of measurements of As concentrations found in the HNO_3 and NaOH eluents also show a difference associated with the presence of CO_2 carrier gas. Recovery experiments carried out using nitric acid with CO_2 resulted in a relatively greater albeit still very low percentage of arsenic recovered from the separated carbon phase (Figure 9) while nitric acid extractions of the ME media used in the absence of CO_2 carrier gas showed a relatively greater arsenic mobilization in the sample with both ZVI and carbon (Figure 10). Overall, As recovery was low albeit it was higher for samples generated in the experiments without CO_2 carrier gas (40% versus less than 1% of As recovery measurements without and with CO_2, respectively). Additionally, it was consistently observed that less arsenic was recovered from Fe/C solids used in the experiments with CO_2 flux as opposed to experiments where CO_2 flux was absent (Figure 11). This finding indicates that CO_2 flux impacts the catalytic activity of ZVI. The data also indicate that the As is preferentially retained by the PAC. This also implies a mechanism for the formation of volatile arsines generated as a result of interactions between ZVI and acid. This phenomenon will be explored further through gas composition analysis.

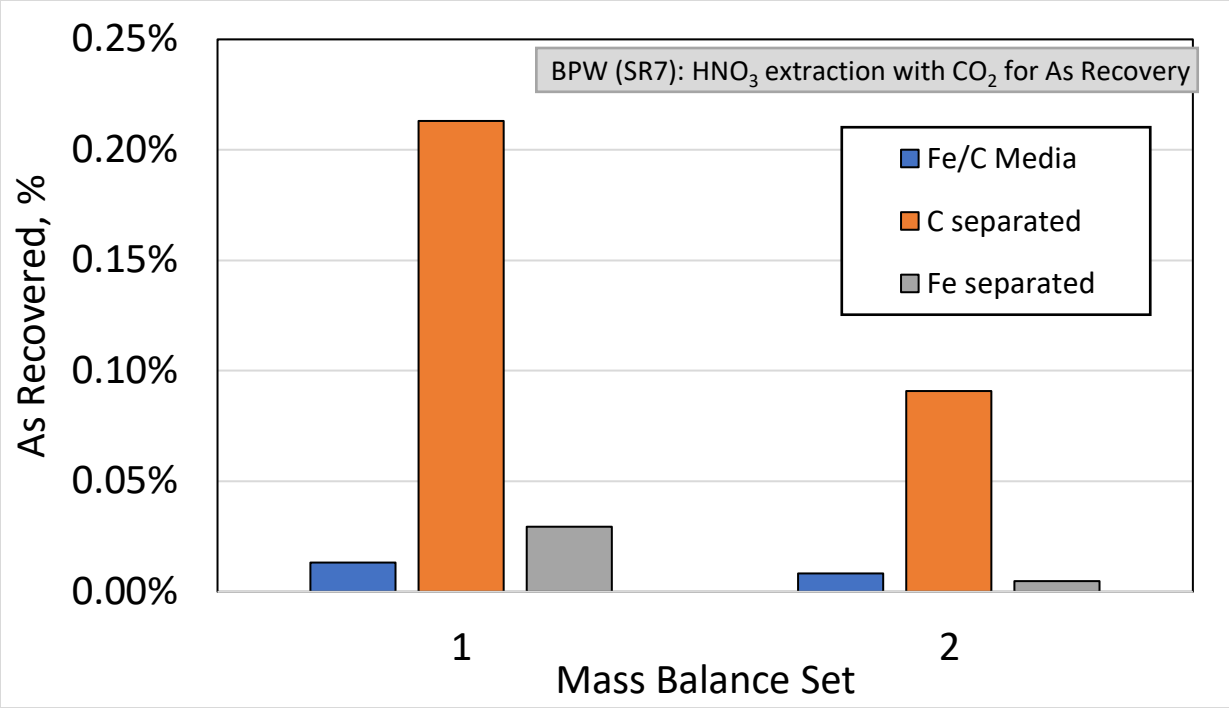

Figure 9. As mobilization from separated PAC and ZVI media, and mixed PAC/ZVI active phase using HNO_3 as a mobilizing agent. Results of the experiments carried out in the presence of CO_2. Fe/C 2:1, LCPF|PAC, 5g/L, pH 5. (Data generated in Nanoscience 1/29/21).

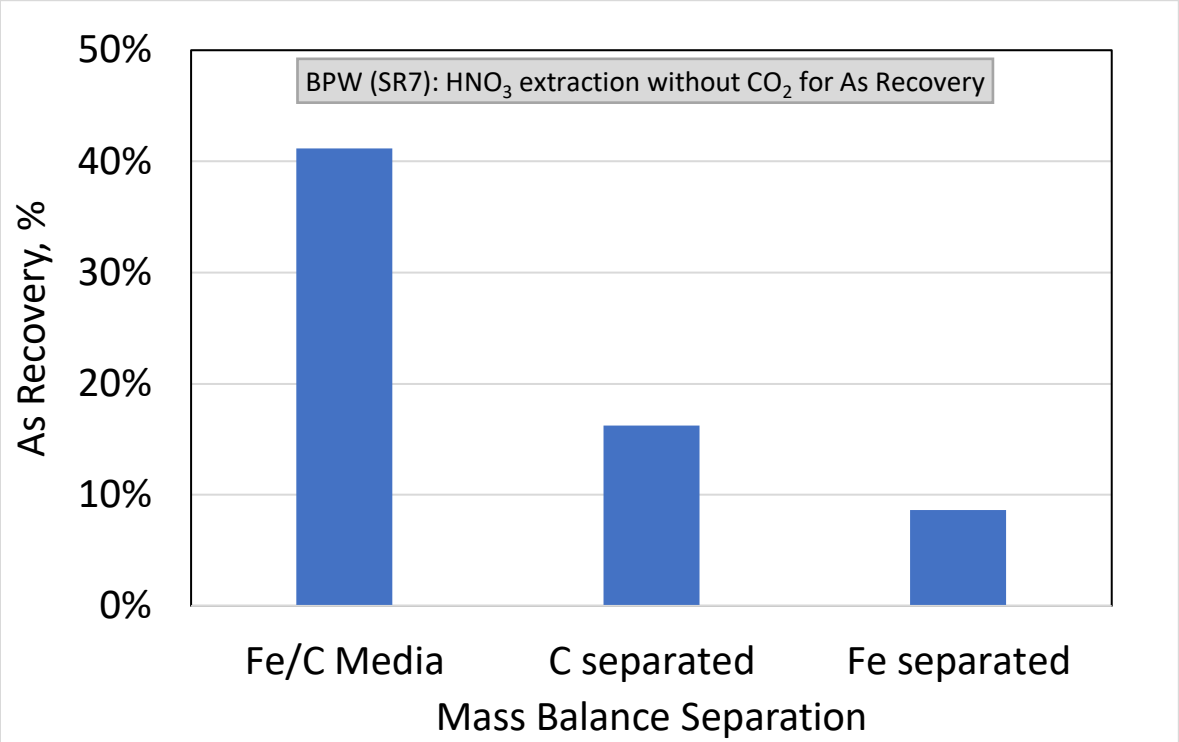

Figure 10. As mobilization in from separated PAC and ZVI phases, and mixed PAC/ZVI active media using HNO_3 as a mobilizing agent. Results of the experiments carried out in the absence of CO_2. Fe/C 2:1, LCPF|PAC, 5g/L, pH 5. (Data generated in Nanoscience 2/5/21).

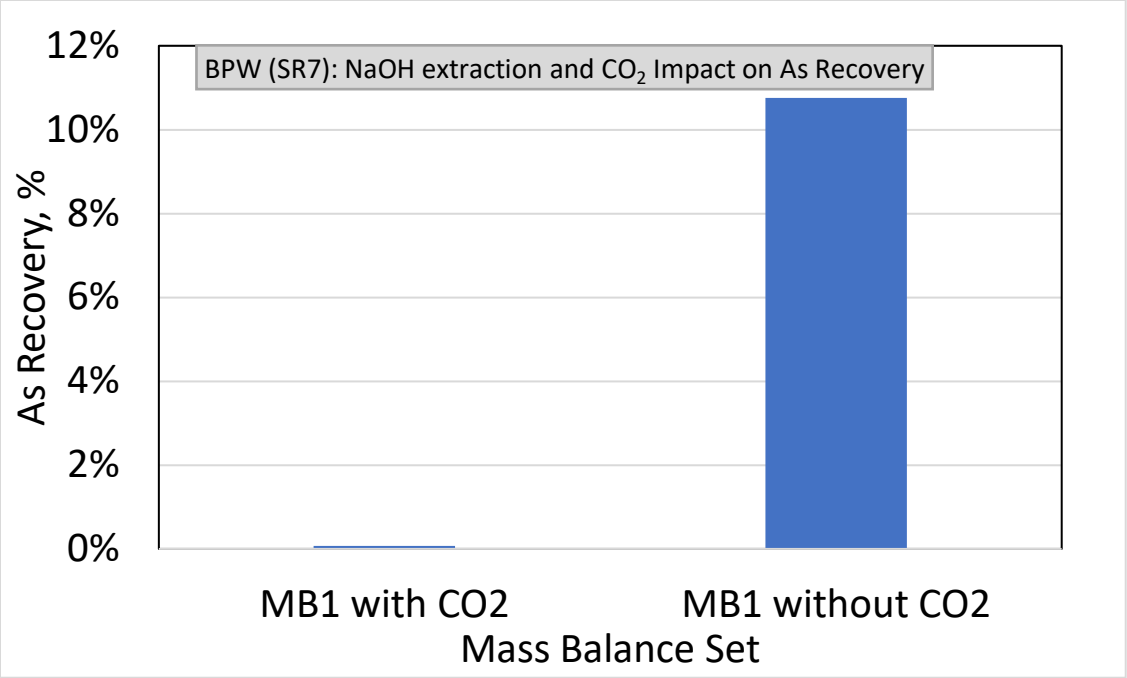

Figure 11. Comparison of As recoveries in the first mass balance experiment from the PAC and iron-containing sample with and without CO_2 flux. Fe/C 2:1, LCPF|PAC, 5g/L, pH 5. (Data generated in Nanoscience 2/5/21). (MB1 refers to Mass Balance Experiment Type 1, MB2 refers to Mass Balance Experiment Type 2).

The results discussed above clearly demonstrate that further experiments are needed to close the overall mass balance for As in ME treatment. For instance, only 0.08% of the removed arsenic was recovered by NaOH elution from the unseparated Fe/C solids in the first mass balance experiment with CO_2, while 0.01% was recovered from the same experiments when nitric acid was used. In the experiments that measured the mass balance of arsenic in the ME media used for BPW treatment without CO_2, approximately 11% of the retained arsenic was mobilized with sodium hydroxide from the sample containing unseparated iron and carbon, while up to 41% of the retained As was recovered using nitric acid under the same conditions. It can be concluded that there is no large difference in arsenic recovery between sodium hydroxide and nitric acid for experiments with CO_2 albeit further experiments are needed to determine whether this is the case for experiments without CO_2.

Antimony is a second element of interest in the treatment of BPW. While arsenic is present in the BPW SR7 samples at a concentration around 6000 to 7000 ppb, antimony concentrations range from 600 to 700 ppb. Although Sb levels in BPW are lower than those of As, its control in landfill gas condensates may become important in the future as safety regulations develop to better address this co-occurring health concern. ME experiments by our group have shown to result in Sb removal rates > 80% in the BPW samples with CO_2 flux (Figure 12). This contrasts with findings from experiments without CO_2 flux, where 60-70% removal was seen (Figure 13).

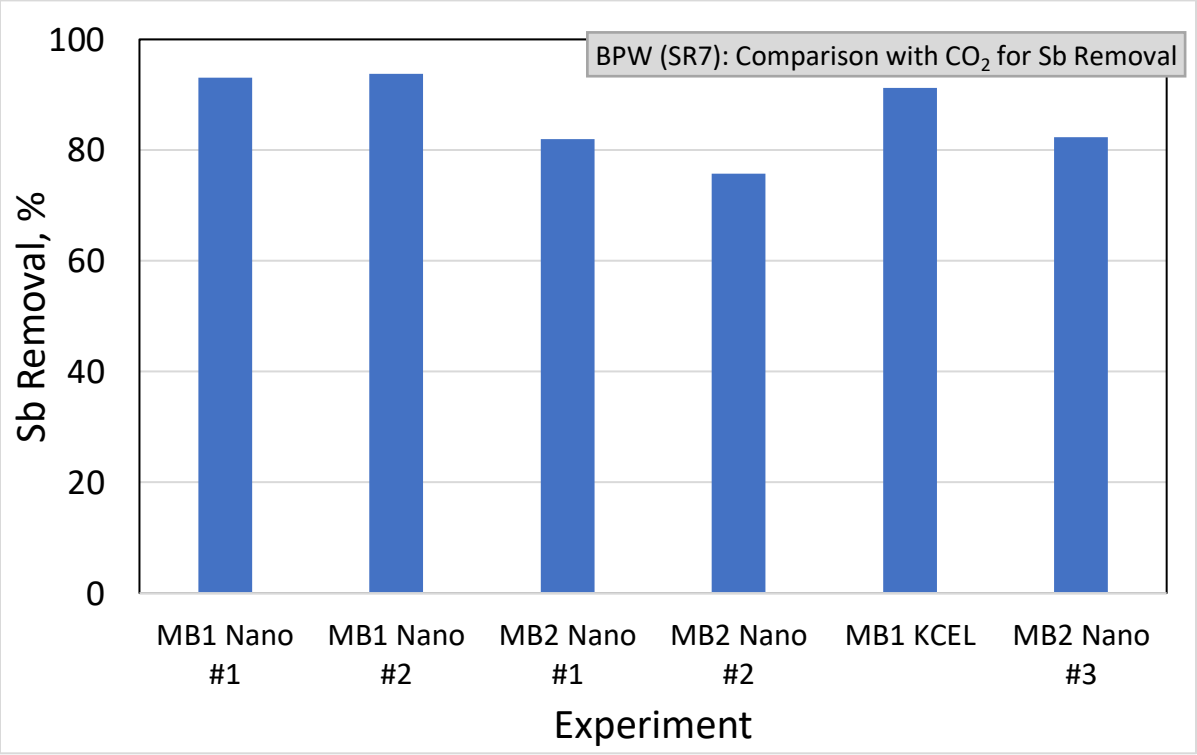

Figure 12. Reproducibility of Sb removal from BPW (SR7) in the presence of CO_2 flux. Fe/C 2:1, LCPF|PAC, 5g/L, pH 5. (Data generated in Nanoscience 1/29/21, 2/5/21 and KCEL 1/19/21.) (MB1 refers to Mass Balance Experiment Type 1, MB2 refers to Mass Balance Experiment Type 2).

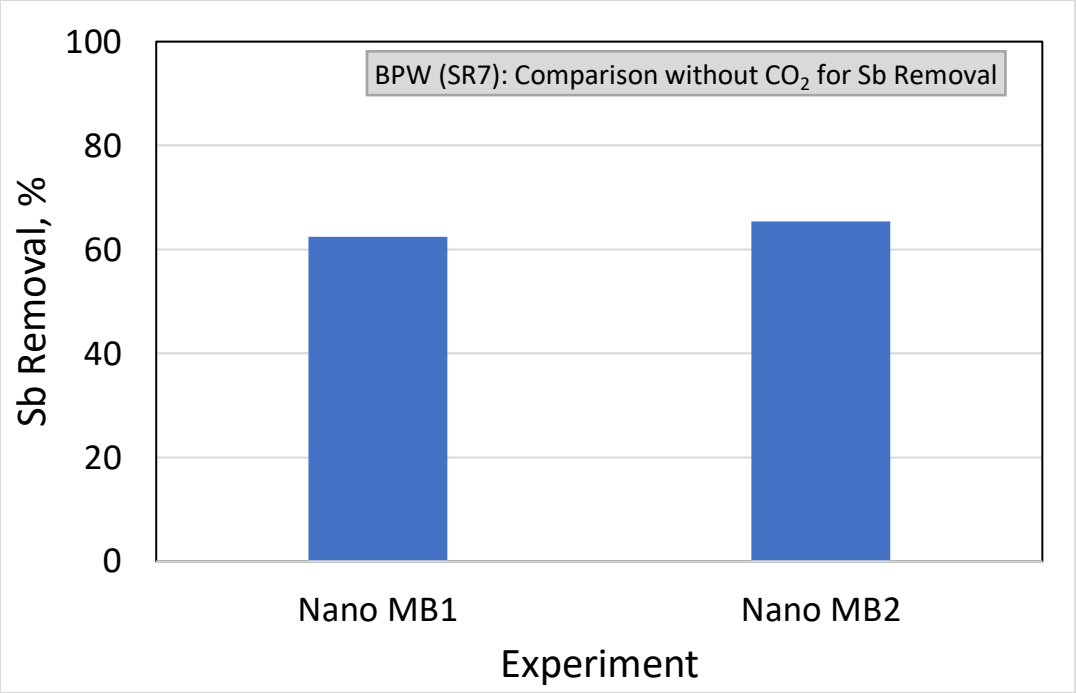

Figure 13. Removal of Sb in the absence of CO_2 flux. Fe/C 2:1, LCPF|PAC, 5g/L, pH 5. (Data generated in Nanoscience 2/5/21). (MB1 refers to Mass Balance Experiment Type 1, MB2 refers to Mass Balance Experiment Type 2).

Antimony recovery was also impacted by CO_2 flux present during the ME experiments in which the Fe/C media were used (Figure 14). Sb recovery measurements for the experiments with CO_2 flux resulted in about 5% or less recovery, compared to up to 20% in the experiments without CO_2 . However, the difference between extraction using nitric acid or sodium hydroxide was not as impactful. The mobilization from the separated phases of carbon and iron in the case of experiments with CO_2 did not surpass 2% regardless of extraction media.

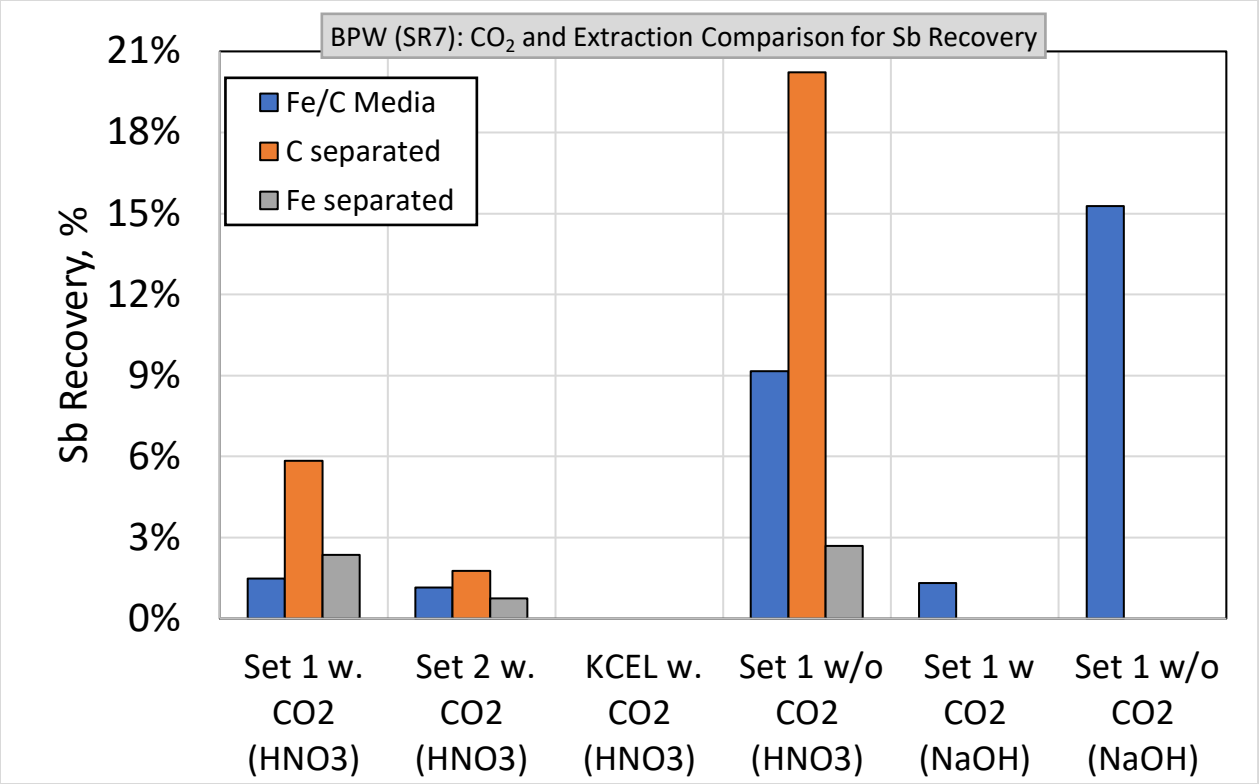

Figure 14. Comparison of Sb recoveries for different BPW treatment scenarios and eluent compositions. Fe/C 2:1, LCPF|PAC, 5g/L, pH5 (0.1M HNO3/1M NaOH). (Data generated in Nanoscience 1/29/21, 2/5/21 and KCEL 1/19/21.)

To better understand the fate of arsenic in the BPW treatment, ME experiments were conducted with model solutions of As (III) (arsenite), As (V) (arsenate), and dimethylarsinic acid (DMA) with a concentration of 10 mg/L as arsenic and a background salt concentration of 0.1 M $NaSO_4$. (While TMA has been shown to be the most prevalent arsine present in the landfill gas, experiments with the TMA precursor trimethylarsine oxide TMAO were not conducted due to its very high cost. While such measurements may be conducted in the future when more cost-efficient TMAO sources are found, DMA was used in this study as a sufficiently acceptable alternative because its reduction results in the formation of dimethylarsine whose properties are sufficiently close to those of .) The results show nearly 100% removal at 24 hours for the As (III) and As (V) solutions regardless of CO_2 treatment conditions. In contrast, the removal of As from the DMA solution ranges from 40% to 80% (Figure 15). These data indicate that methylated As

species such as DMA are less easily removed through ME treatment (Figure 16) although this observation need to be confirmed by more extensive measurements for a representative range of model compounds that can generate As volatiles with varying degrees of methylation and other properties.

The observed difference implies that ZVI may not be not as catalytically effective at removing methylated As species, and possibly that As (III) and As (V) are more easily volatilized to arsines in the conditions typical for ME treatment. A second important finding demonstrated by the data shown in Figure 16 is that the presence or absence of CO_2 results in relatively small changes of DMA As removal (70% and 69%, respectively). Depending on the chosen treatment scheme, this could have consequential design impacts, and such design choices will need to be better informed by the behavior of the more common but less accessible TMA.

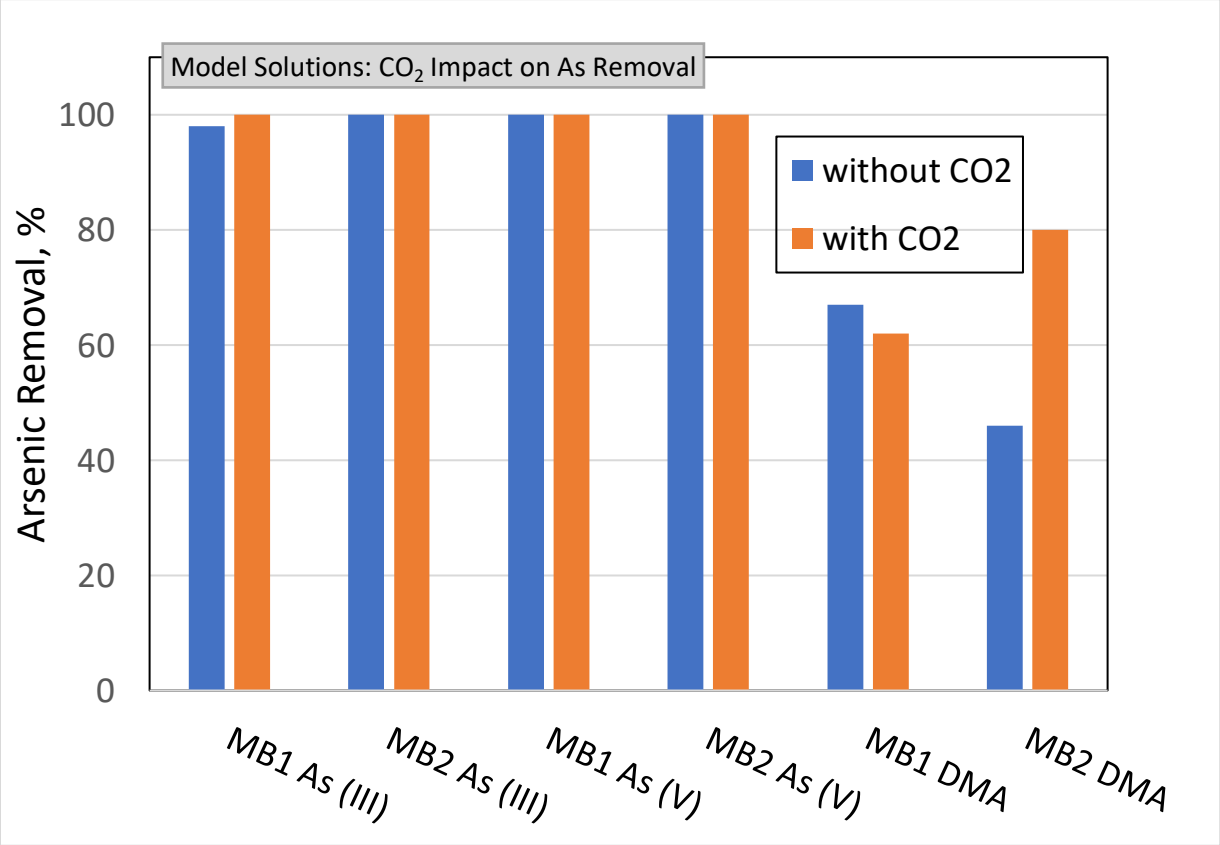

Figure 15. As removal by ME treatment of model As species (arsenite As(III), arsenate As(V) and DMA). Contact time in hours, Fe/C 2:1, LCPF|PAC, 5g/L, pH 5. (Data generated in KCEL 3/11/21.) (MB1 refers to Mass Balance Experiment Type 1, MB2 refers to Mass Balance Experiment Type 2).

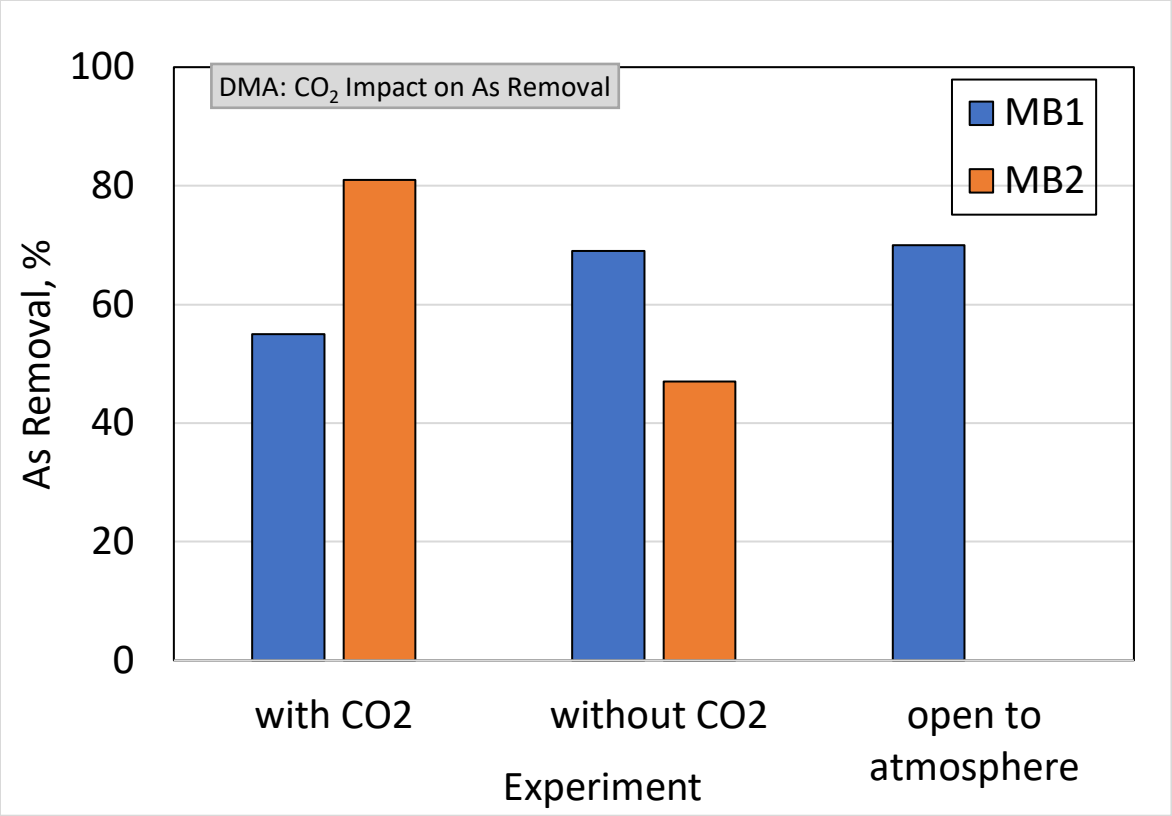

Figure 16. Comparison of DMA-As removal in the presence and absence of CO2 flux. Contact time 24 hours, Fe/C 2:1, LCPF|PAC, 5g/L, pH 5. (Data generated in Nanoscience 2/18/21). (MB1 refers to Mass Balance Experiment Type 1, MB2 refers to Mass Balance Experiment Type 2).

Arsenic recovery from the solids generated in the experiments with DMA solutions showed considerable differences compared with the trend reported above for BPW SR7. While comparatively greater recovery was observed in the DMA experiments that did use CO_2 carrier gas with a maximum of 21% recovery from the separated carbon phase when CO_2 was used in treatment, a 60% maximum recovery was seen for treatment without CO_2. This high albeit incomplete recovery was not seen for the other solutions of either As(III) or As(V) solutions, or BEW process water (Figures 17 – 19). Because SR7 treatment resulted in a relatively greater

(compared with that from the ZVI phase) As recovery from the carbon phase formed in the case of CO_2, it can be tentatively hypothesized that a higher proportion of arsenic in BEW is in the form of DMA or similar methylated compounds or possibly thiolated compounds albeit the latter possibility must be explored in the future. This data also shows that more arsenic was mobilized from the PAC phase in the case of treatment without CO_2 for all three model solutions. This differs from the results for SR7 without CO_2 treatment that showed greater recovery from the combined carbon and iron eluent (Figure 10).

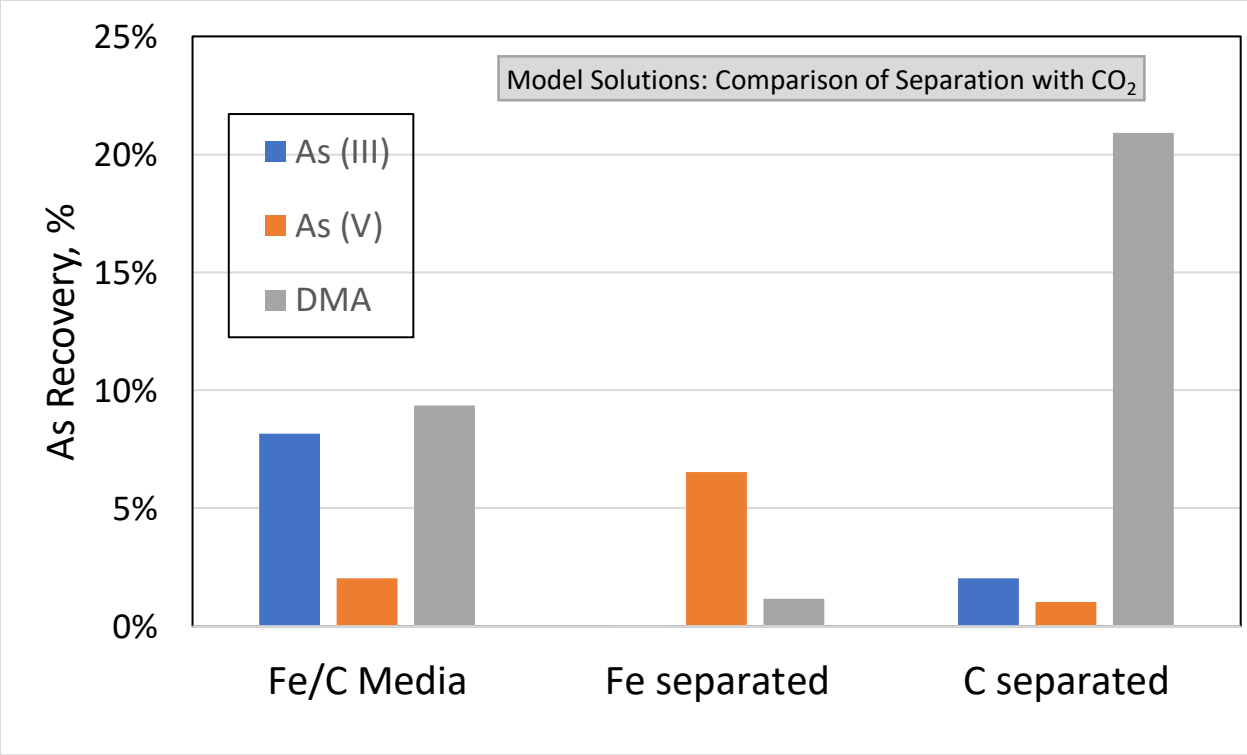

Figure 17. As recovery from solids phases generated during ME treatment of model solutions of As (III), As (V), and DMA in the presence of CO_2 flux. Fe/C 2:1, LCPF|PAC, 5g/L, pH 5. (KCEL data reported on 3/11/21).

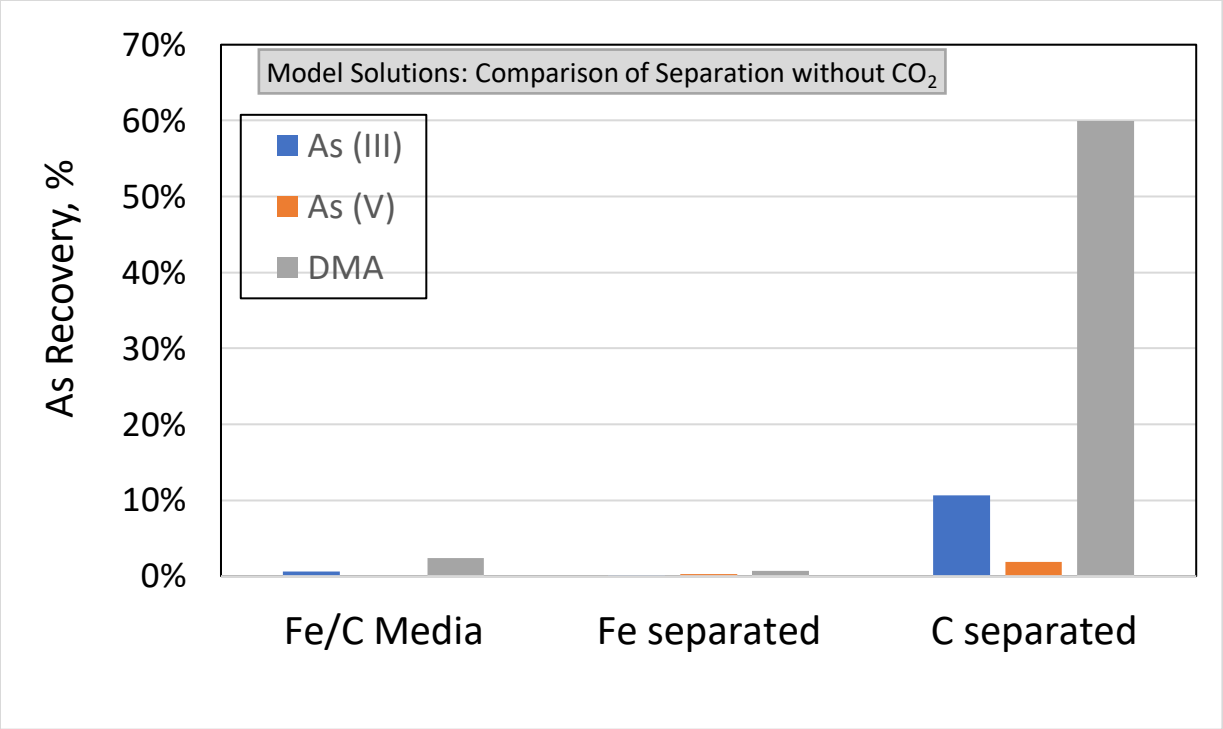

Figure 18. As recovery from solid phases generated during ME treatment of model solutions of As (III), As (V), and DMA in the absence of CO_2 flux. Fe/C 2:1, LCPF|PAC, 5g/L, pH 5. (KCEL data reported on 3/11/21).

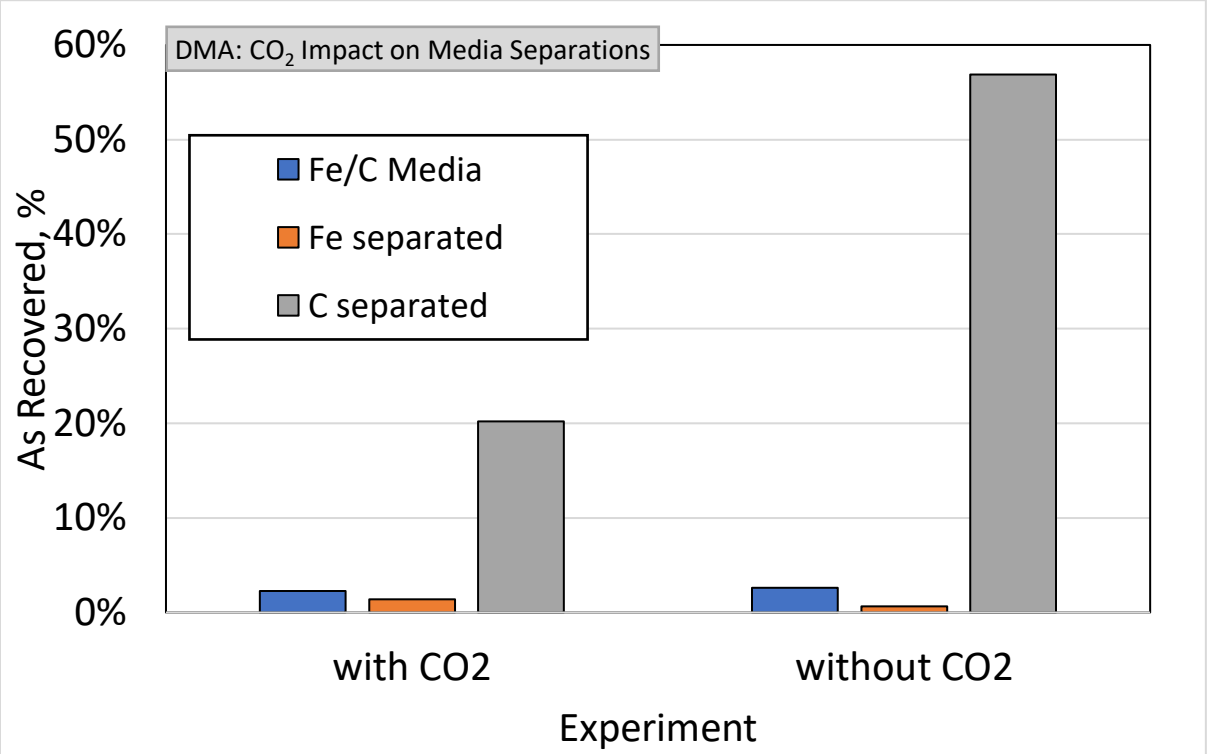

Figure 19. Comparison of As recoveries from Fe/C solids generated during ME treatment of DMA. Fe/C 2:1, LCPF|PAC. 5g/L, pH 5 (Results generated in Nanoscience, 2/18/21).

Results of X-Ray Photoelectron Spectroscopy (XPS) of ZVI and PAC solids Used in ME Treatment

XPS spectroscopy was used to examine whether more possibly unrecovered arsenic remains in the Fe/C media used in ME treatment and, if it is present, compare its properties with those in representative model. The samples sent for XPS analysis are detailed in the following Table 3 As shown in that table, not all samples have produced reasonable data and as a result, a complete analysis of the carbon and iron ME solids from each scenario was not possible. The XPS spectra generated in our measurements with the MAF instrument were also more noisy than those reported in prior studies for arsenic and sulfur containing compounds (Kovalskiy et al. (2017), Yao et al. (2018)). The reason for the increased noise observed in our measurements may be related to the lower sensitivity of the available XPS instrument.

Table 3. Summary of XPS Samples

Sample Class	Samples Sent	Sufficiently Intense As Signal Obtained?
Model Compounds	Arsenopyrite (FeAsS)	Yes
	Realgar (As_4S_4)	Yes
	Orpiment (As_2S_3)	Yes
Fe/C active media separated and dried after ME treatment (100 mg/L As in solution, model compounds arsenate, arsenite and DMA)	As (V) Carbon	Yes
	As (V) Iron	No, sample was magnetized
	As (III) Carbon	Yes
	As (III) Iron	No, sample was magnetized
	DMA Carbon	No, As not detected
	DMA Iron	No, sample was magnetized
Dried Colloidal Particles Isolated Rinse Water (190 mg/L As in ambient solution)	Fe/C	No, As not detected
Dried Colloidal Particles Isolated from SR 8 (12 mg/L As in ambient solution)	Fe/C	No, As not detected
Dried Colloidal Particles Isolated from SR 7 (7 mg/L As in ambient solution)	Fe/C	No, As not detected

XPS Data for Model Compounds

Arsenopyrite

Arsenopyrite (AsFeS) XPS spectra show a range of chemical environments for the arsenic present (Figure 20, Table 4). Oxidation states of both +5 and +3 are inferred, demonstrating at least two separate bond types. However, the +5 state is likely to be a result of surface oxidation prior XPS measurements rather than that which is inherently characteristic for arsenopyrite. As (III) observed peaks are confirmed by Yao et al. (2018) as arsenic-sulfur bonds. Both sulfur peaks at 163.594 and 162.414 eV can be attributed to a metal thiol bond (Figure 21, Table 5). The binding energy (BE) shift for arsenopyrite spectra is 13.88 eV, which is the value needed to adjust the 1s C from the original reading to 285 eV.

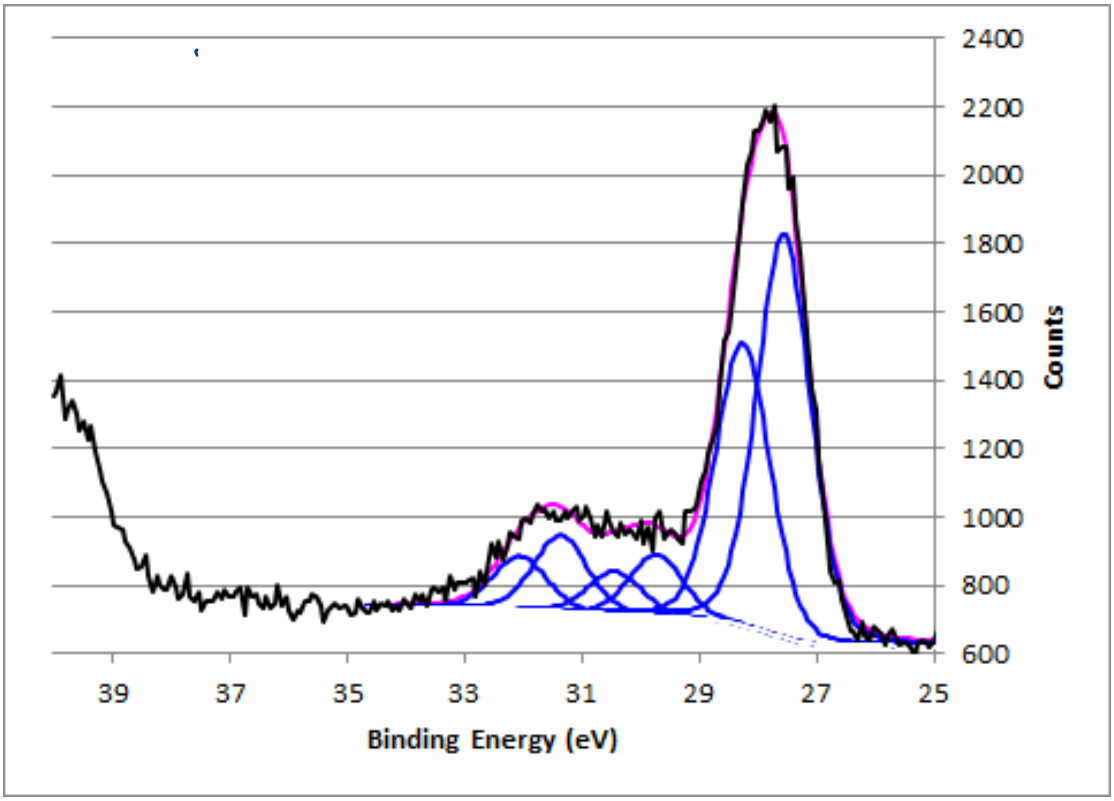

Figure 20. Arsenopyrite arsenic XPS spectra (MAF 5/26/21).

Table 4. Summary of As Binding Energies in Arsenopyrite

Line	Value (eV)	State	FWHM	Integration Area
1	45.936	As (V)	1.085	2973
2	45.236**	As (V)	1.084	4260
3	44.313*	As (III)	1.085	2433
4	43.613*	As (III)	1.084	3479
5	42.135	As (III) or 3d 5/2	1.084	15815
6	41.435	As (III) or 3d 5/2	1.085	22563

*May correspond to 43.4 eV for an As (III)-S bond reported by Yao et al. (2018).
**Likely due to surface oxidation.

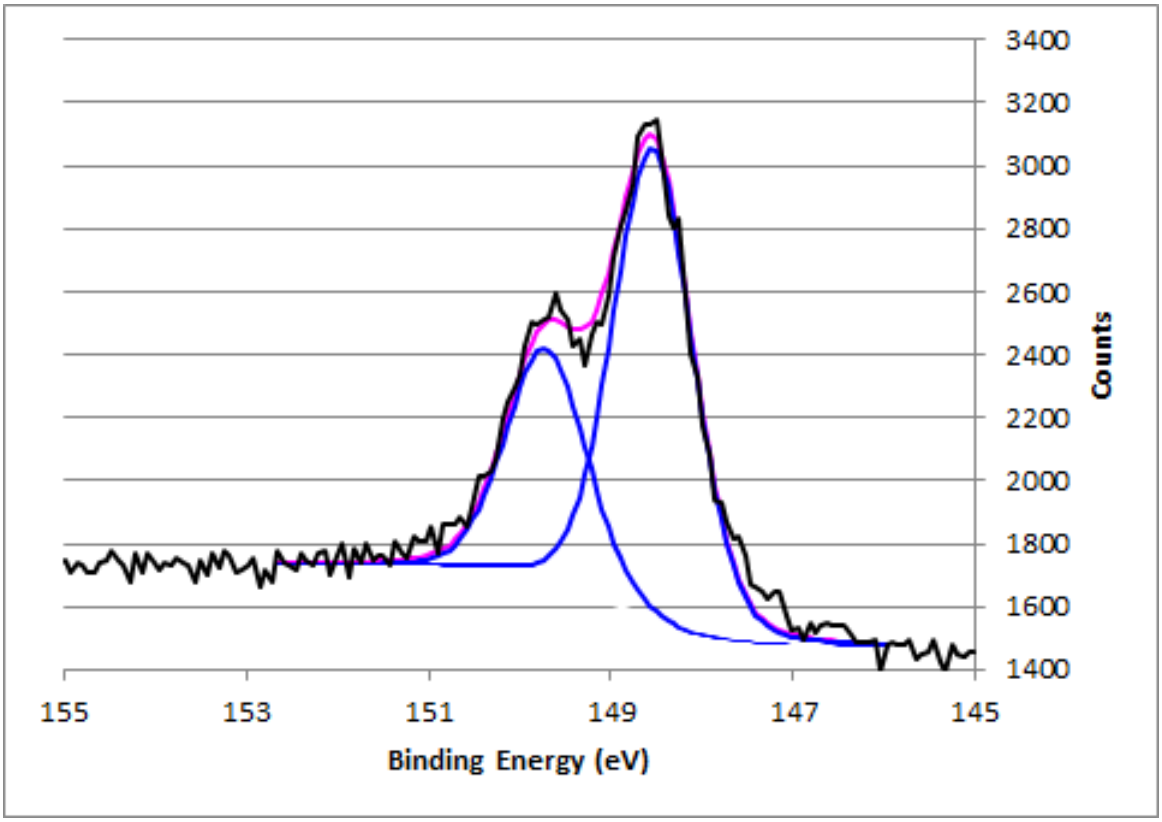

Figure 21. Arsenopyrite sulfur XPS spectra (MAF 5/26/21).

Table 5. Summary of S Binding Energies in Arsenopyrite

Line	Value (eV)	State	FWHM	Integration Area
1	163.594	Metal thiol	1.046	13670
2	162.414	Metal thiol	1.046	27310

Realgar

Realgar (As_4S_4) spectra exhibit two distinct chemical environments for both the arsenic and sulfur species present. Arsenic binding energies at 44.271 and 43.571 eV are indicative of the As (III) oxidation state, as Yao et al. (2018) reports a value of 43.4 eV for an As (III)-S bond (Figure 22, Table 6). Both sulfur peaks at 164.364 and 163.184 eV represent a sulfide bond (Figure 23). The second value (163.184 eV) is confirmed by Yao et al. (2018) which reports the S- As (II) bond in realgar at 163.1 eV. Binding energy shift of reported data from MAF is 12.42 eV.

Table 6. Summary of Realgar Binding Energies for As and S

	Value (eV)	State	FWHM	Integration Area
Arsenic				
Line 1	43.571	As (III)	1.346	24215
Line 2	44.271	As (III)	1.347	16940
Sulfur				
Line 1	164.364	sulfide	1.283	21066
Line 2	163.184	sulfide	1.284	42155

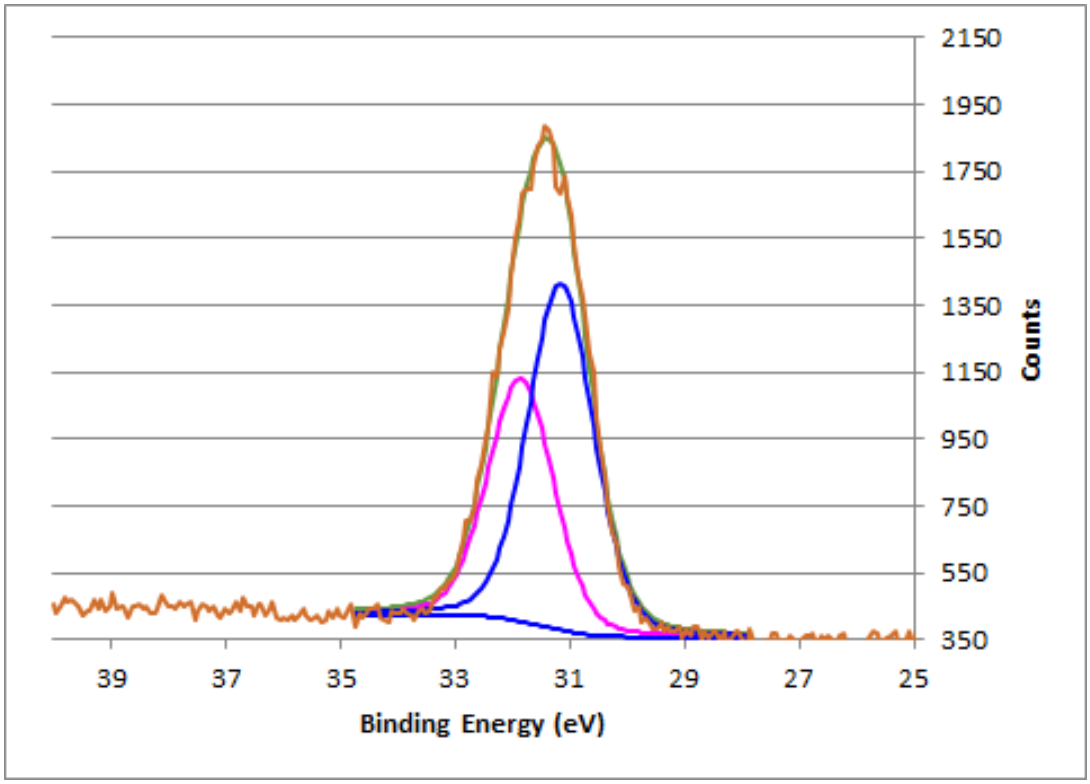

Figure 22. Realgar arsenic XPS spectra (MAF 5/26/21).

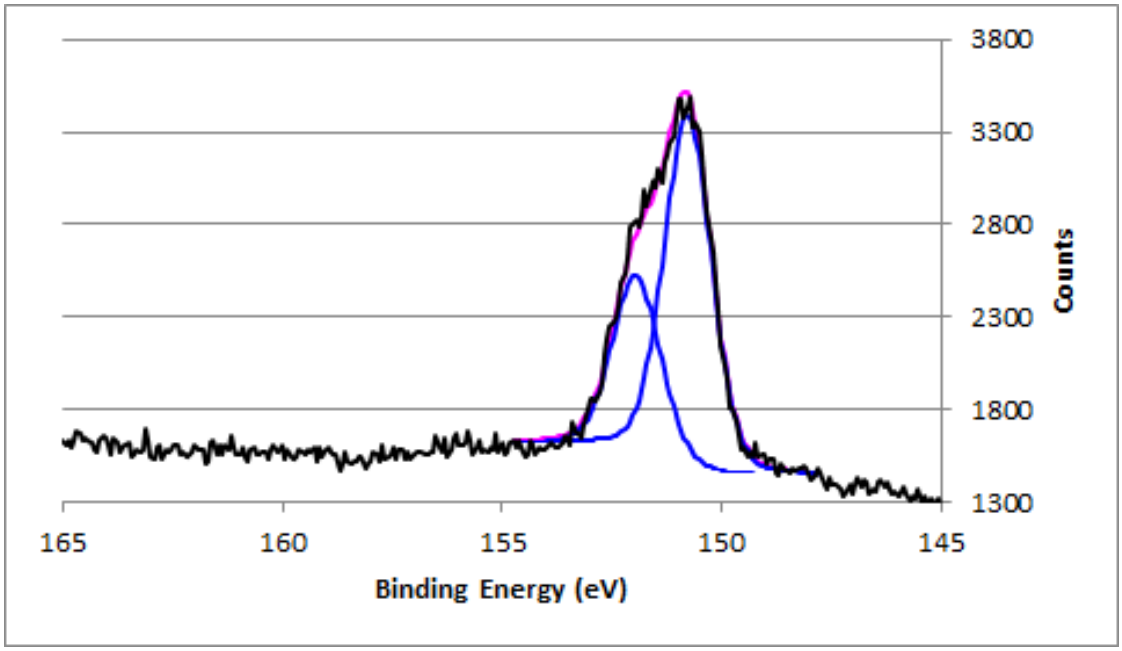

Figure 23. Realgar sulfur XPS spectra (MAF 5/26/21).

Orpiment

Like arsenopyrite, orpiment (As_2S_3) data demonstrates a range of binding energies for arsenic, though all appear to correspond to the largely same environment of a +3 oxidation state (Table 7, Figure 24). Sulfur was observed to show four binding energies, with all values indicating either a metal thiol or metal sulfide bond (Table 8, Figure 25). The binding energy shift is 10.4 eV.

Table 7. Summary of Orpiment Binding Energies for As

	Arsenic			
	Value (eV)	State	FWHM	Integration Area
Line 1	43.386**	As (III)	1.305	3188
Line 2	42.686*	As (III)	1.305	4562
Line 3	41.993	As (III) or 3d 5/2 spin	1.307	7783
Line 4	41.293	As (III) or 3d 5/2 spin	1.306	11096

*Values match those reported by Kovalskiy et al. (2017) for $As_{40}S_{60}$.
**Yao et al. (2018) reports 43.4 eV as an As (III) – S peak.

Table 8. Summary of Orpiment Binding Energies for S

	Sulfur			
	Value (eV)	State	FWHM	Integration Area
Line 1	162.504*	Metal thiol	1.104	3674
Line 2	161.485	Metal sulfide	1.104	7199
Line 3	161.324*	Metal sulfide	1.104	7374
Line 4	160.305	Metal sulfide	1.104	14382

*Values match those reported by Kovalskiy et al. (2017) for $As_{40}S_{60}$.
**Yao et al. (2018) reports 43.4 eV as an As (III) – S peak.

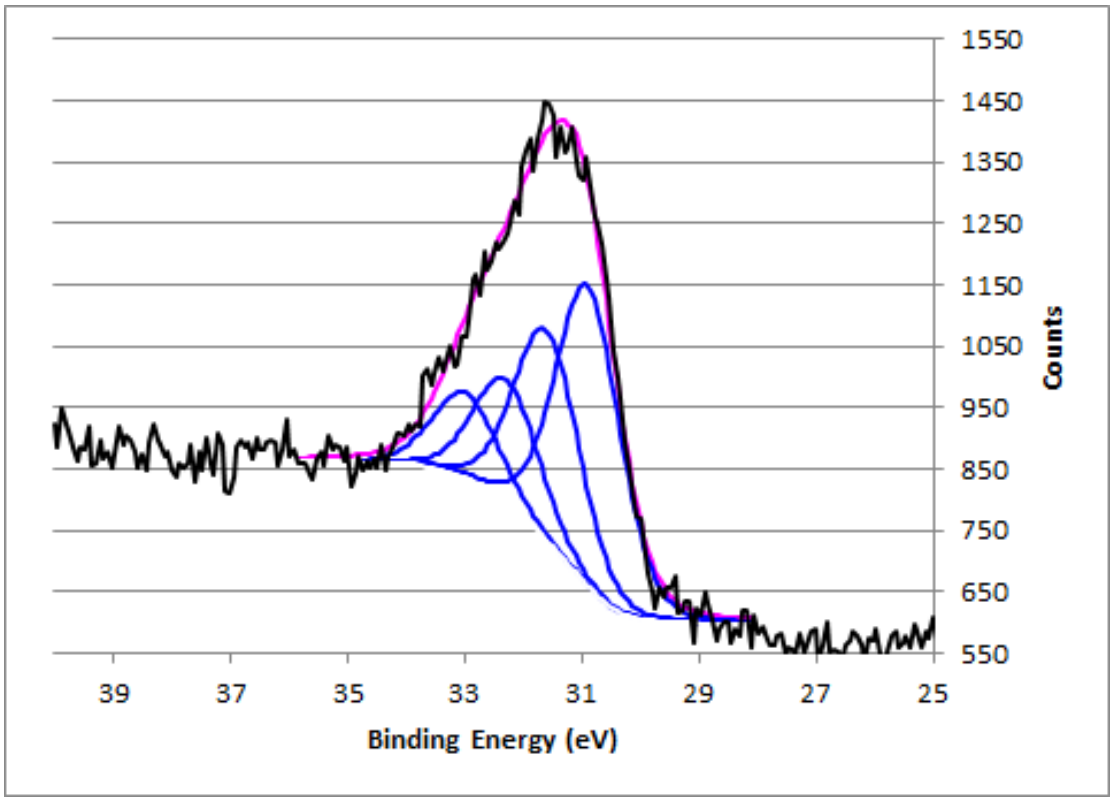

Figure 24. Orpiment arsenic XPS spectra (MAF 5/26/21).

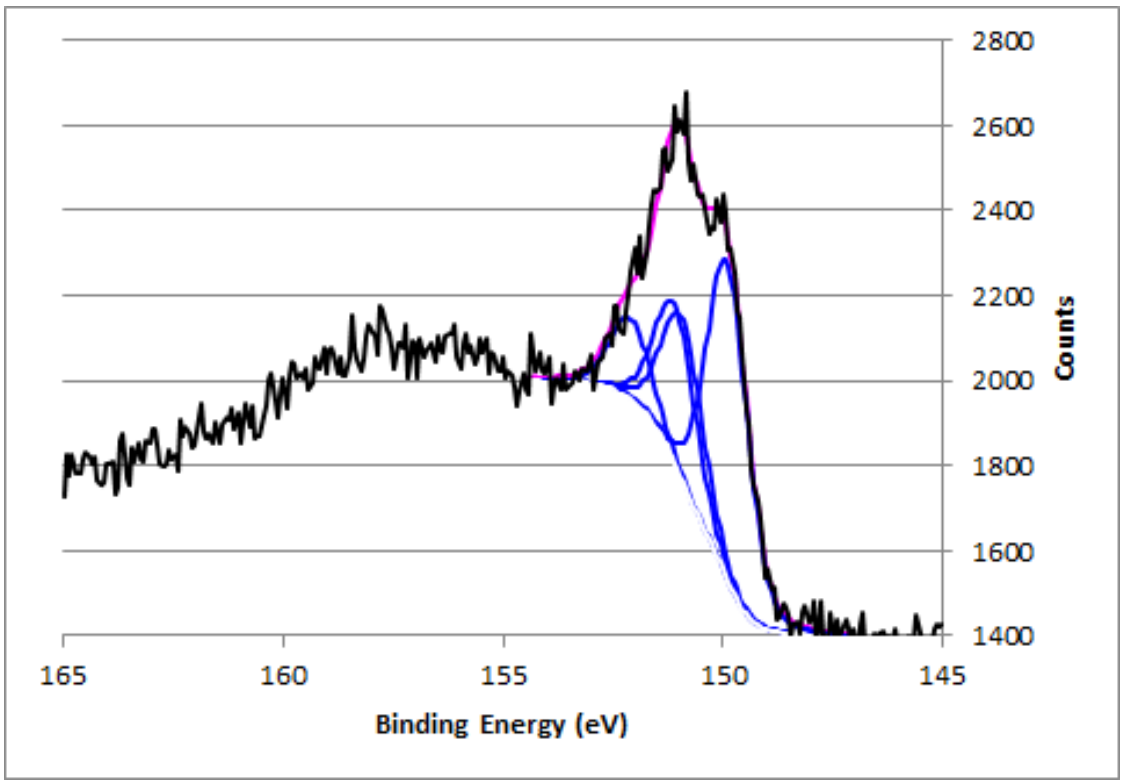

Figure 25. Orpiment sulfur XPS spectra (MAF 5/26/21).

Both of these spectra can be interpreted considering reported spectra by Kovalskiy et al. (2017) for analysis of $As_{40}S_{60}$, which has the same empirical formula as orpiment. Kovalskiy et al. (2017) also reports the presence of four separate peaks for As, as observed from the MAF results (Figure 26). The two stronger peaks appear to correspond to the bonding of arsenic with sulfur, while the other two can be assigned to As-As bonds, according to the color-coded key povided by Kovalskiy et al. (2017) (Figure 26). While intensity units of Kovalskiy et al. (2017) do not match the counts seen from the MAF data, the reported binding energies are almost identical if the BE shift of 10.4 eV is taken into account for the MAF data. As with the arsenic data, the comparison of sulfur data from MAF and Kovalskiy et al. (2017) is very similar considering the BE shift of 10.4 eV (Figure 27). The difference in peak intensity again describes bonding differences, though the MAF results do not demonstrate this as clearly. Although four lines are seen, Kovalskiy et al. (2017) reports this as three doublets, indicating only three unique sulfur

environments. It is important to note also that the scale is not identical on these figures, with counts referring to electrons ejected from the surface of the sample and intensity (a.u.) as according to the Beer-Lambert law.

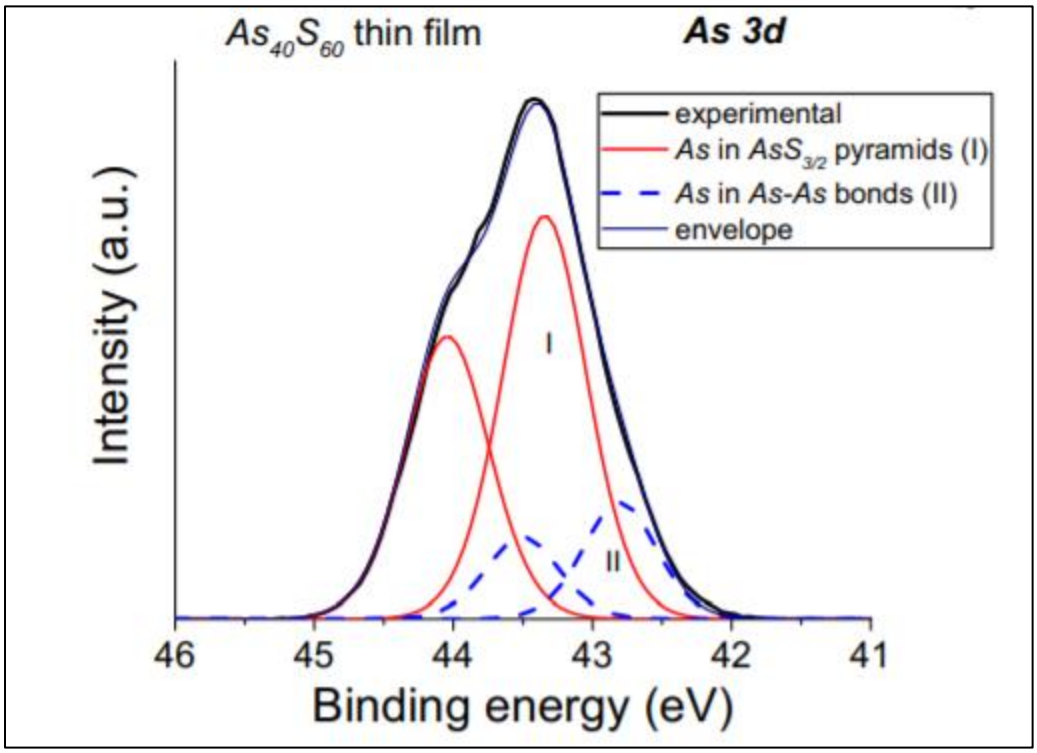

Figure 26. Arsenic 3d spectra reported by Kovalskiy et al. (2017), Figure 1.

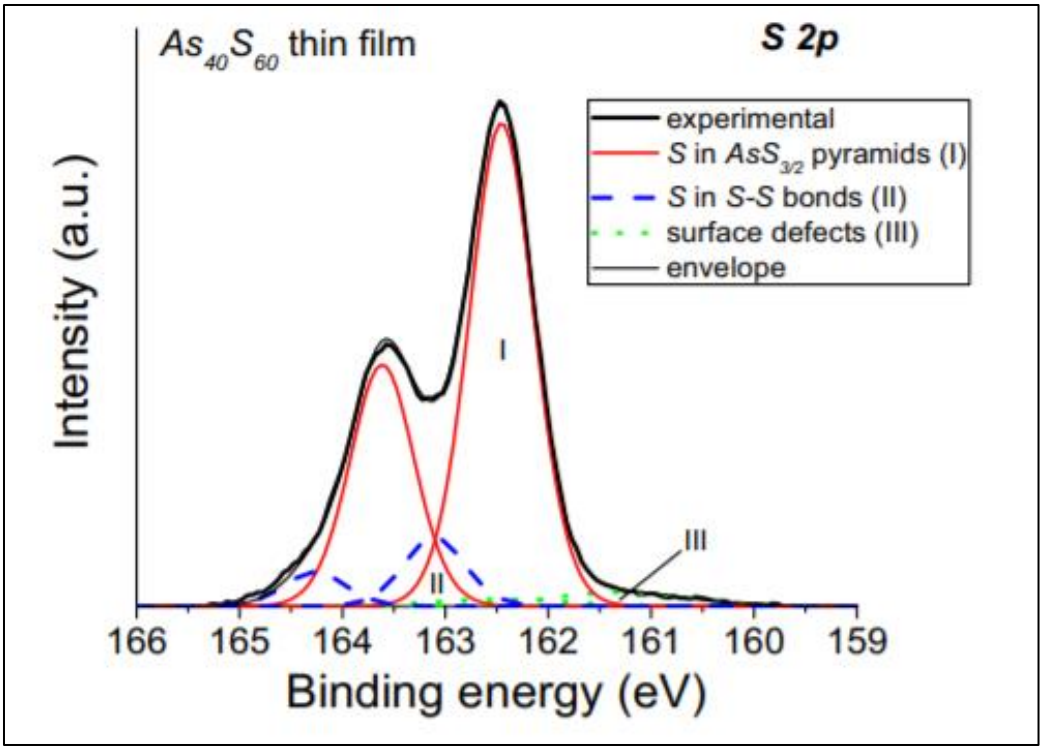

Figure 27. Sulfur 2p spectra reported by Kovalskiy et al. (2017), Figure 1.

ME Dried Solids

Using the model compound XPS results, information about the bonding behavior and chemical environments of arsenic found in the solid phases used in ME treatment or colloidal particles naturally present in BPW samples can in principle be inferred. However, as noted in Table 3, only the samples of the carbon phase used, together with the ZVI particles, in the ME experiments with As (V) and As (III) models yielded reasonable results. The other samples did not yield meaningful XPS data due to the magnetization that interferes with XPS measurements.

ME solids generated in experiments with As (V) model

Similarly to the reported literature interpretations, the XPS spectra for ME solids with As (V) show two strong peaks and two peaks with fewer counts (Figure 28). This could indicate the presence of two As-As bonds and two As-S bonds, as explained by Kovalskiy et al. (2017). The signal from sulfur has a low intensity and it is associated with the small amount of sulfur

naturally present in PAC. In this spectrum, the arsenic is mostly found in the +5 oxidation state, though it possibly is also observed in the +3 oxidation state (Table 9). Sulfur data shows only two environments and higher binding energies than observed with the model compounds, where metal sulfur bonds are expected (Figure 29, Table 10). This data has a binding energy shift of 12.35 eV.

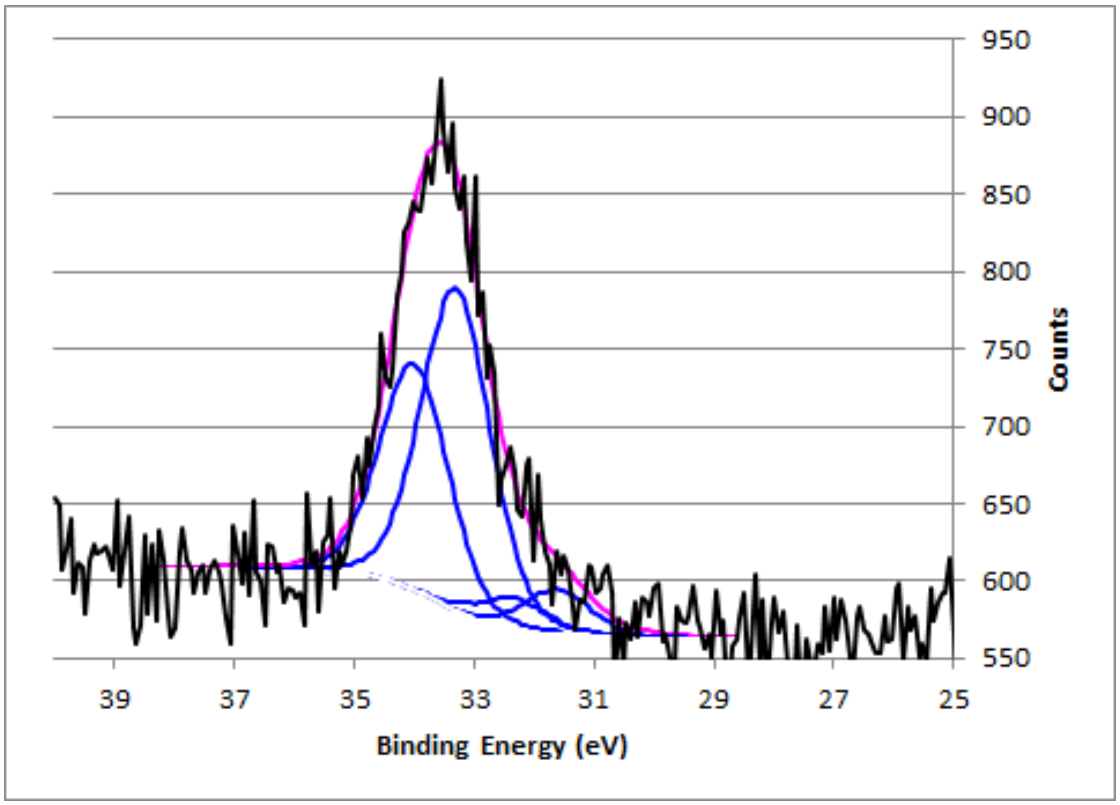

Figure 28. ME solids with As (V) arsenic XPS spectra (MAF 5/26/21).

Table 9. Summary of As Data for ME Dried Solids with As (V)

	Arsenic			
	Value (eV)	State	FWHM	Integration Area
Line 1	46.353	As (V)	1.355	3466
Line 2	45.653	As (V)	1.355	4953
Line 3	44.67	As (V)	1.355	495
Line 4	43.97	As (III)	1.355	705

Table 10. Summary of S Data for ME Dried Solids with As (V)

	Sulfur			
	Value (eV)	State	FWHM	Integration Area
Line 1	170.054	Metal-sulfur bond	1.537	2421
Line 2	168.874	Metal-sulfur bond	1.537	4851

-

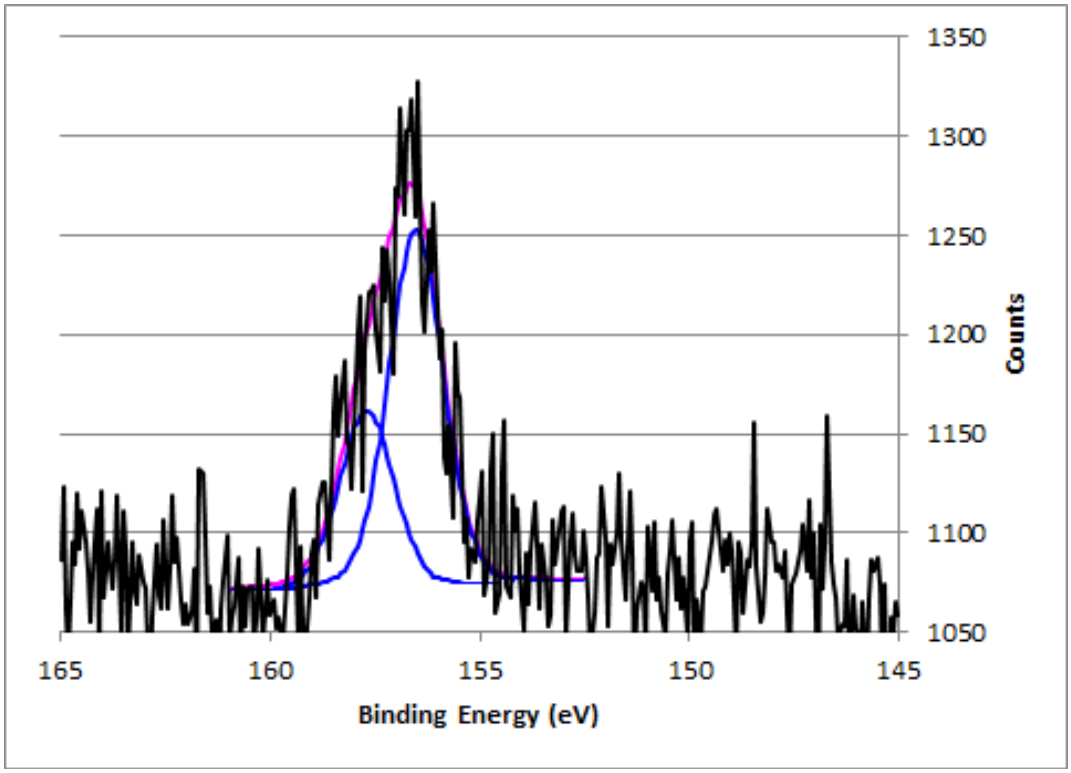

Figure 29. ME solids with As (V) sulfur XPS spectra (MAF 5/26/21).

ME solids generated in experiments with As (III) model

The spectra for ME solids with As (III) show less variation in the range of binding energies. Only two peaks are reported for both arsenic and sulfur (which has a very low intensity) with the second line for arsenic suspected to be an artifact (Table 11, 12). This data has a binding energy shift of 11.2 eV. The binding energies for arsenic are more indicative of the As (V) state than the As (III) state, while sulfur peaks again indicate a metal sulfate bond (Figures 30, 31).

Table 11. Summary of As Data for ME Dried Solids with As (III)

	Arsenic			
	Value (eV)	State	FWHM	Integration Area
Line 1	45.947	As (V)	2.408	1946
Line 2	45.247	As (V)	2.408	2781

Table 12. Summary of S Data for ME Dried Solids with As (III)

	Sulfur			
	Value (eV)	State	FWHM	Integration Area
Line 1	169.998	Metal-sulfur bond	1.704	1832
Line 2	168.818	Metal-sulfur bond	1.703	3669

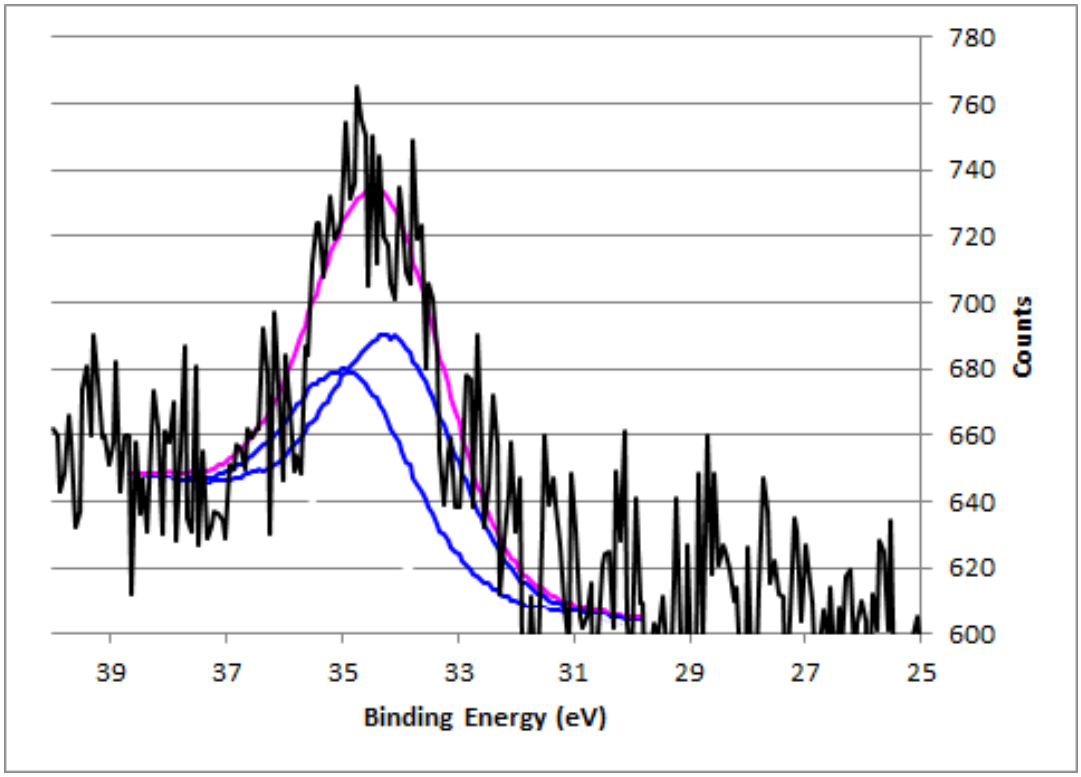

Figure 30. ME solids with As (III) arsenic XPS spectra (MAF 5/26/21).

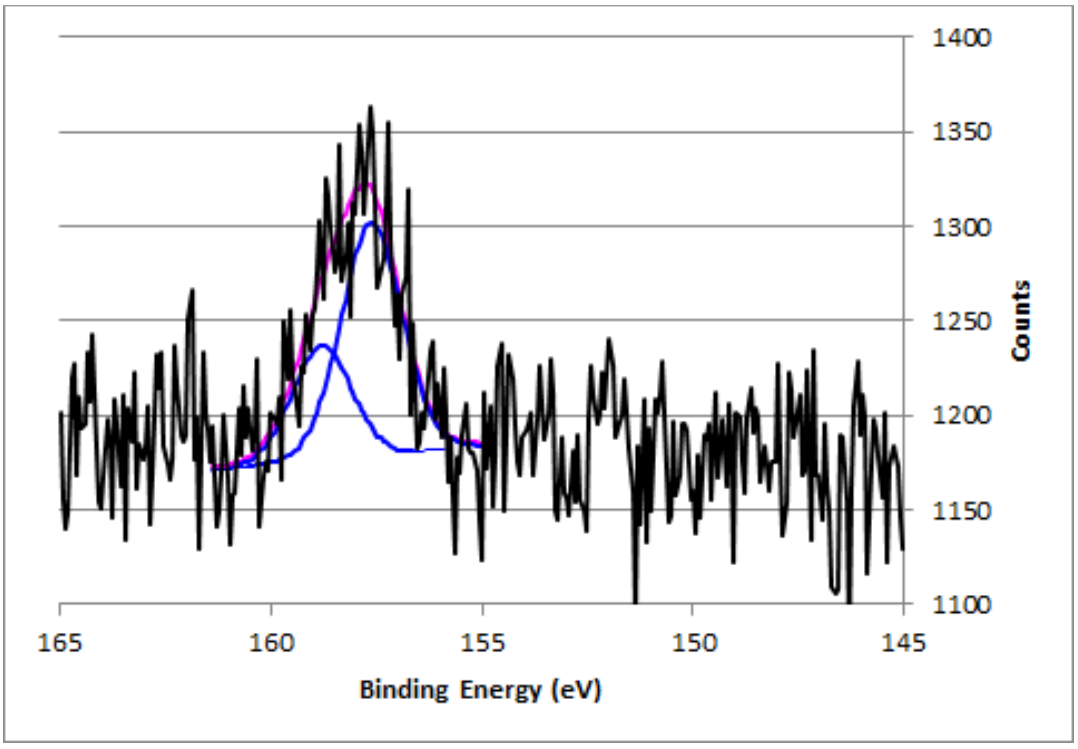

Figure 31. ME solids with As (III) sulfur XPS spectra (MAF 5/26/21).

In comparing the XPS data for the model compounds and ME solids, it can be noted that the reported counts in both the cases of arsenic and sulfur differ by several hundred counts and that this may be contributing to the low signal to noise ratio. In the case of arsenic, the model compounds had counts of 1450 or greater, while the dried ME solids had counts of under 950. For sulfur, model compounds had counts of over 2600 while ME solids had counts of half that at 1350 or less. Additionally, the sulfur in the ME solids has a binding energy range of 168.818 to 170.054 eV while the model compounds show sulfur peaks ranging from 160.305 to 163.594 eV. This may imply a more positive oxidation state as a result of a metal sulfate bond. Based on reported values from Yao et al. (2018), it is expected that this bond is an As (III) – S bond. It can also be inferred that arsenic is volatilizing from the low intensity of the As lines in these spectra, because the lack of clarity represents low signal to noise ratio and therefore a low arsenic concentration.

Chapter 4: Initial Examination of the Formation of Arsenic Volatile Species in ME treatment

Goals

This chapter aims to close the mass balance data that were left unanswered by the previous mass balance experiments. In the mass balance experiments, recovery of arsenic from the ME treatment media was negligible, typically $< 1\%$. This finding combined with the XPS spectroscopic data showing little to no arsenic present in the ME treatment media led us to believe that the arsenic which was removed by ME but not recovered from the ME treatment media in the mass balance experiments may be lost to the gas phase. The experiments described in this chapter are accordingly concerned with the generation and capture of arsine gas. The ultimate goal of these measurements was to ascertain whether arsines were indeed generated in the Fe/C treatment of BEW process water and whether and how the arsenic was mobilized from the solid treatment media to the gas phase.

The quantitation of arsine formation was done using the silver diethyldithiocarbamate (AgDDC) method that has been extensively used in prior research (Cross (1979), Kopp (1973), Budesinsky (1979), Sandhu and Nelson (1978), Shaikh and Tallman (1977)). The use of the AgDDC method in this study was deemed appropriate due to the high levels of arsenic in BEW product water and related matrixes, and the need to distinguish between different species of arsines that may be generated in ME treatment of As-containing solutions. Experimental and analytical aspects of the AgDDC method as implemented in this study and relevant results are presented in the sections that follow.

Results

Wavelengths of Maximum Absorbance

The absorbance spectra and their specific parameters, for instance the wavelength of maximum absorbance can be a valuable indicator to characterize the forms of arsenic and to a lesser extent antimony in the BPW SR solutions. To provide a baseline for comparison and reference, data for standard solutions of sodium arsenite, sodium meta-arsenate, dimethylarsinic acid, and ICP standards for arsenic and antimony are presented in this section (Figures 32-36). For better illustration of the absorbance bands and the corresponding wavelengths of maximum absorbance, the absorbance spectra obtained for the highest concentration tested (200 μg/L) are shown. In the case of sodium arsenite, which contains arsenic in the +3 oxidation state, a clear wavelength of maximum absorbance is observed at 525 nm (Figure 32). This is very similar to the expected wavelength of 520 nm identified in the standard methods consulted in the design of these experiments. Sodium meta-arsenate however, where arsenic has a +5 oxidation state, did not yield a similarly strong response, despite the addition of 2N HCl as recommended in the standard method (Figure 33). This suggests that this form of arsenic (formal As oxidation state +5) is more difficult to reduce and convert to arsine. This also implies that the As volatiles potentially formed during ME treatment of the BPW solutions are not likely to be a result of As (V) reduction and conversion to AsH_3. (For this matter, practically no arsenate was found to be present in BEW process water) This aspect of the reductive treatment of BPW will be further explored through gas-phase analysis of ME treatment byproducts.

The borohydride reduction of DMA that is assumed to generate dimethyl arsine $(CH_3)_2AsH$ resulted in a distinctly different absorbance spectra of AgDDC/$(CH_3)_2AsH$ complexes (Figure 34). Their absorbance spectra had a pronounced peak at 420 to 430 nm and a secondary peak at ~480 nm, a clear difference compared with the spectra of AgDDC/AsH_3 complexes. This

difference helps to distinguish the nature of arsine released in ME treatment and the speciation of As in BPW solutions.

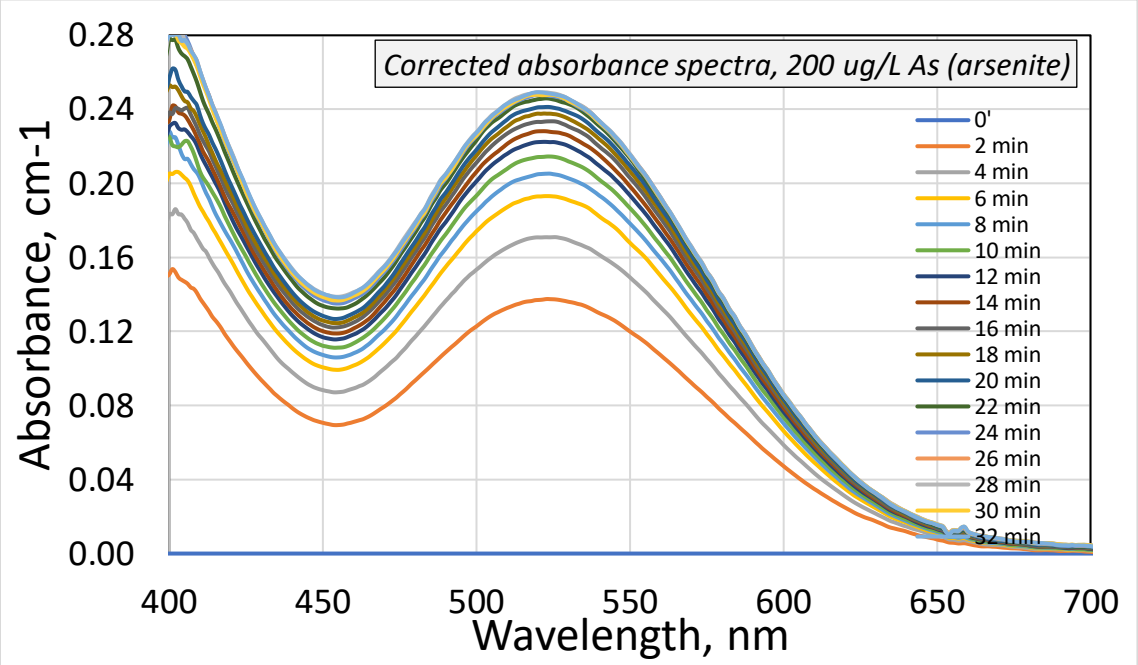

Figure 32. Development of the background-corrected absorbance spectra of AgDDC in the case of borohydride reduction of 200 □g/L As (arsenite).

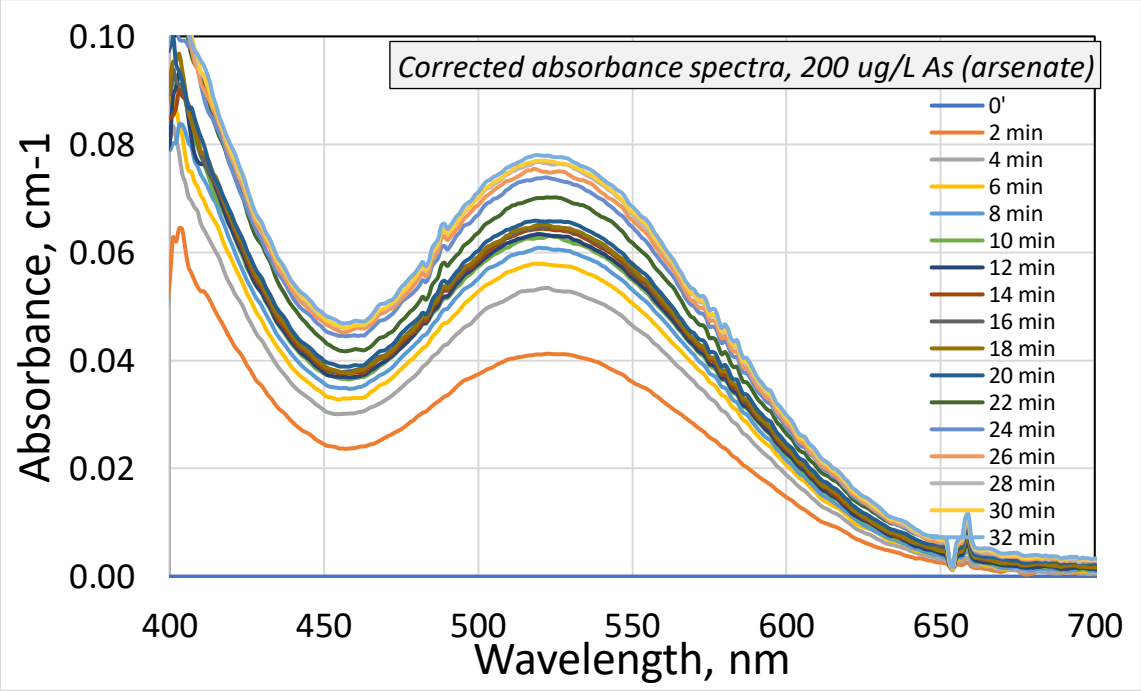

Figure 33. Development of the background-corrected absorbance spectra of AgDDC in the case of borohydride reduction of 200 □g/L As (arsenate).

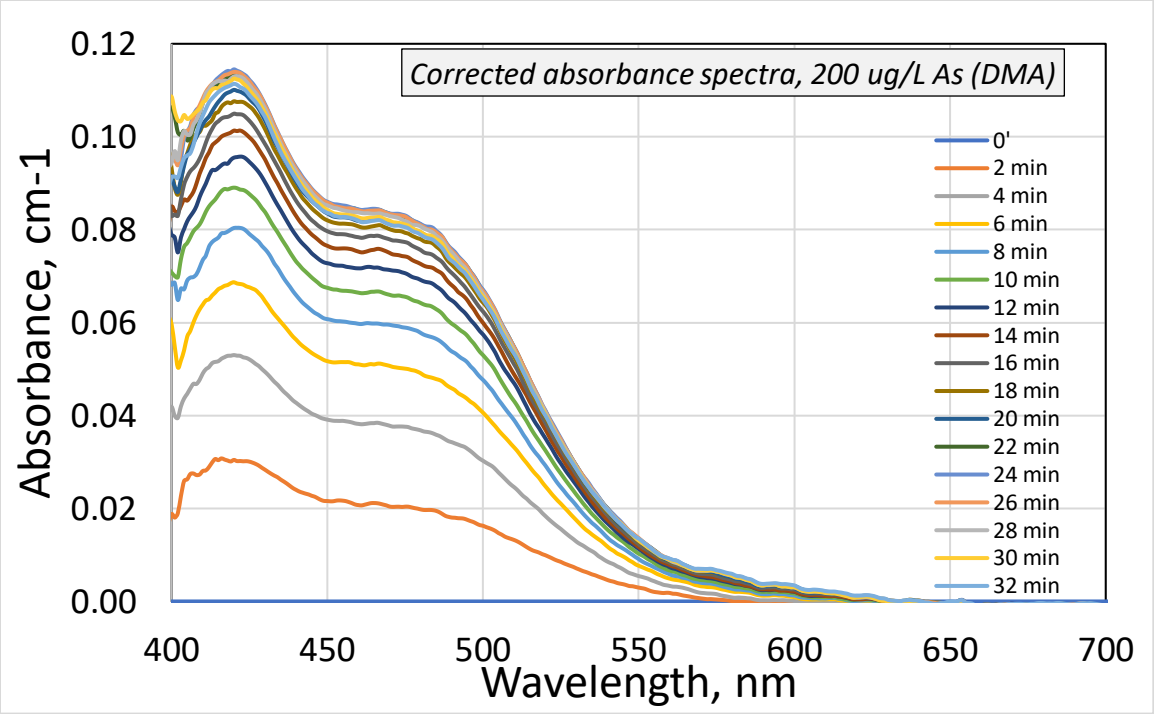

Figure 34. Development of the background-corrected absorbance spectra of AgDDC in the case of borohydride reduction of 200 μg/L As (DMA).

In addition to the measurements that utilized As(III) and As(V) salts as arsine precursors, ICP standards for arsenic and antimony were also used as arsenic and antimony sources in AgDDC analyses. The absorbance spectra obtained for the As ICP standard used as the arsine source are identical to those in the case of arsenite salt, with a maximum again seen at 525 nm (Figure 35). The difference lies in the reported intensities, which requires further exploration.

To determine whether this method (borohydride reduction) would successfully generate stibines and could be used to determine possible contributions and formation of volatiles in ME treatment of BPW, an antimony standard was also tested, assumedly forming stibine SbH_3 (Figure 36). The observed intensity of the AgDDC/SbH_3 complexes was considerably lower than those observed in the case of the arsenic standard, about 20%, and the wavelength of maximum absorbance is closer to 507 nm. This suggests that while there is a possibility of distinguishing the antimony

and arsenic contributions in the generation of As and Sb volatiles, their separation depends on both the different intensity of the spectra and the notable intensity difference observed for the absorbance bands of the $AgDDC/AsH_3$ and $AgDDC/SbH_3$ complexes.

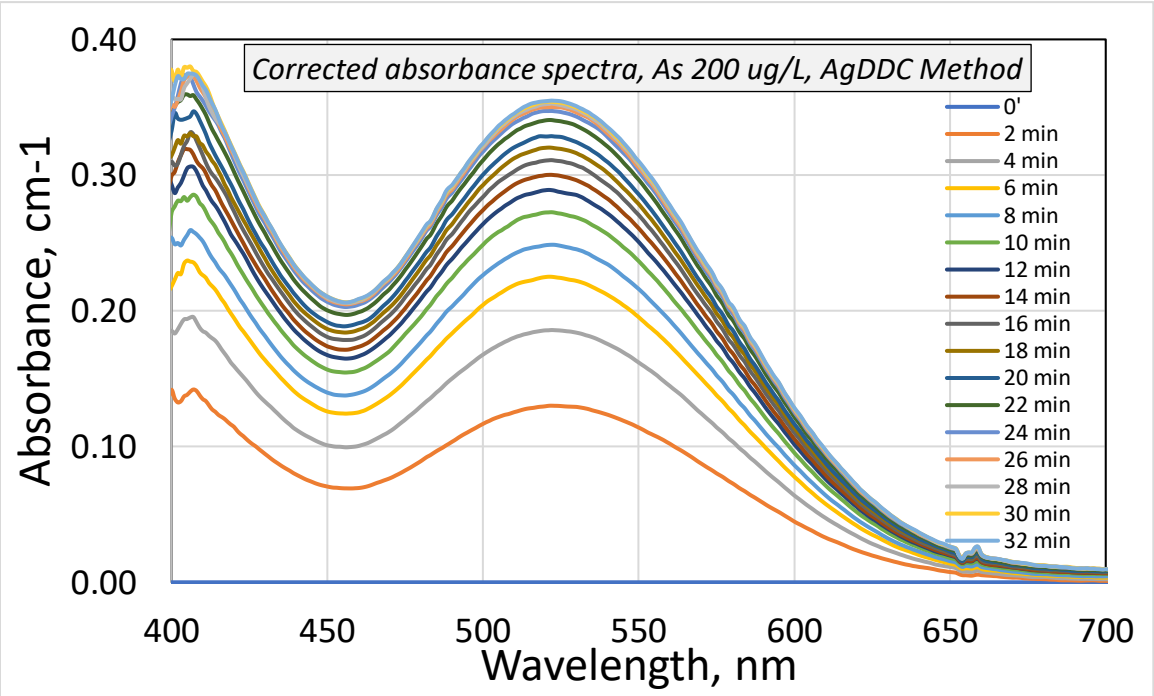

Figure 35. Development of the background-corrected absorbance spectra of AgDDC in the case of borohydride reduction of 200 µg/L (ICP standard was the source of arsenic).

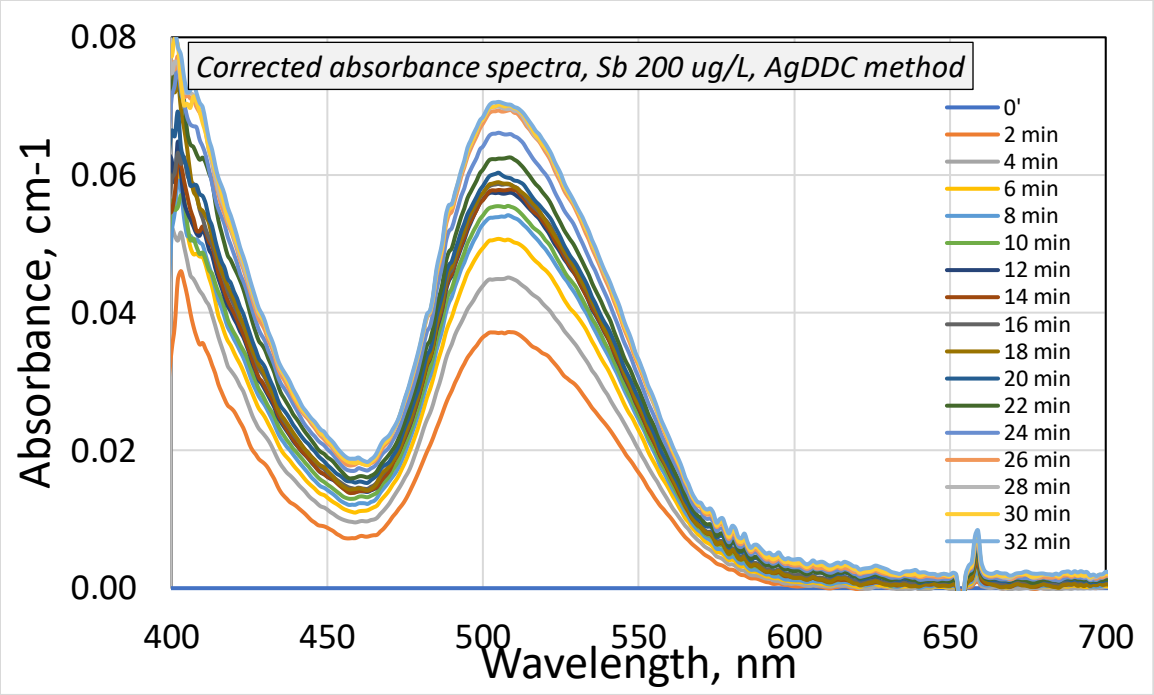

Figure 36. Development of the background-corrected absorbance spectra of AgDDC in the case of borohydride reduction of 200 µg/L Sb (ICP Sb standard was the source of antimony).

Following the measurements carried out for the As(III). As(V), DMA and Sb reference systems, formation of As volatiles was also examined in the case of the borohydride reduction of several BPW samples. SR8 to SR12 samples were used in this measurements (Figures 37-41). The measurements were carried BPW samples dilutions ranging from 100x to 10x.

The evolution of As volatiles following the borohydride reduction of SR12, the most recent sample, resulted in the development of a pronounced peak at ca. 420 nm (Figure 37). The shape of the spectra shown in Figure 37 was different compared with the data for the other BPW samples. Interestingly, the spectra generated for SR9 to SR11 samples very closely resemble that of DMA, with similar intensities for SR9 and SR11. The SR8 spectra also resembles that of DMA, although not as closely.

These observations suggest that a large portion of arsenic volatilized as a result of the borohydride reduction of the samples comprises methylated arsines, possibly predominantly dimethylated or trimethylated arsines $(CH_3)_2AsH$ and $(CH_3)_3As$. This point needs to be explored further using a more detailed range of As precursors, for instance MMA, TMAO and others. This work will be carried out in the future.

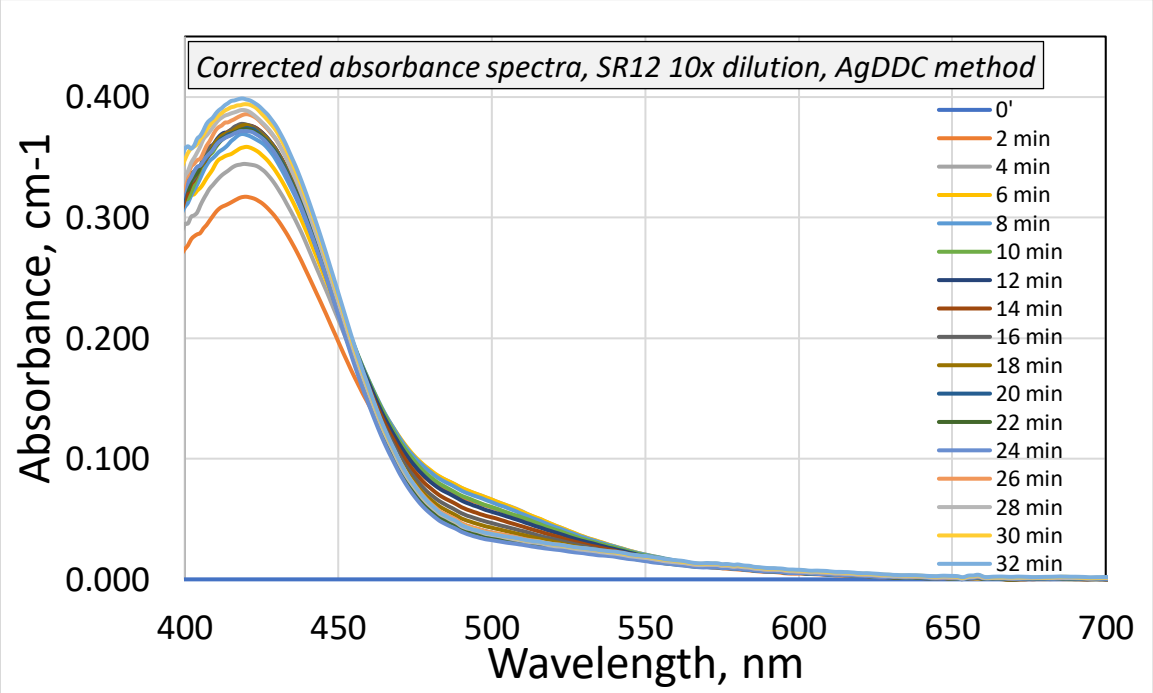

Figure 37. Development of the background-corrected absorbance spectra of AgDDC in the case of borohydride reduction of BEW product water, SR12 sample, 10x dilution (687 ug/L As).

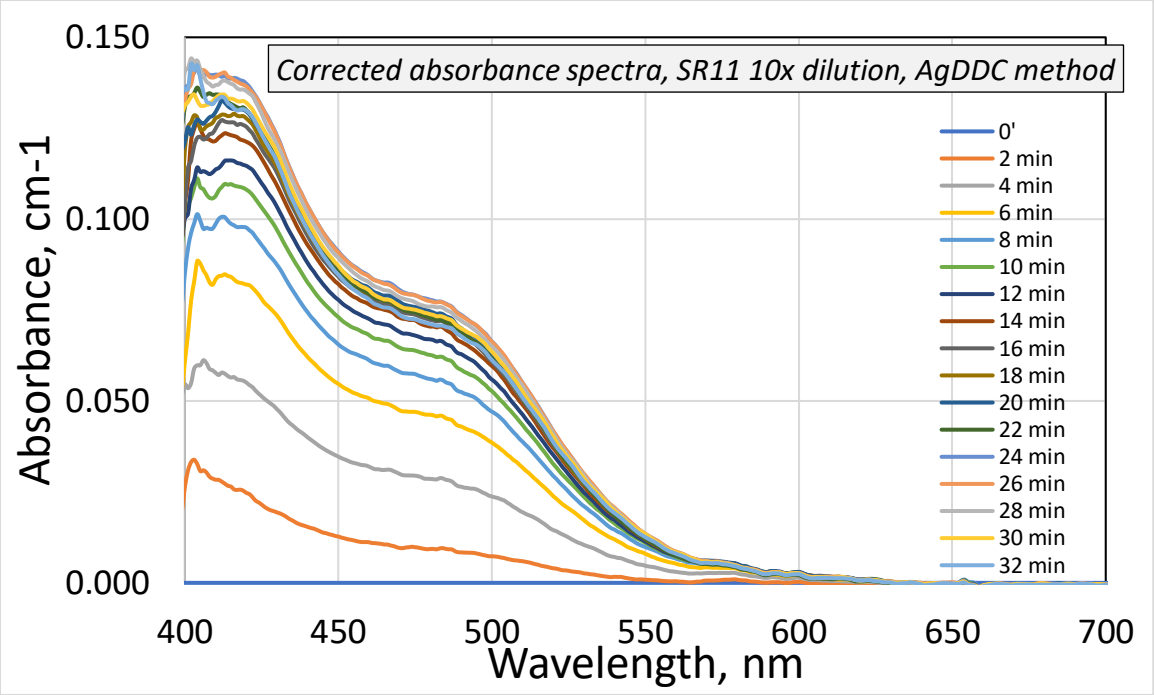

Figure 38. Development of the background-corrected absorbance spectra of AgDDC in the case of borohydride reduction of BEW product water, SR11 sample, 10x dilution (434 ug/L As).

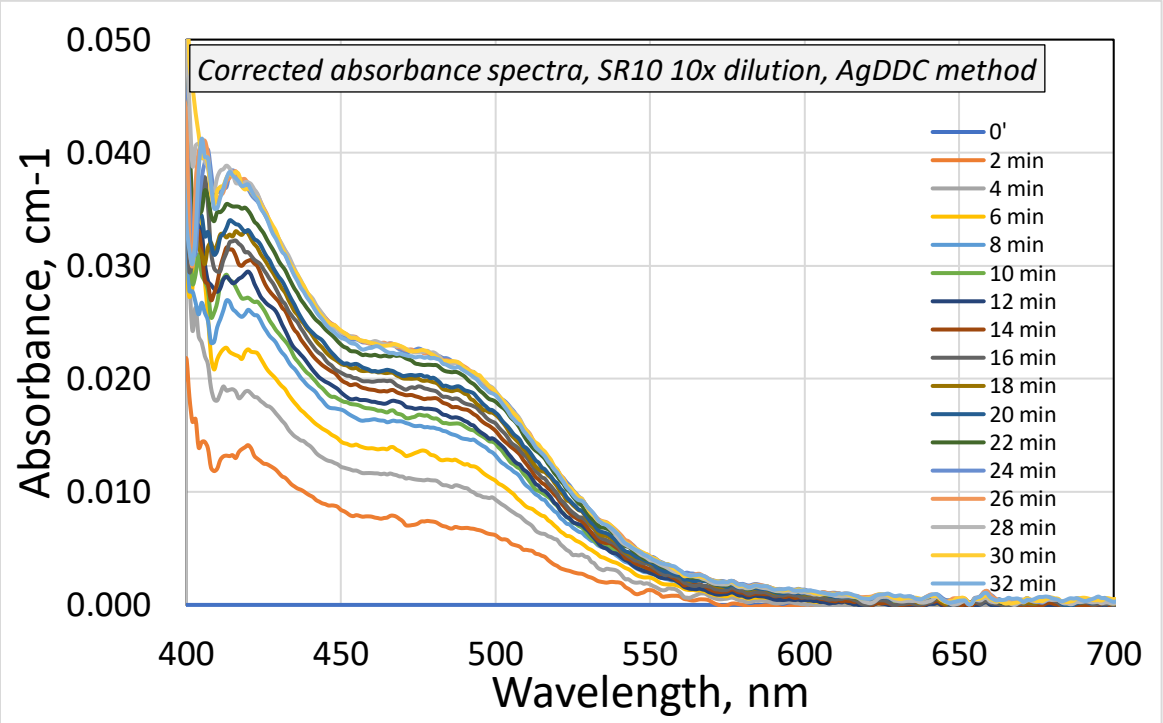

Figure 39. Development of the background-corrected absorbance spectra of AgDDC in the case of borohydride reduction of BEW product water, SR10 sample, 10x dilution (445 ug/L As).

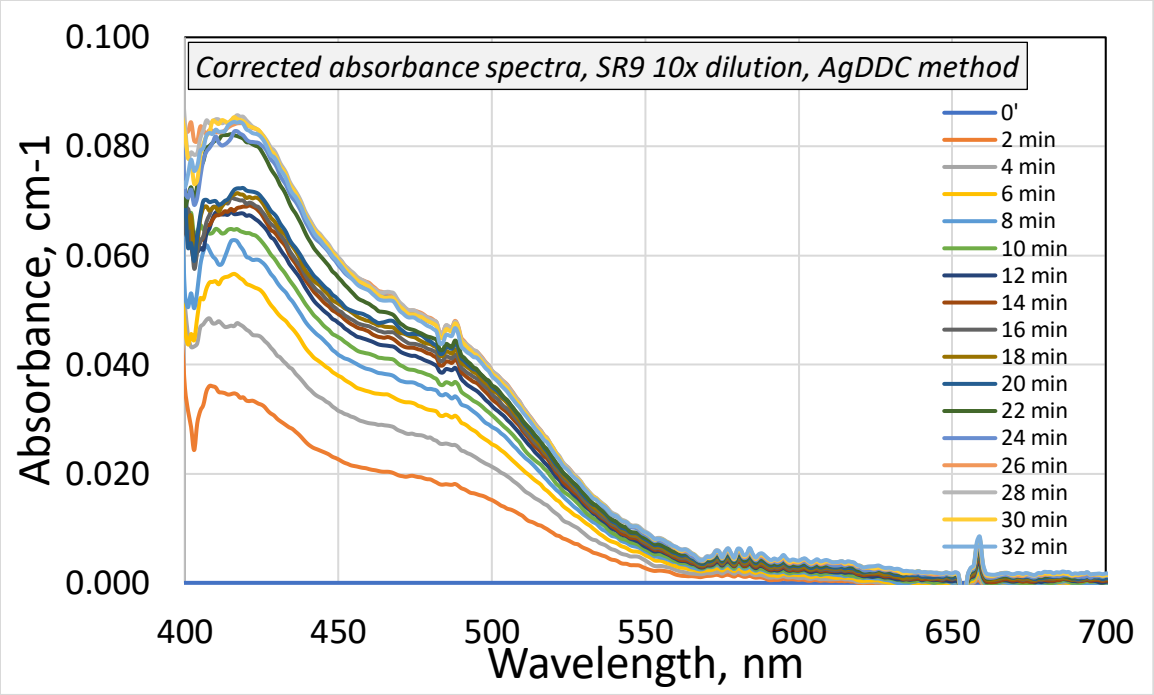

Figure 40. Development of the background-corrected absorbance spectra of AgDDC in the case of borohydride reduction of BEW product water, SR9 sample, 10x dilution (1120 ug/L As).

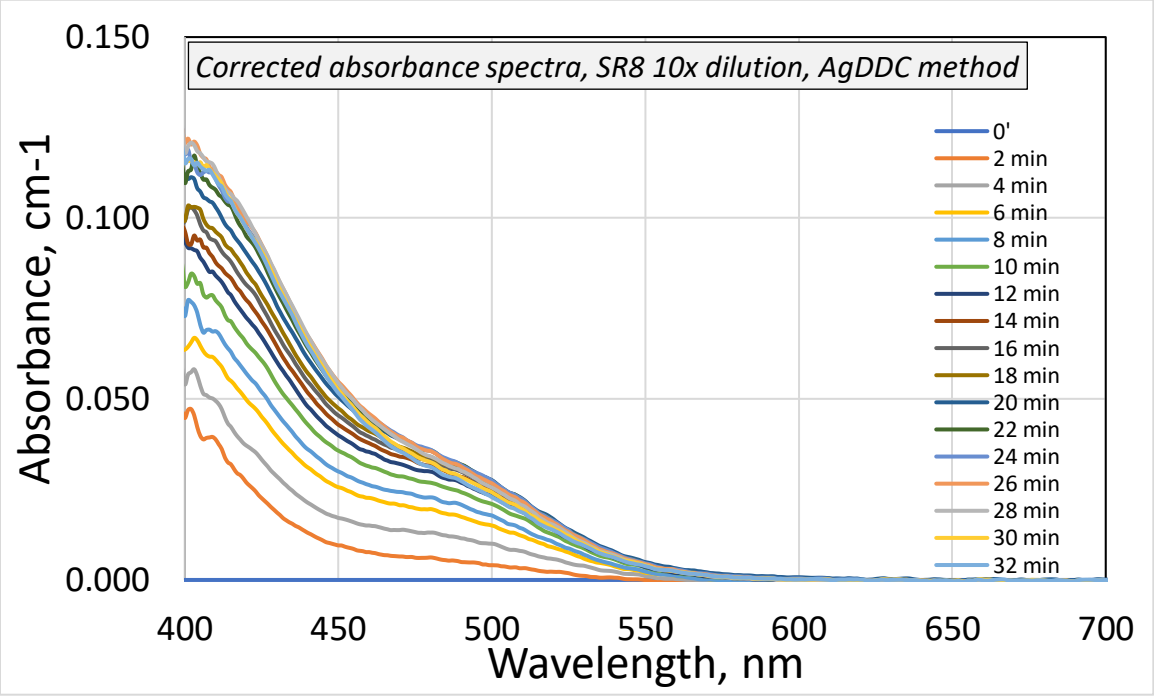

Figure 41. Development of the background-corrected absorbance spectra of AgDDC in the case of borohydride reduction of BEW product water, SR8 sample, 10x dilution (1210 ug/L As).

Kinetic Profiles

In order to compare the generation of arsines over time in the borohydride-reduced SR8 to SR12 samples of BPW and characterize the speciation and reactivity of arsenic compounds present in these samples, the development of the absorbance of AgDDC/arsine complexes was tracked during a 40 minute period. Arsine generation was carried out for 20 minutes and a scan of the AgDDC/pyridine solution was taken every 2 minutes. After the 20 minutes, the scrubber and Erlenmeyer were disconnected and an empty Erlenmeyer flask was substituted. The absorbance of the AgDDC/pyridine solution was monitored for an additional 20 minutes, with a scan again taken every 2 minutes.

Given the positions of the characteristic maxima in the absorbance spectra, the development of the absorbance of the borohydride-reduced solutions of the reference As compounds (arsenite, arsenate, DMA) was examined at the 525 and 430 nm wavelengths (Figures 42-50). For the experiments that used the arsenic ICP standard, a constant increase in absorbance at both 525 and 430 nm was seen during the 20 minute experiment and in the 10 minutes following the completion of the arsine generation phase of the experiment. The slight increase of the absorbance of the AgDDC/arsine solution may suggest that either the trapped arsines continue to react with the AgDDC/pyridine to cause a darker color development (Figures 42, 43) or there are other interactions (e.g., the ingress of oxygen) that affect the absorbance of the AgDDC/arsine complexes.

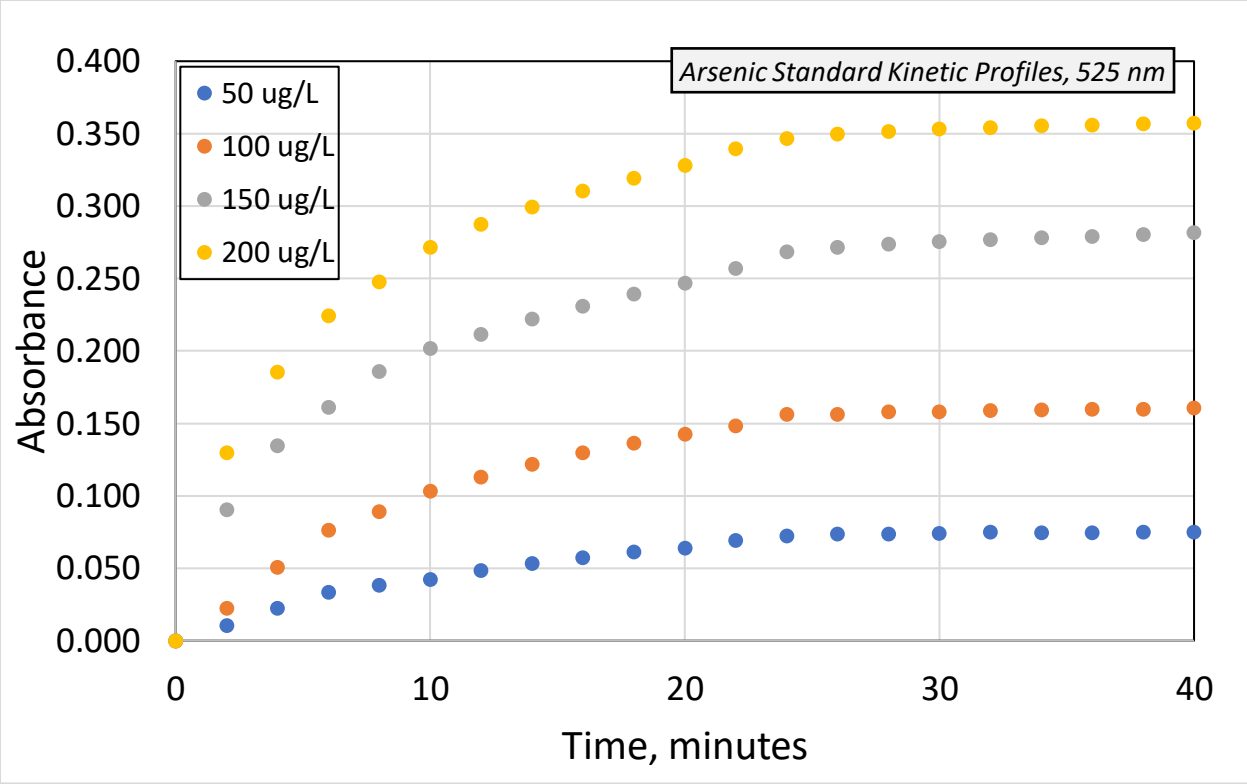

Figure 42. Effects of arsenic concentrations on the kinetic profiles of absorbance measured at 525 nm. Arsenic ICP standard arsine precursor.

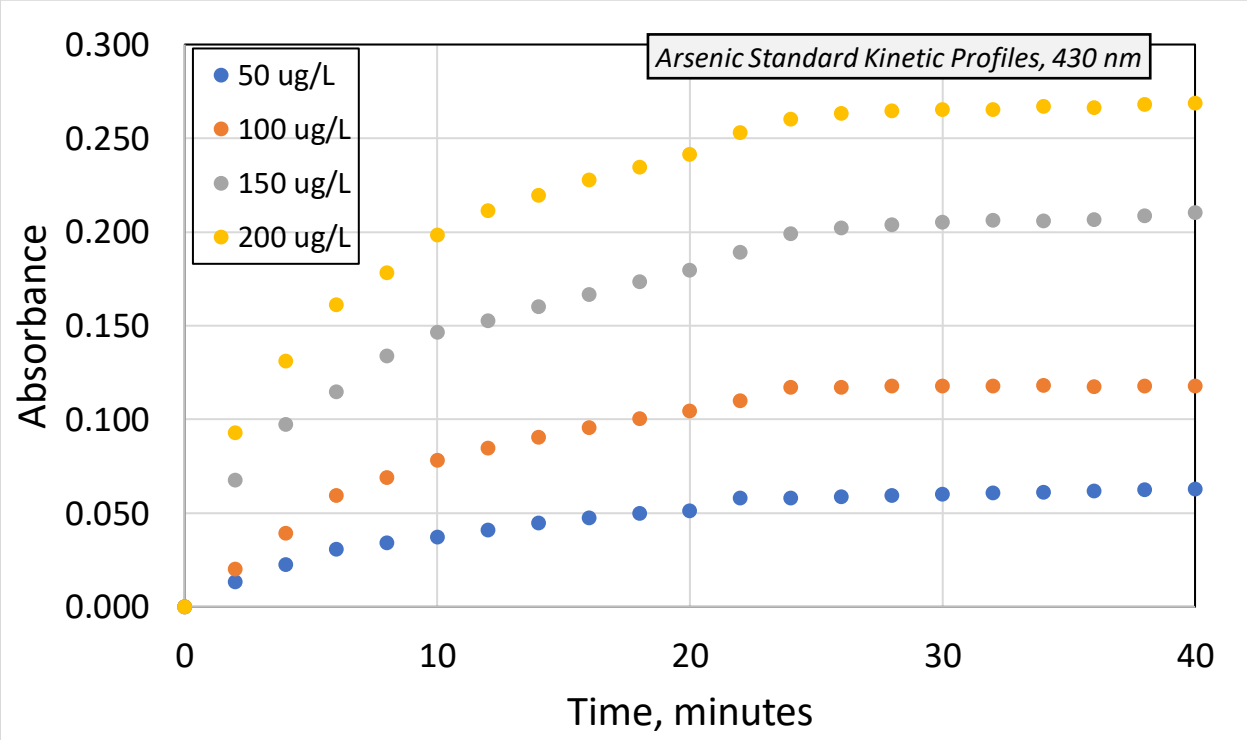

Figure 43. Effects of arsenic concentrations on the kinetic profiles of absorbance measured at 430 nm. Arsenic ICP standard arsine precursor.

In the case of the antimony standard used a stibine precursor there is a greater discrepancy between the reported absorbance development in the concentration range tested (Figures 44-46). Similarly to the observations made with the arsenic standard, a clear increase in absorbance is noted during the initial 10 minutes of stibine generation. Because the wavelength corresponding to the maximum absorbance was close to 507 nm, a kinetic profile at this wavelength was also included; it is visually very close to that at 525 nm (Figure 46).

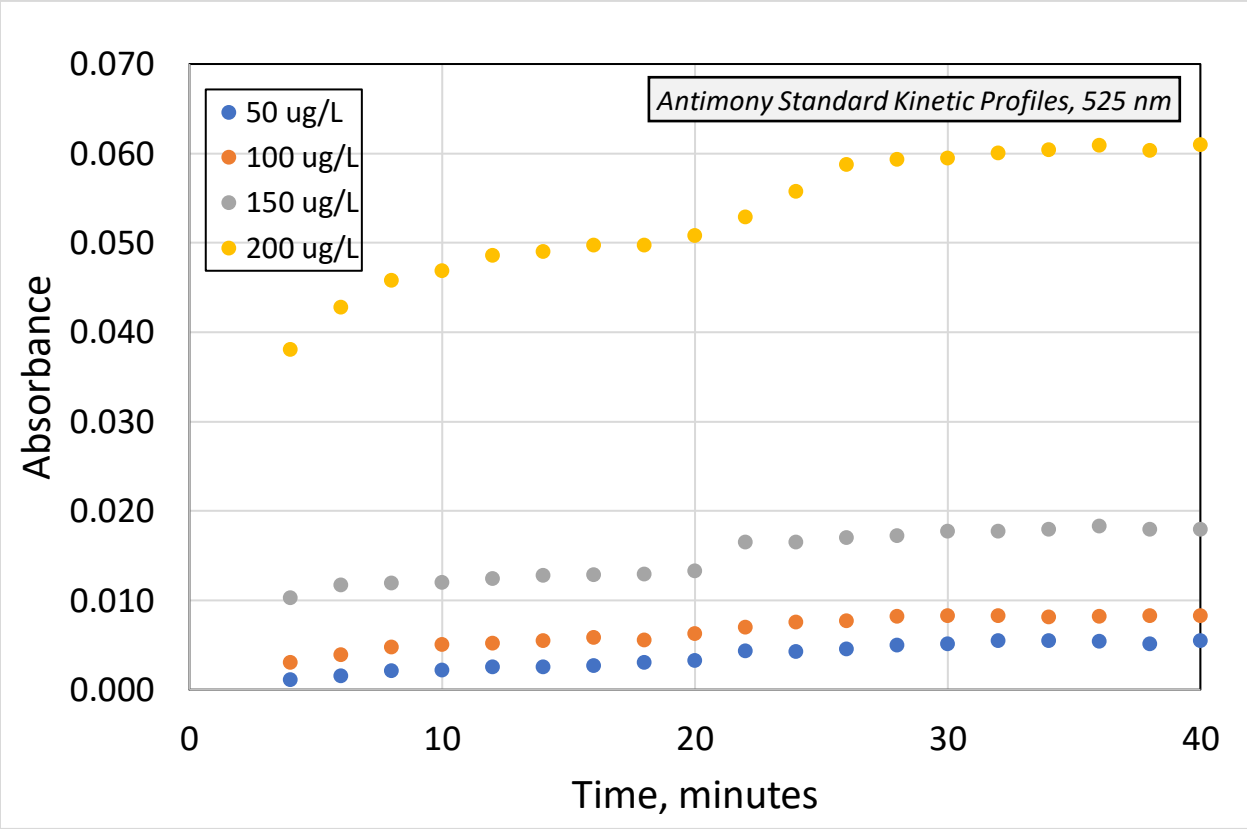

Figure 44. Effects of antimony concentrations on the kinetic profiles of absorbance measured at 525 nm. Antimony ICP standard stibine precursor.

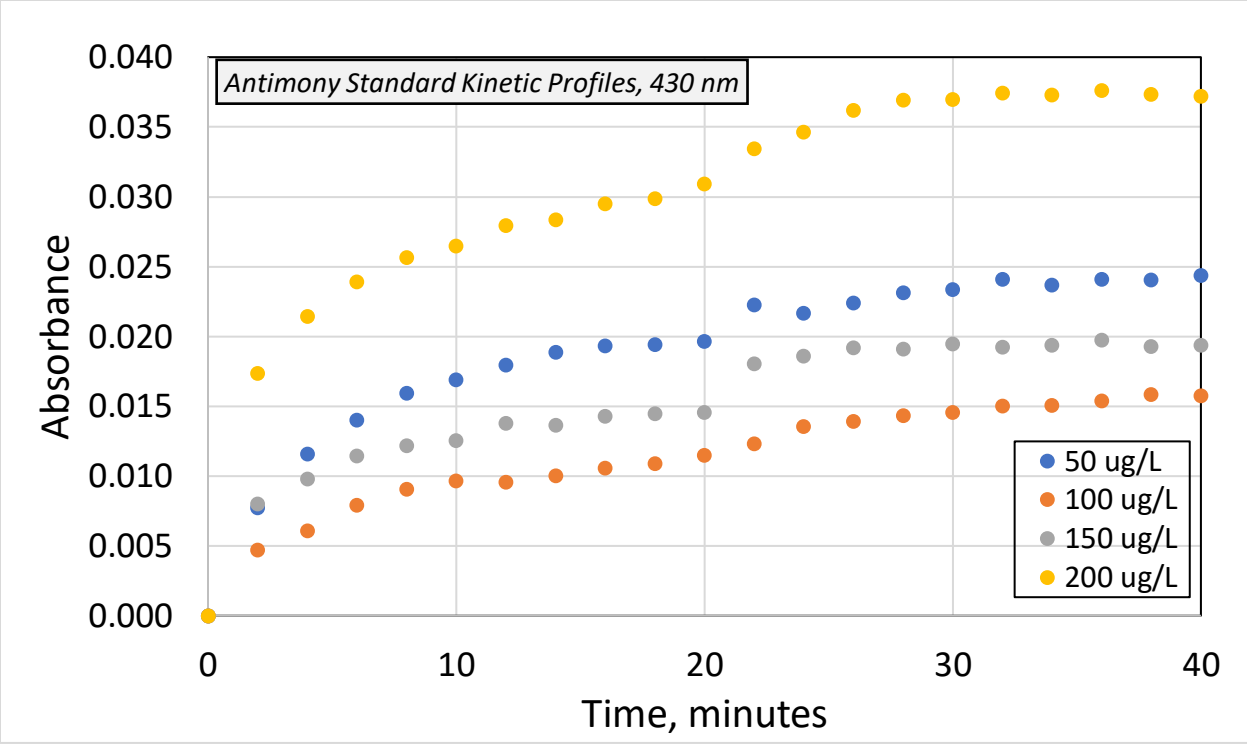

Figure 45. Effects of antimony concentrations on the kinetic profiles of absorbance measured at 430 nm. Antimony ICP standard stibine precursor.

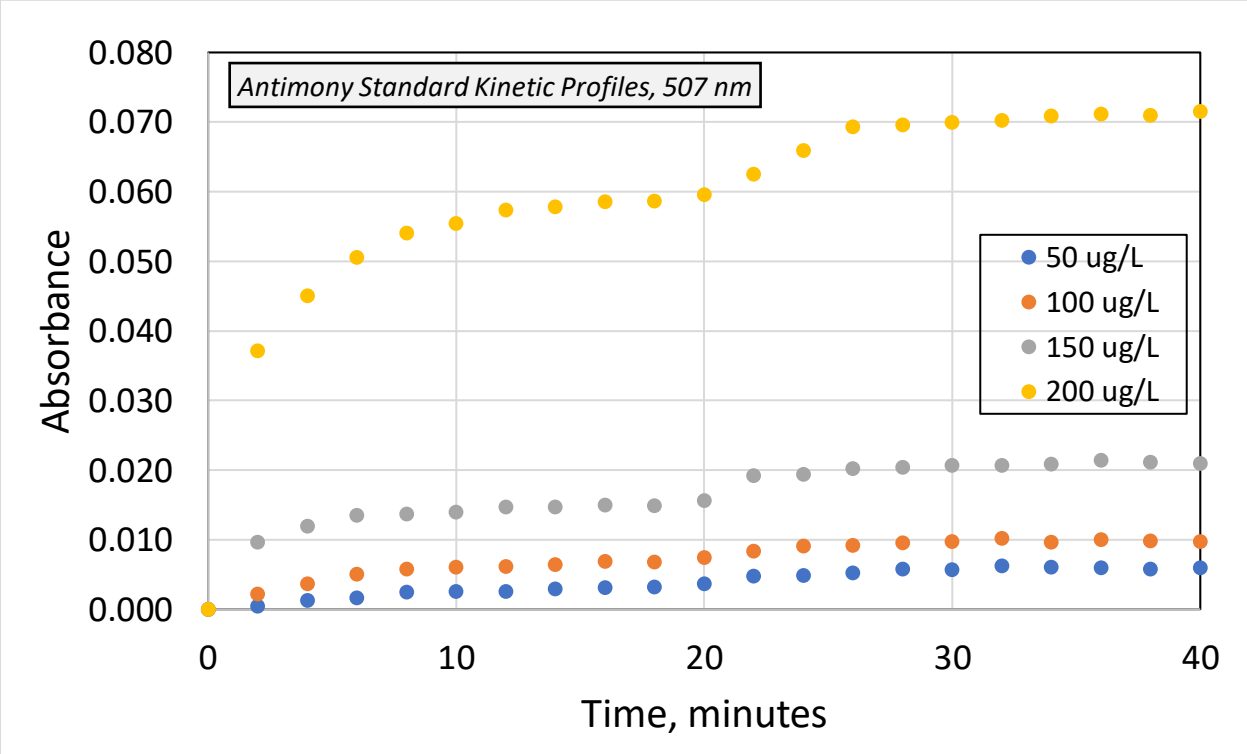

Figure 46. Effects of antimony concentrations on the kinetic profiles of absorbance measured at 507 nm. Antimony ICP standard stibine precursor.

The profiles for arsenite during the generation experiment again reflect that of the arsenic ICP standard, though they demonstrate a lower intensity (Figures 47, 48). However, the absorbance for arsenite in the 20 minutes following plateaus much more quickly, with almost negligible increase in the first 10 minutes at both wavelengths considered.

The kinetic profiles for DMA noticeably differ from those for arsenite as the absorbance clearly decreases following the cessation of the ingress of the borohydride-generated dimethylarsine originating from the DMA precursor, rather than reaching a plateau (Figures 49-50, 83-84 in Appendix). For both 525 and 430 nm observation wavelength, a maximum absorbance is observed between 22 and 26 minutes, 2-6 minutes after ending the generation experiment, after which the absorbance clearly decreases. This color fading was observed in the lab and is unique to DMA of all the solutions tested, making it a potentially useful indicator for the presence of methylated arsine.

Arsenate, however, exhibits a curve more reminiscent of the antimony trends (Figures 51, 52). At the end of the 20-minute arsine generation, a clear increase in absorbance during the following ten minutes is observed, with a much less continuous jump than in the case of arsenite. Again, a maximum absorbance is reached in the final ten minutes of the 20 minute monitoring period.

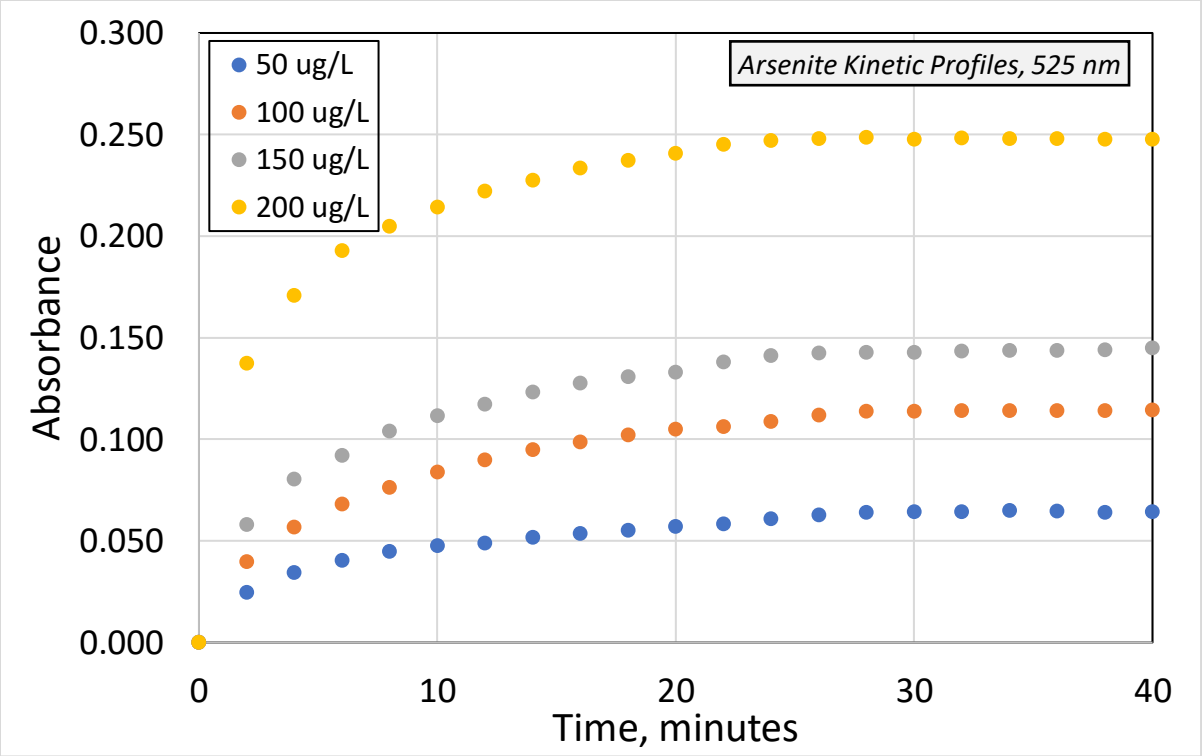

Figure 47. Effects of arsenic concentrations on the kinetic profiles of absorbance measured at 525 nm. Arsenite salt arsine precursor.

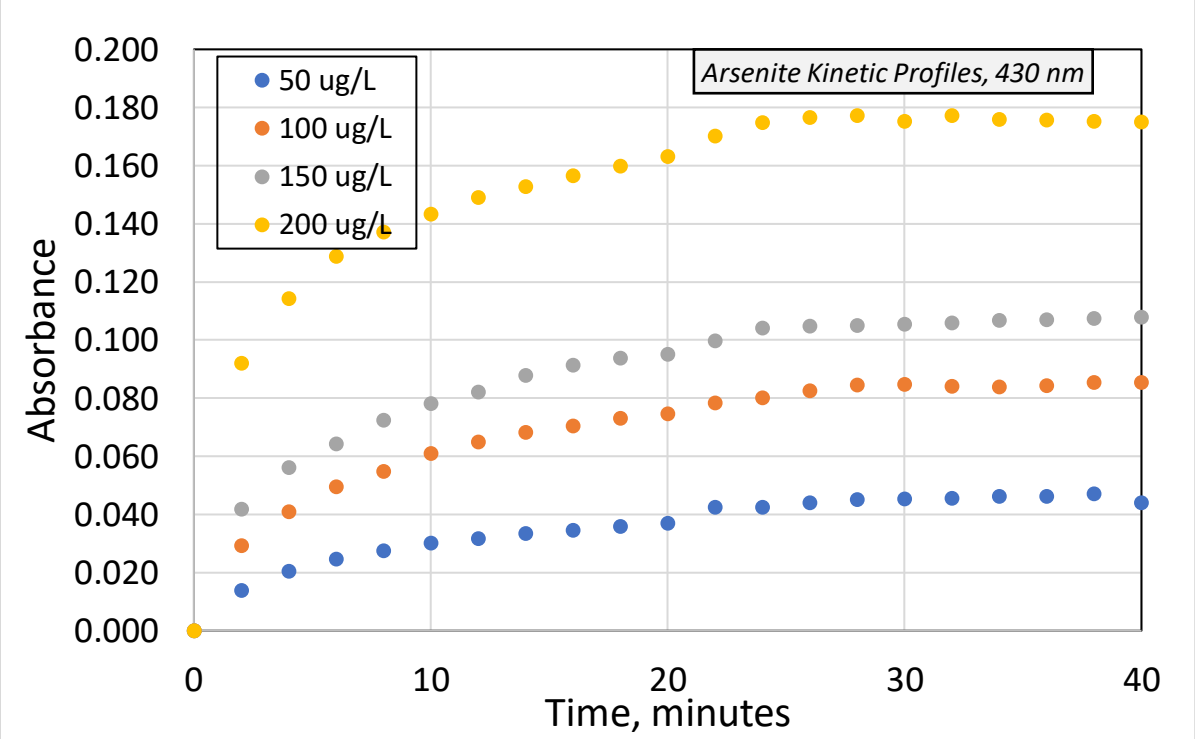

Figure 48. Effects of arsenic concentrations on the kinetic profiles of absorbance measured at 430 nm. Arsenite salt arsine precursor.

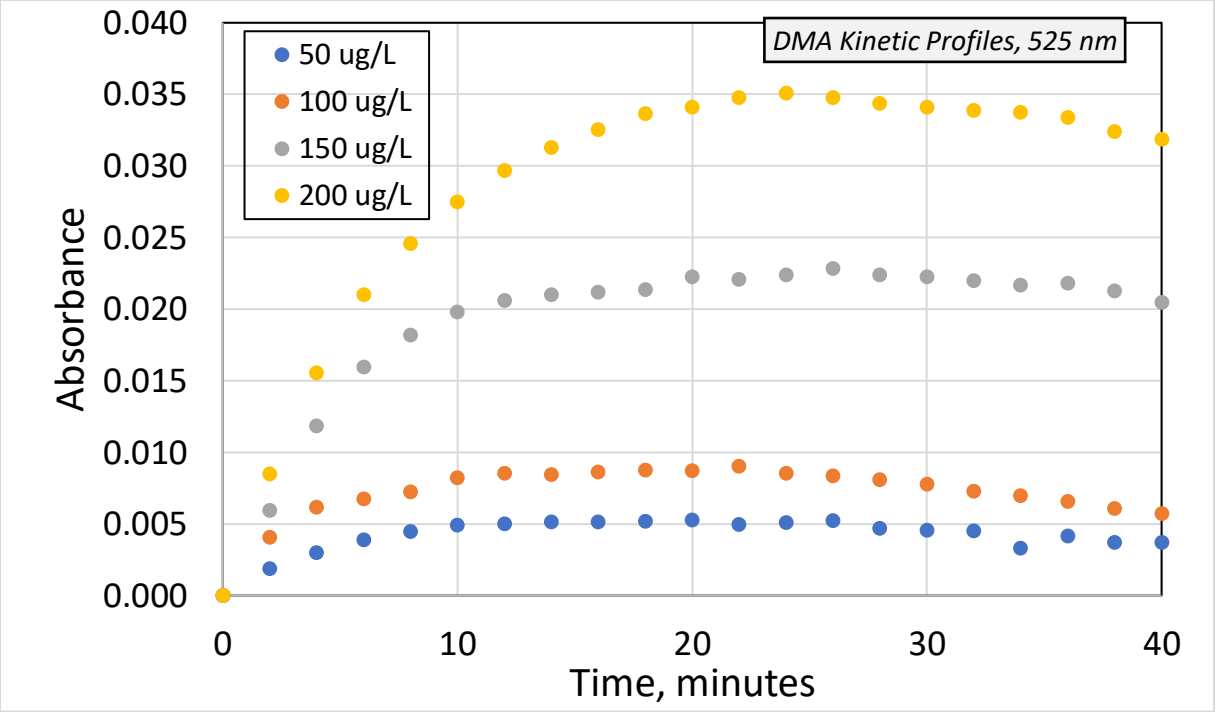

Figure 49. Effects of arsenic concentrations on the kinetic profiles of absorbance measured at 525 nm. DMA arsine precursor.

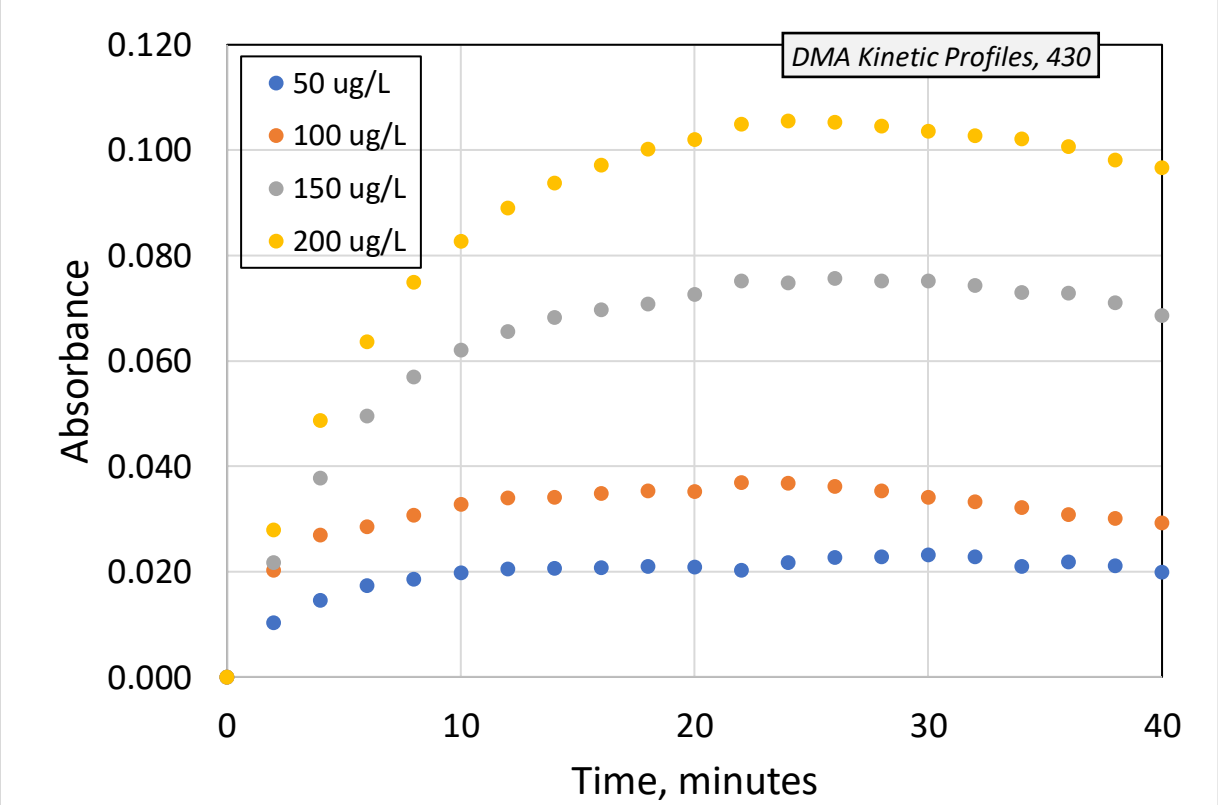

Figure 50. Effects of arsenic concentrations on the kinetic profiles of absorbance measured at 430 nm. DMA arsine precursor.

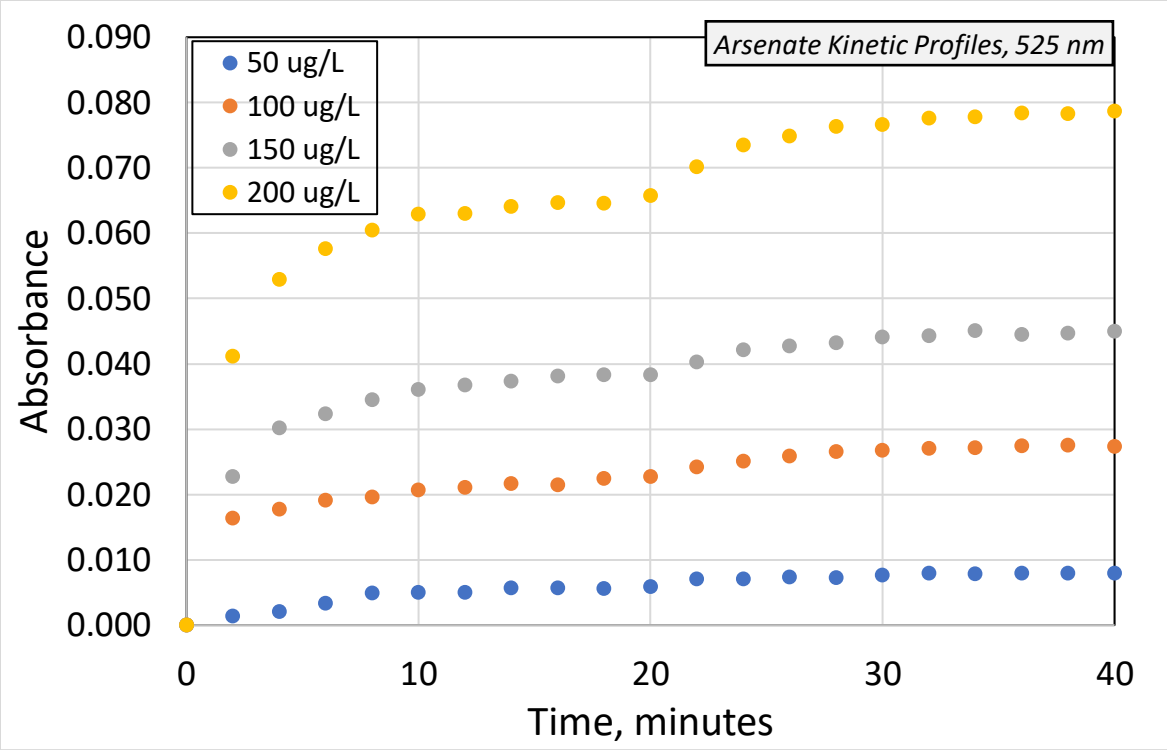

Figure 51. Effects of arsenic concentrations on the kinetic profiles of absorbance measured at 430 nm. Arsenate salt arsine precursor.

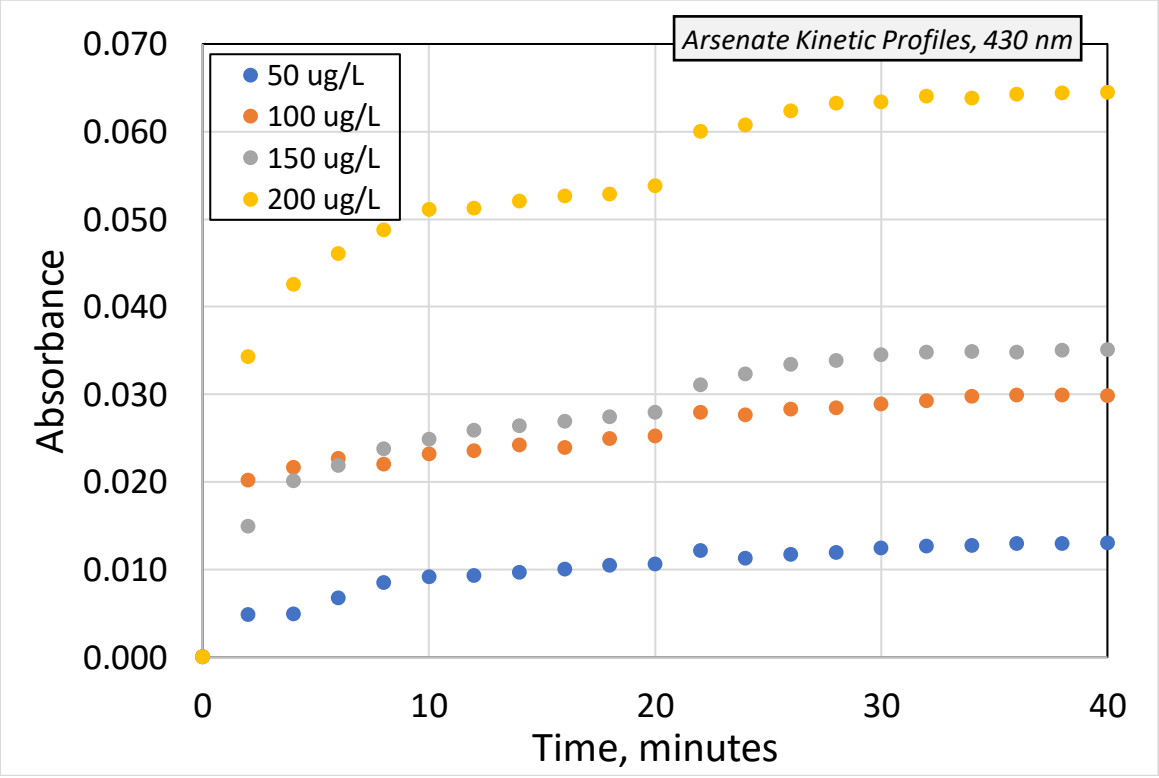

Figure 52. Effects of arsenic concentrations on the kinetic profiles of absorbance measured at 430 nm. Arsenate salt arsine precursor.

The kinetic profiles for the reference arsenic compounds can now be compared to those for the BPW samples (Figures 53-62). In the case of SR8, the absorbance trend at 525 clearly decreases in the last 10 minutes of the experiment for all concentrations, resembling the data for DMA (Figure 53). However, the trend at 430 nm rather demonstrates a plateau while seemingly not following a concentration-dependent pattern (Figure 54). This could be a result of sample age, as SR8 was collected in 2020 and the arsenic may have converted to another form or been impacted by chemical and physical conditions of storage.

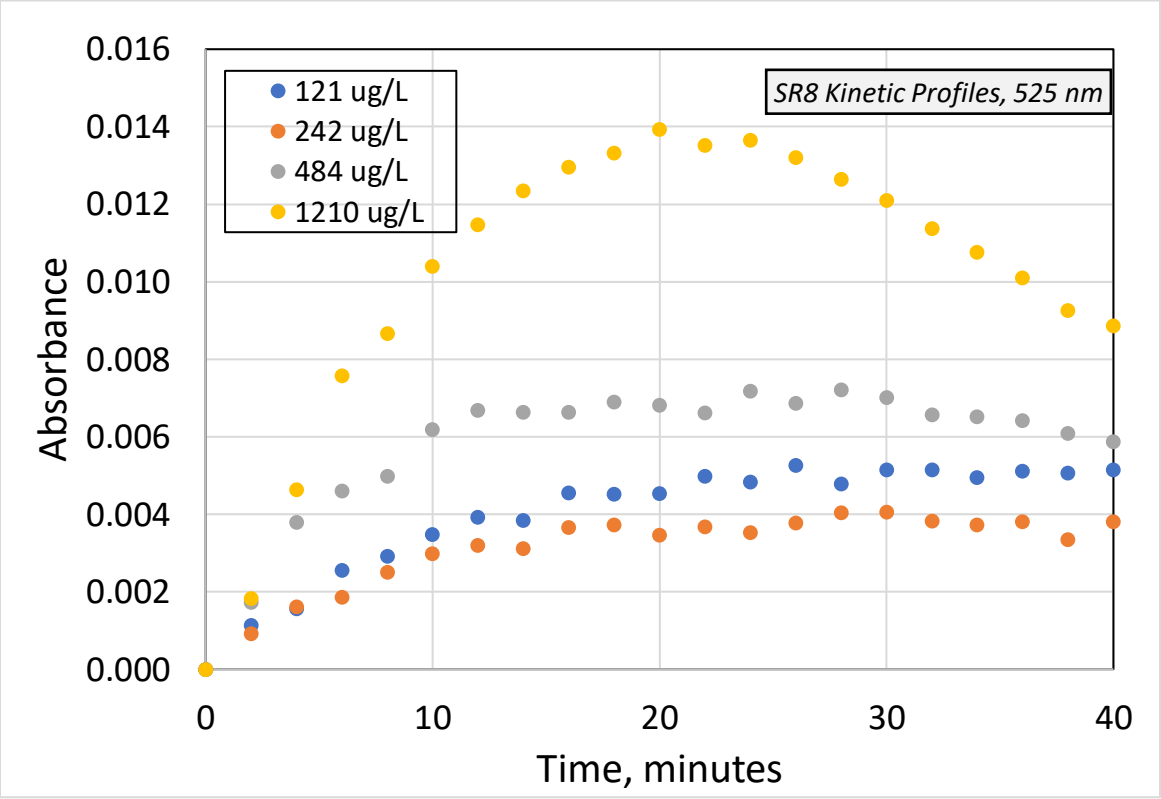

Figure 53. Effects of SR sample dilution on the kinetic profiles of absorbance measured at 525 nm. BPW SR8 arsine precursor.

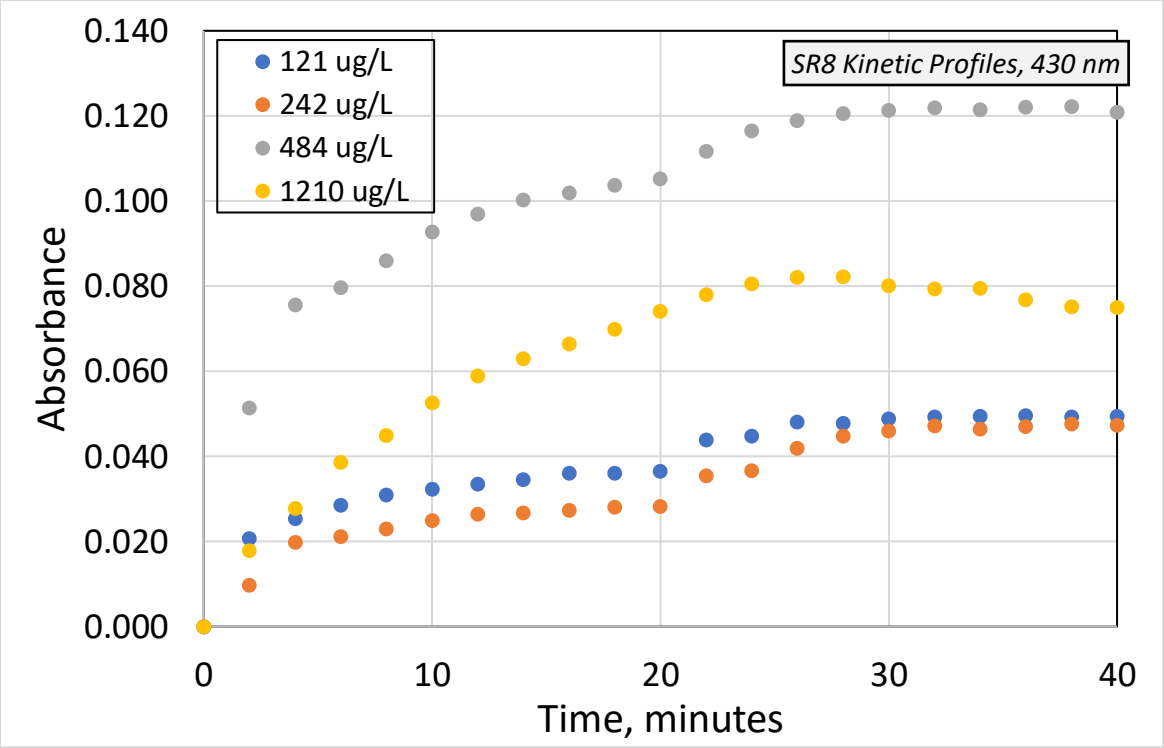

Figure 54. Effects of SR sample dilution on the kinetic profiles of absorbance measured at 430 nm. BPW SR8 arsine precursor.

SR9 similarly shows a peak in the 10 minutes following the arsine generation phase and a decrease in the last 10 minutes of the monitoring period for both the 525 and 430 nm wavelengths, indicating the presence of a methylated arsenic form (Figures 55, 56). Although not as old as SR8, it is important to note that age may also affect the SR9 sample. The trend for SR10 is not as clear (Figures 57, 58). The concentration profiles overlap during the 20 minutes of arsine generation, but exhibit both decreasing and increasing in the 20 minutes following the experiment. Although the less diluted samples more closely follow the trend shown for DMA, it is difficult to distinguish whether this is because of structural similarities as the intensity of SR10 data is much less than DMA and not consistent at all concentrations.

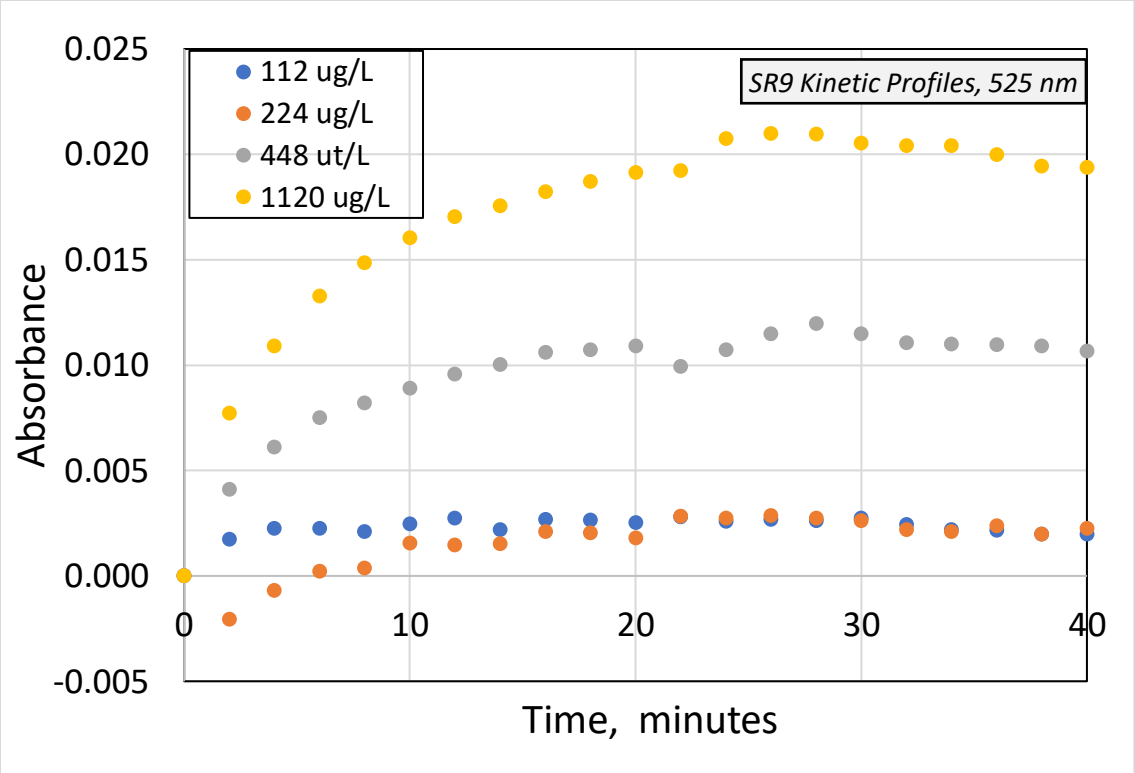

Figure 55. Effects of SR sample dilution on the kinetic profiles of absorbance measured at 525 nm. BPW SR9 arsine precursor.

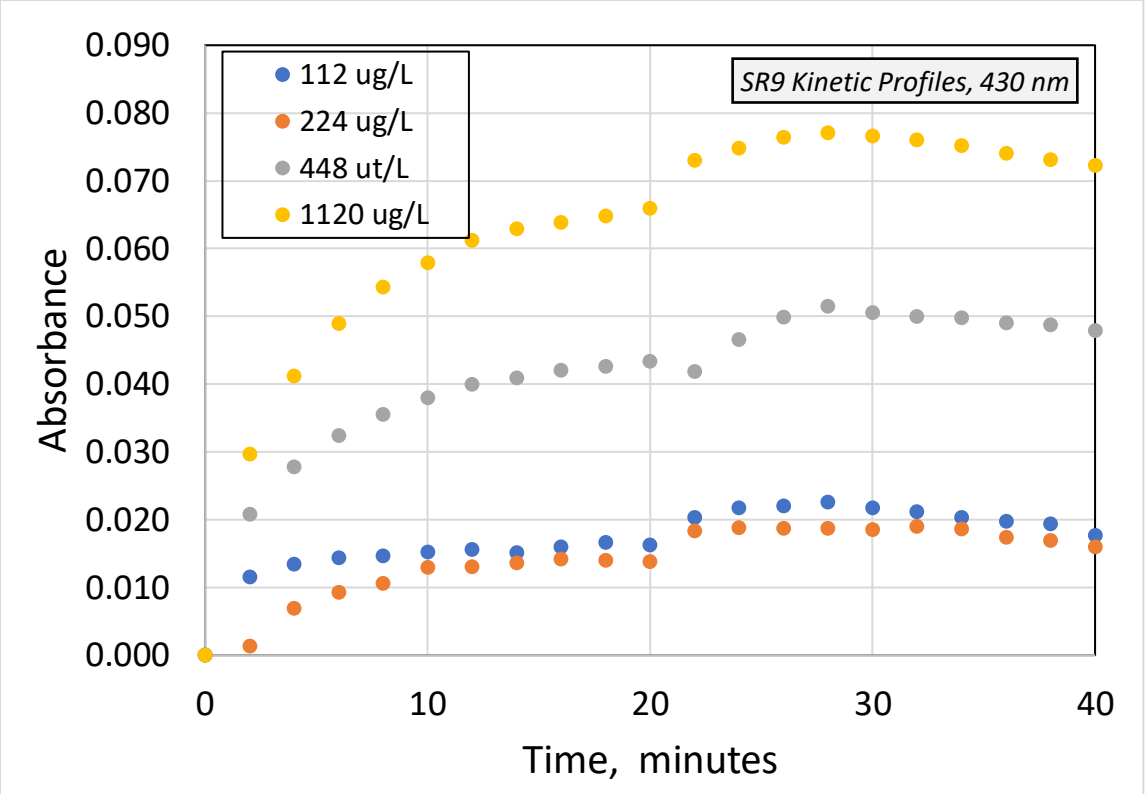

Figure 56. Effects of SR sample dilution on the kinetic profiles of absorbance measured at 430 nm. BPW SR9 arsine precursor.

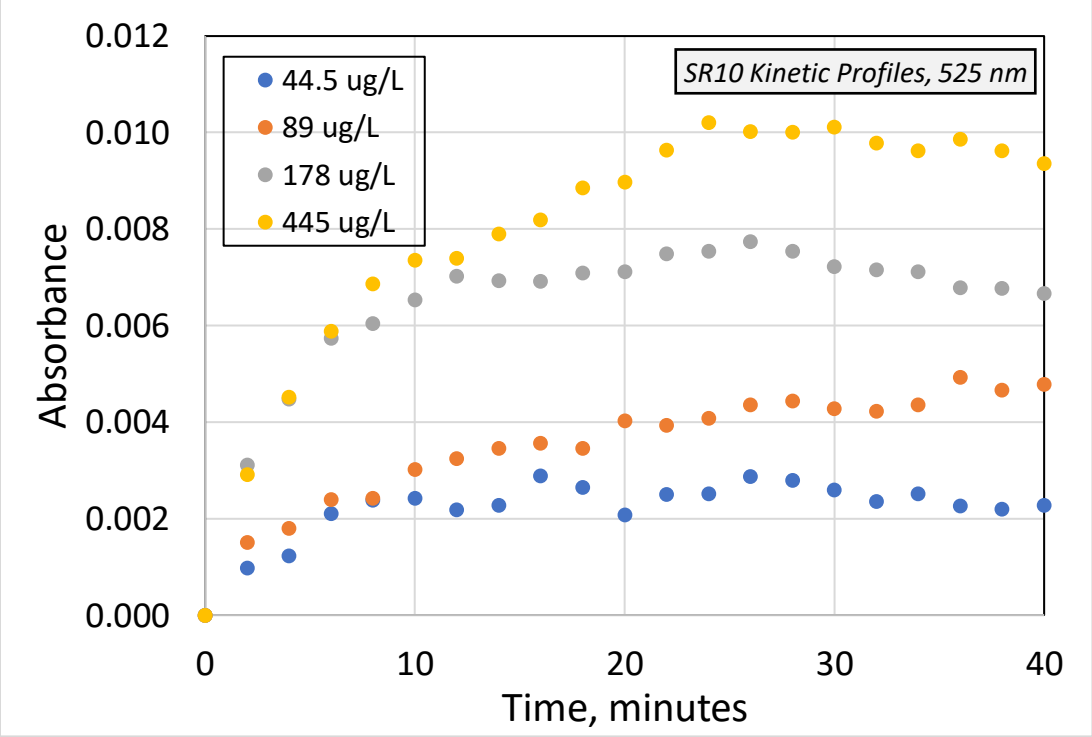

Figure 57. Effects of SR sample dilution on the kinetic profiles of absorbance measured at 525 nm. BPW SR10 arsine precursor.

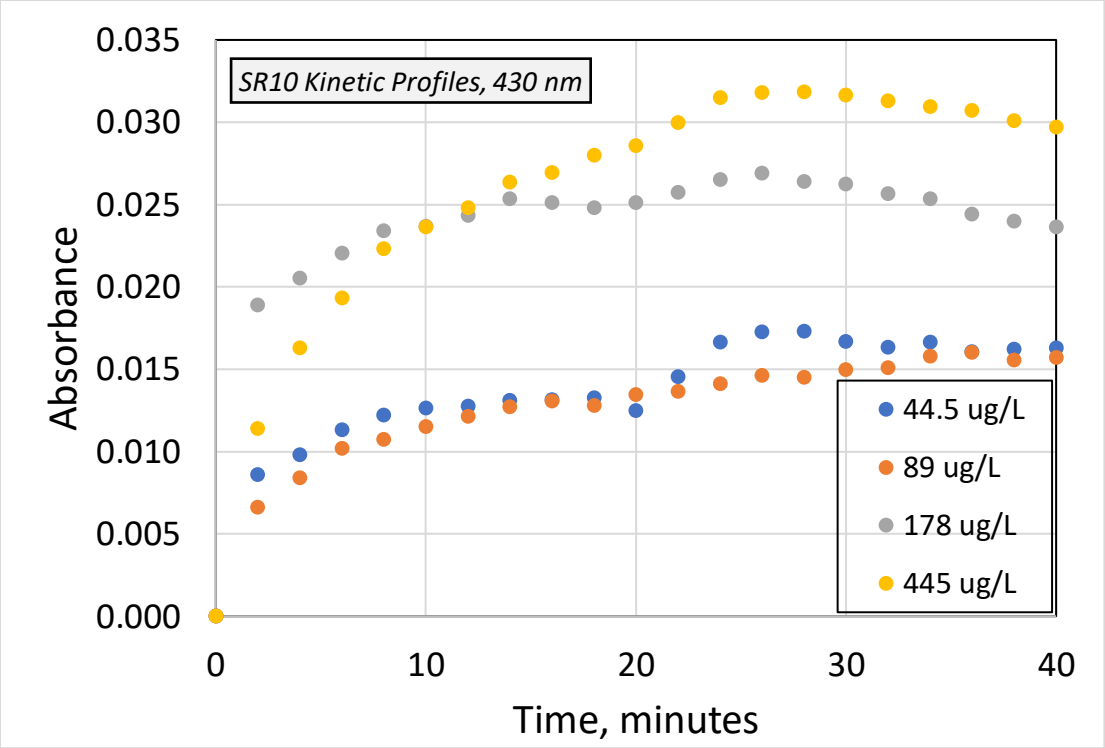

Figure 58. Effects of SR sample dilution on the kinetic profiles of absorbance measured at 430 nm. BPW SR9 arsine precursor.

SR11 and SR12 are relatively newer samples collected in the summer and fall of 2021, respectively. SR11 10x dilution follows a pattern most similar to the DMA at both the 525 and 430 nm wavelengths, but the 25x, 50x, and 100x dilutions more closely resemble the arsenite plateau that is reached in the last 10 minutes of the monitoring period (Figures 59, 60). This difference could indicate disparity in response due to varying concentration or suggest the presence of more than one form of arsenic. While the SR12 10x trend at 525 nm reaches a maximum in the first 10 minutes and then decreases before leveling off, the remaining three dilutions reflect the arsenite kinetic profile (Figure 61). The SR12 10x trend at 430 similarly demonstrates unique behavior, with an increasing absorbance throughout the 40 minutes, while the lower concentrations reach a clear plateau in the last 15 minutes of the experiment (Figure 62).

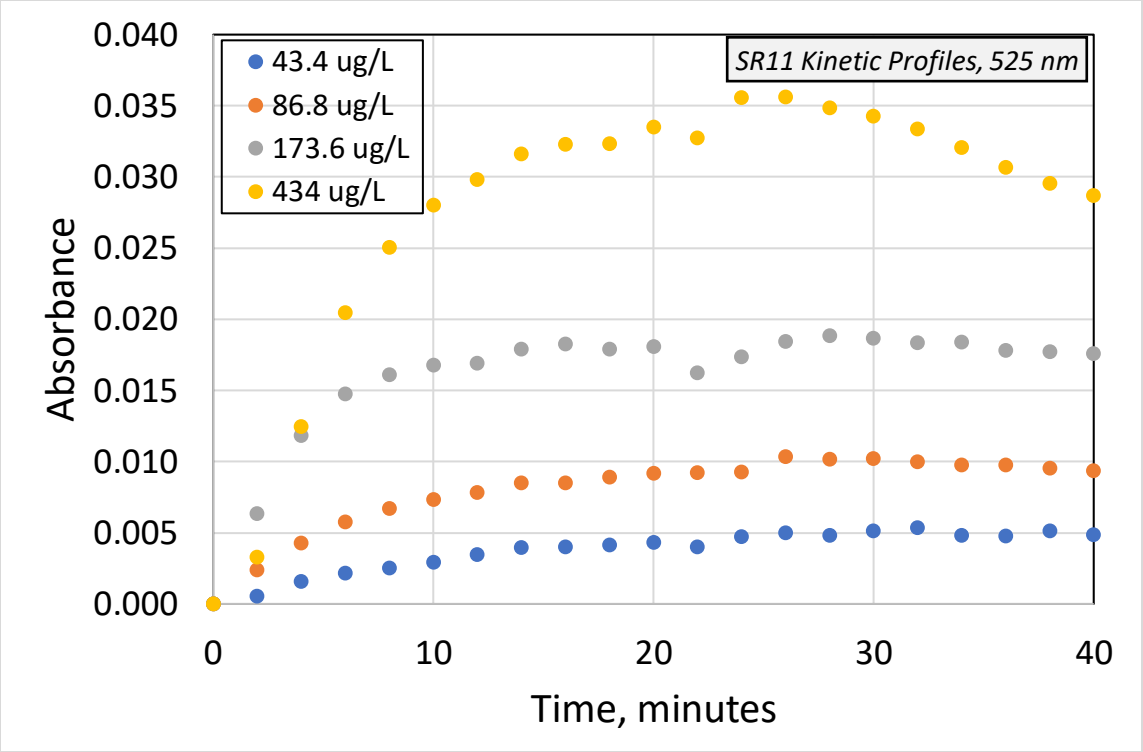

Figure 59. Effects of SR sample dilution on the kinetic profiles of absorbance measured at 525 nm. BPW SR11 arsine precursor.

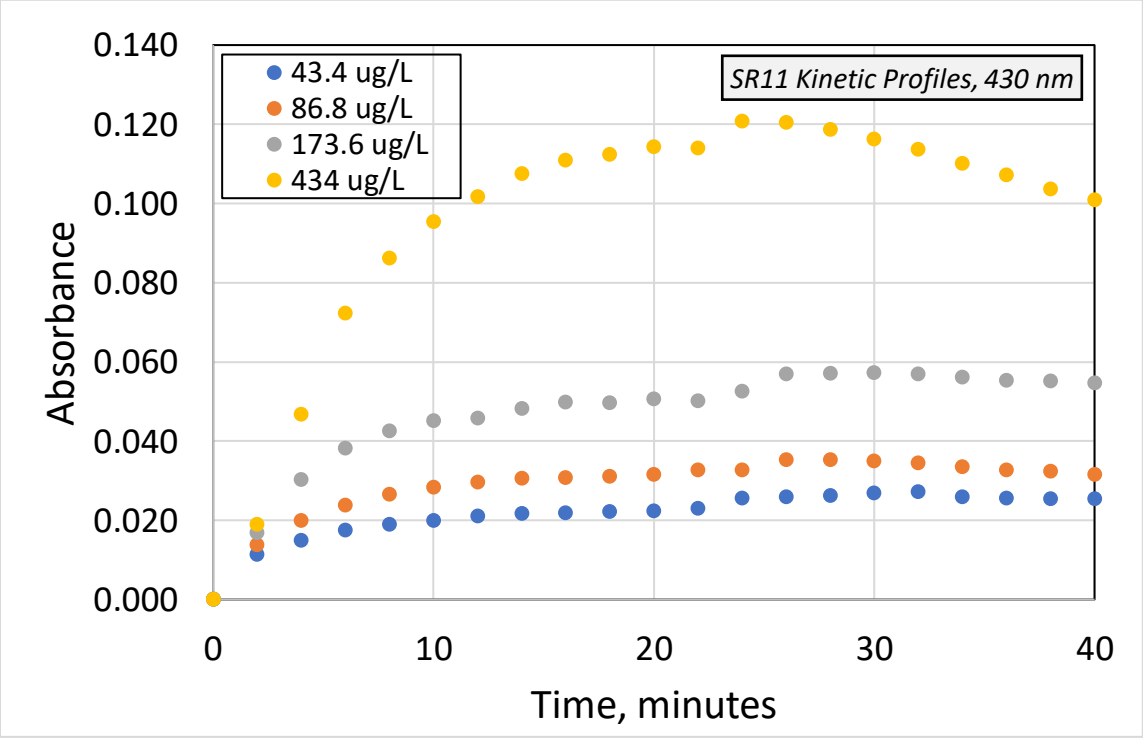

Figure 60. Effects of SR sample dilution on the kinetic profiles of absorbance measured at 430 nm. BPW SR11 arsine precursor.

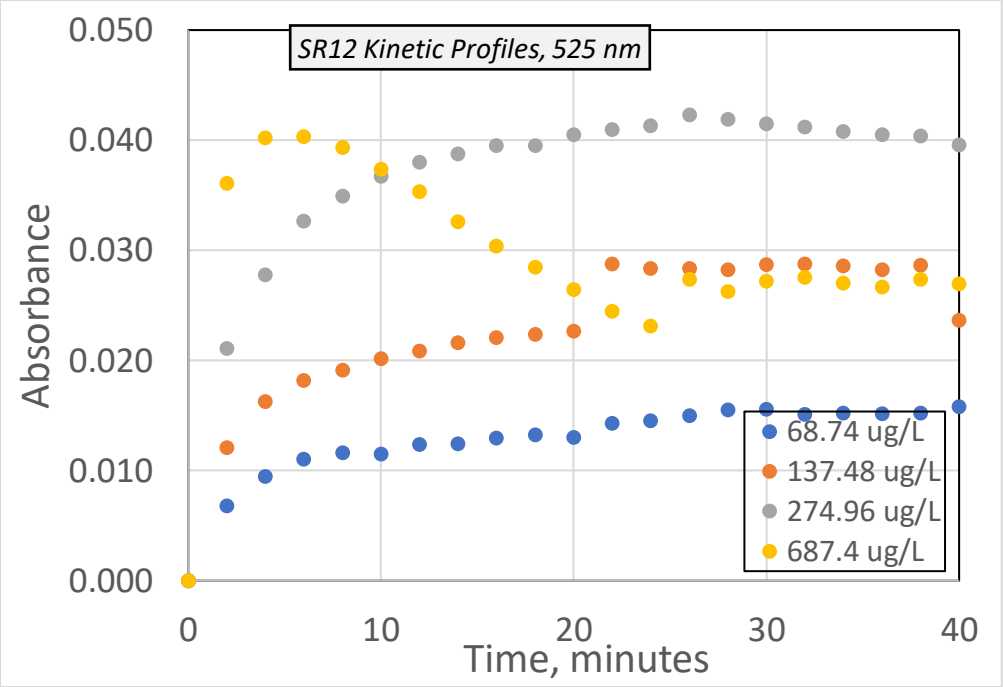

Figure 61. Effects of SR sample dilution on the kinetic profiles of absorbance measured at 525 nm. BPW SR12 arsine precursor.

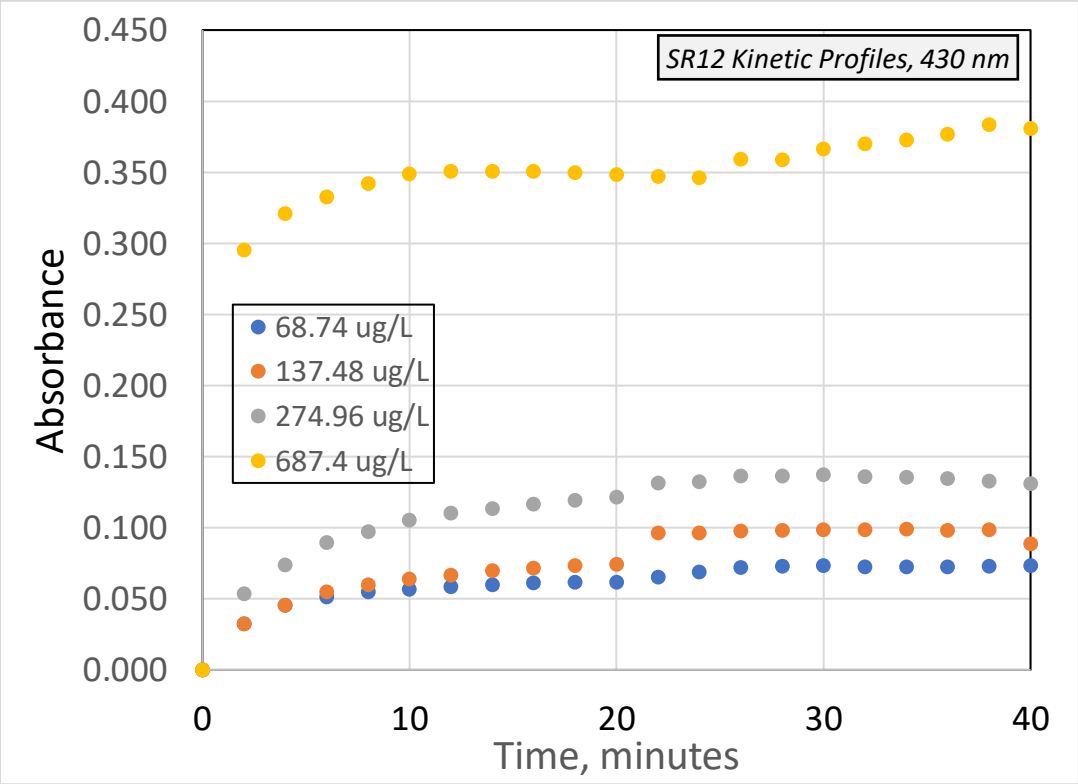

Figure 62. Effects of SR sample dilution on the kinetic profiles of absorbance measured at 430 nm. BPW SR12 arsine precursor.

Impact of Nitrogen Carrier Gas on the Development of AgDDC absorbance Spectra

As suggested in the standard method used in the experiments, the impact of nitrogen gas flow in the arsine generator was explored. While the evolution of hydrogen that takes place during the borohydride reduction process used in the standard AgDDC method helps carry the generated arsine into the scrubber containing the pyridine solutions of AgDDC, the presence of nitrogen gas flow may aid with mixing the solution and flushing arsine into the scrubber. The additional need to use the nitrogen carrier is to expand the use of the AgDDC method to direct measurements of the generation As volatiles in ME reactors that currently use CO_2 carrier gas while N_2 gas was used in the preceding experiments.

For the purpose of examining effects of the N_2 carrier gas on the results of AgDDC measurements, the Erlenmeyer flask used in the experiments described in the preceding section was substituted with a round bottom flask, and nitrogen was bubbled into the flask at 60 mL/min. As a result of this gas flow, a clear change in the kinetic absorbance profiles was observed.

In the case of DMA, the presence of nitrogen resulted in a greater recorded absorbance throughout the 40 minute period at 430 nm (Figure 63). This trend was not seen at 525 nm. While the nitrogen flux through the round bottom flask does increase the absorbance during the 20 minutes of arsine generation, the following decrease in absorbance occurred at a greater rate (Figure 64). Additionally, the maximum absorbance was reached twice as quickly, occurring at the 10 minute mark rather than in the monitoring period following the arsine generation.

Arsine generation in the case of the arsenic ICP standard was not positively affected by the presence of nitrogen at 430 nm (Figure 65). The absorbance in the case of nitrogen was similar but less than the data recorded without nitrogen during the 20-minute arsine generation. The 20 minute monitoring period following arsine generation revealed a greater difference between the

two experimental conditions, as the nitrogen-free trial plateaued at a higher absorbance. At 525 nm, the maximum absorbance for arsine generation from this source, the nitrogen flux again resulted in greater overall absorbance (Figure 66).

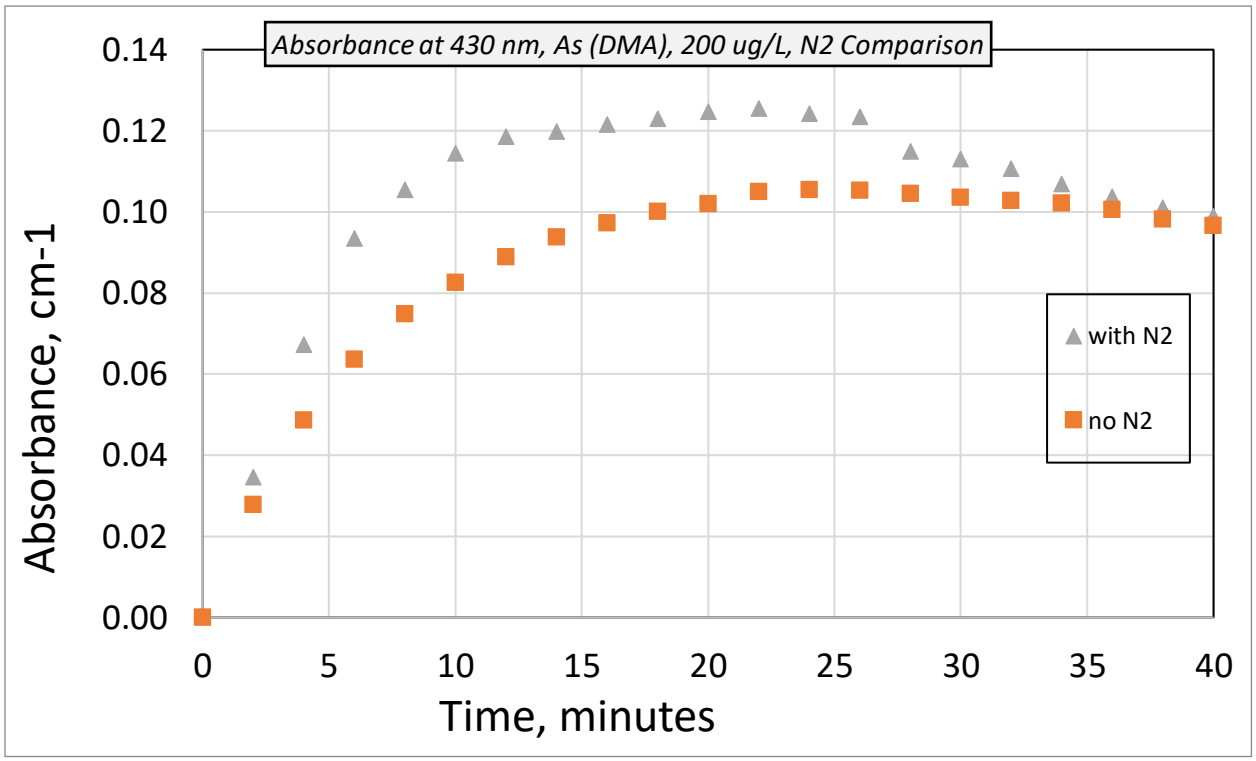

Figure 63. Effects of nitrogen presence on the kinetic profiles of absorbance measured at 430 nm. DMA arsine precursor.

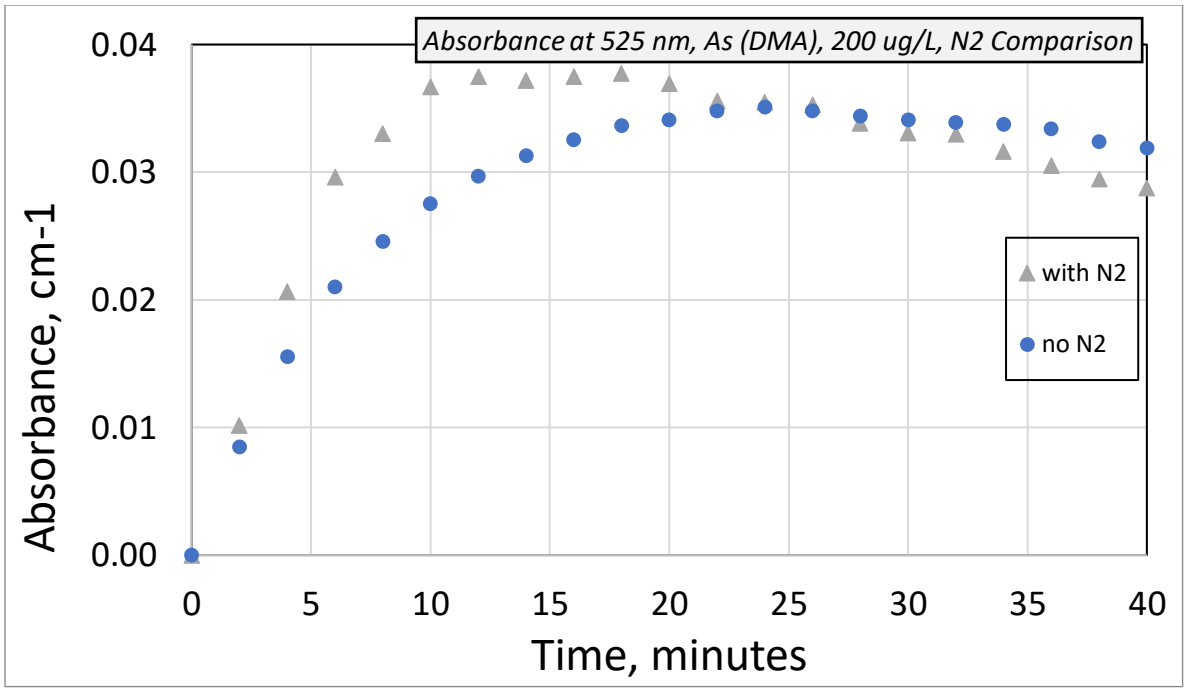

Figure 64. Effects of nitrogen presence on the kinetic profiles of absorbance measured at 525 nm. DMA arsine precursor.

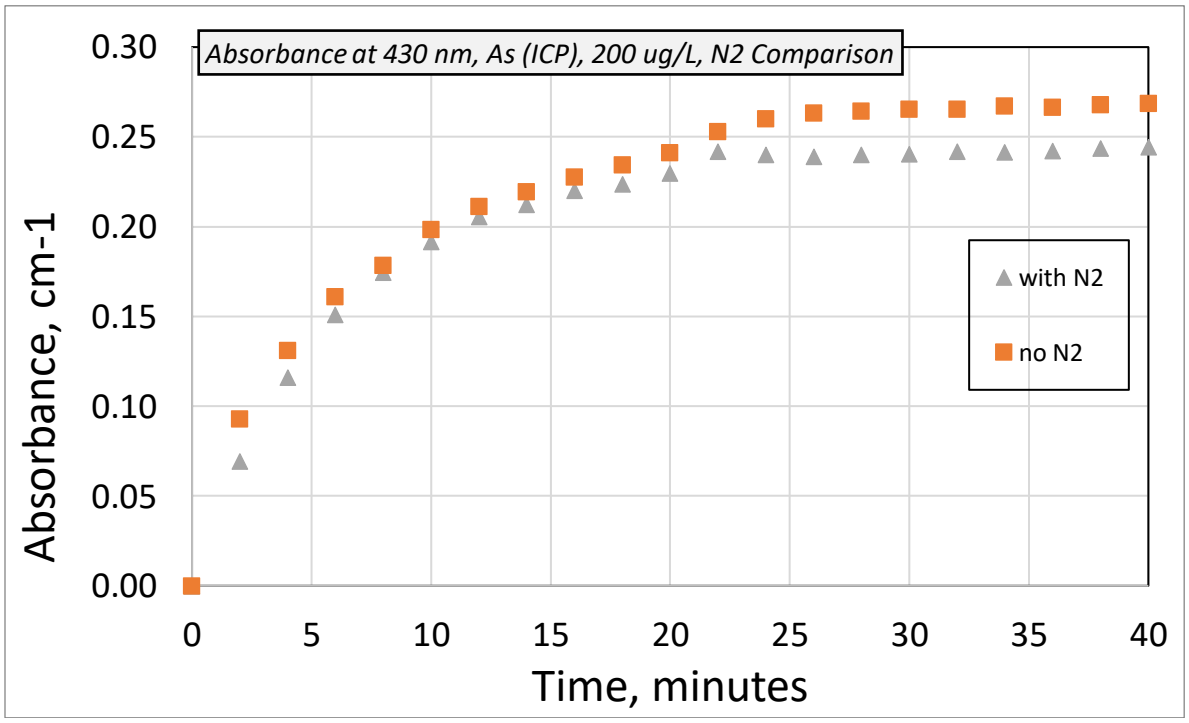

Figure 65. Effects of nitrogen presence on the kinetic profiles of absorbance measured at 430 nm. As ICP arsine precursor.

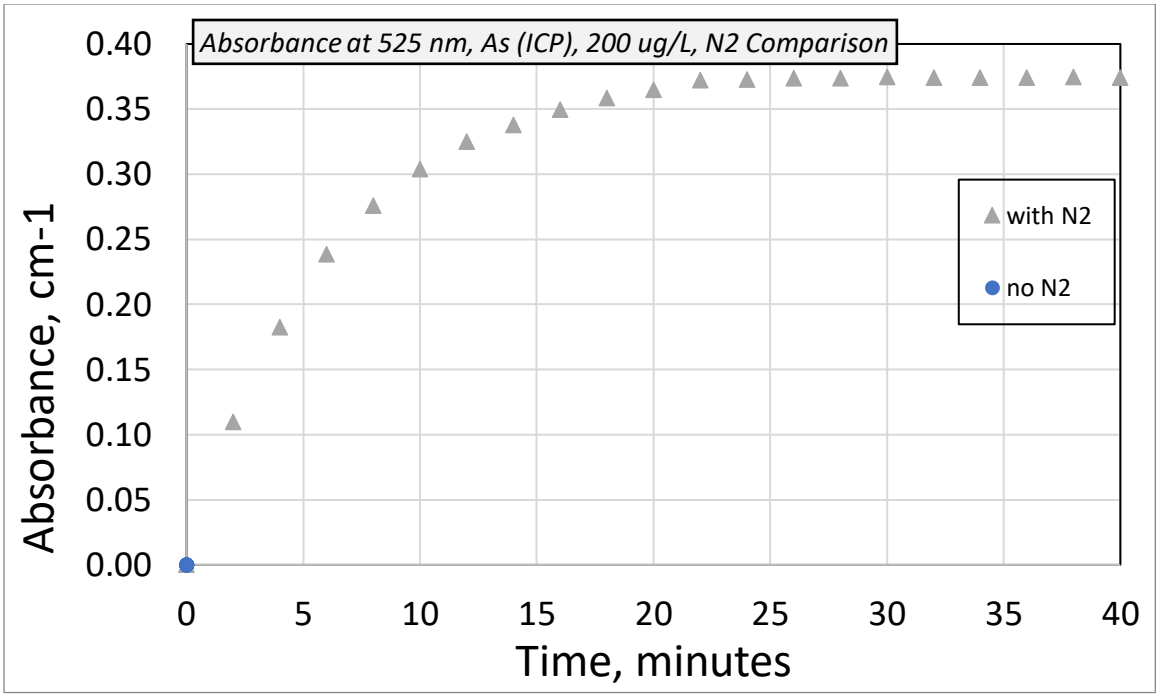

Figure 66. Effects of nitrogen presence on the kinetic profiles of absorbance measured at 525 nm. As ICP arsine precursor.

The effect of nitrogen flux was also tested using the BPW SR12 effluent sample. Nitrogen flow was seen to have a noticeable effect on absorbance at both wavelengths of interest (Figures 67, 68). At 430 nm, the absorbance did not start as high in the presence of nitrogen but much more quickly increased, reaching a maximum absorbance of almost twice the value reported in the absence of nitrogen flow at 20 minutes. At 525 nm, the experiment with nitrogen flow again began with a lower absorbance but surpassed the values in the case without nitrogen after 10 minutes.

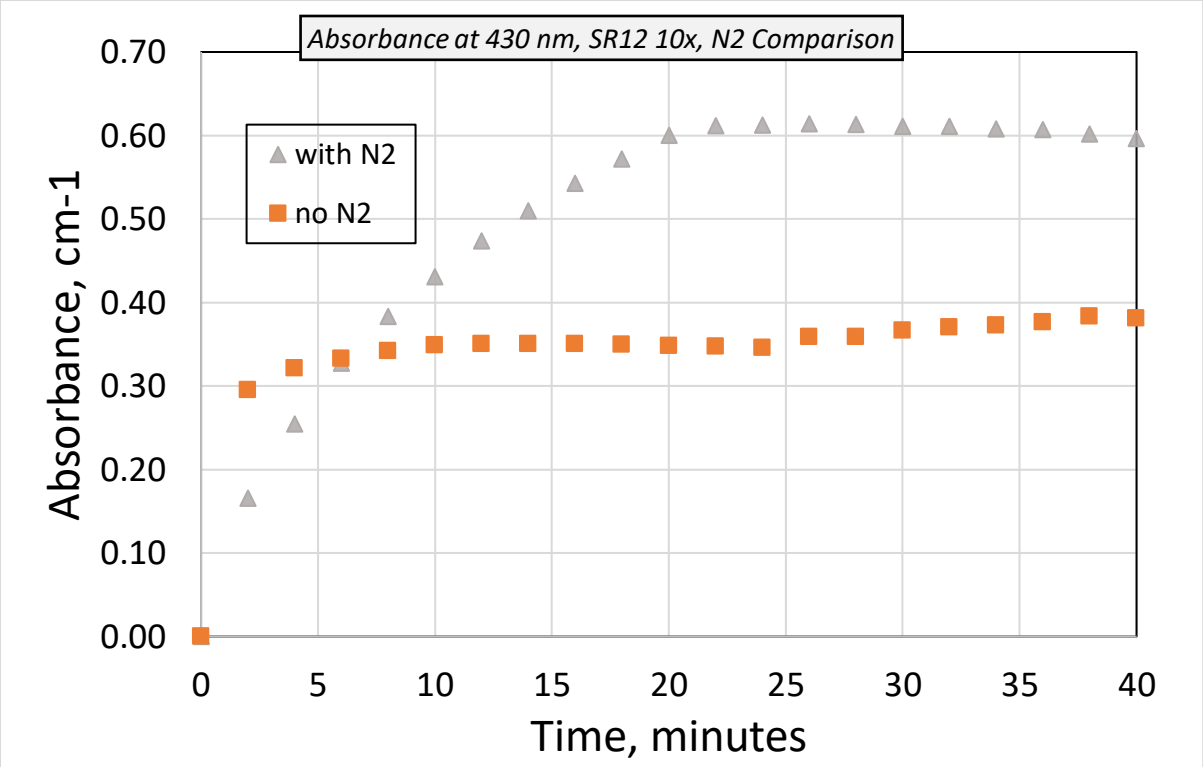

Figure 67. Effects of nitrogen presence on the kinetic profiles of absorbance measured at 430 nm. SR12 10x arsine precursor.

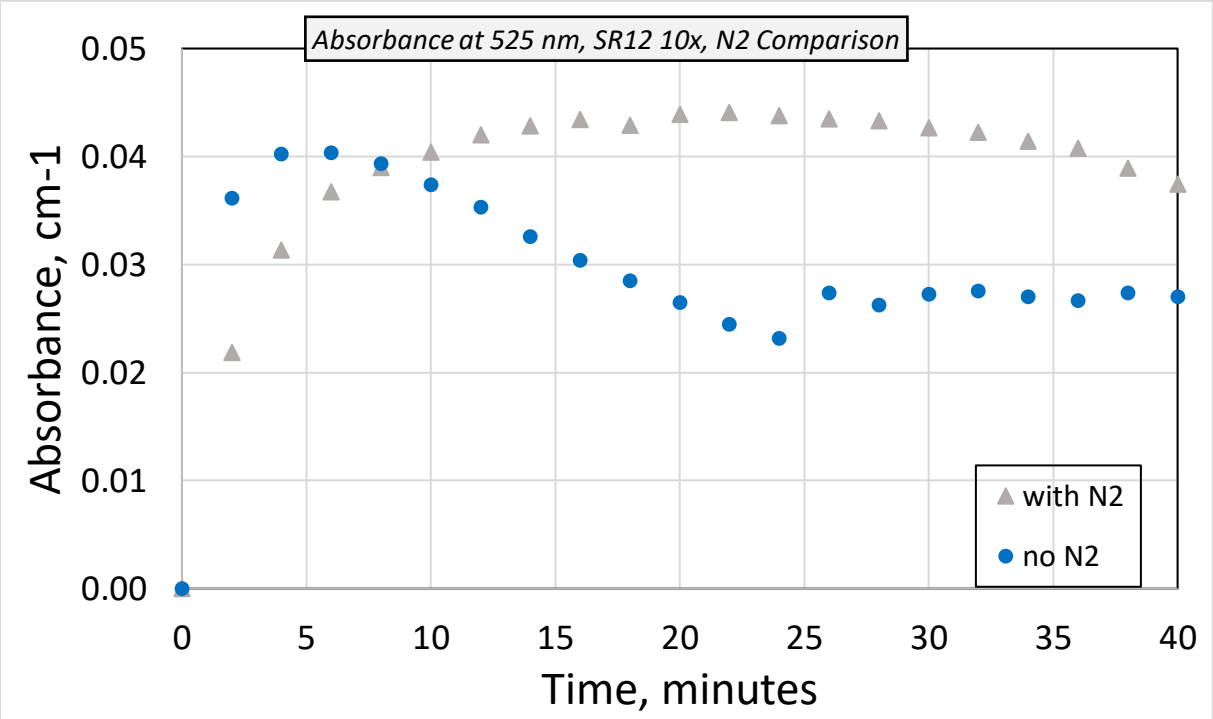

Figure 68. Effects of nitrogen presence on the kinetic profiles of absorbance measured at 525 nm. SR12 10x arsine precursor.

Chapter 5: Conclusions and Recommendations

Conclusions

Mass Balance Experiments

- The experiments described above confirm that > 90% of arsenic can be removed from BPW using ME treatment method at a 24 hours contact time in the presence of CO_2 flux, while only 20% can be removed without CO_2.
- Extractions of the arsenic retained by the Fe/C solids using nitric acid and sodium hydroxide resulted in negligible As recoveries for the samples generated in the experiments with CO_2 flux, while As recovery in the case of the experiments without CO_2 ranged from 10 to 40%.
- Similar results were seen with antimony. More than 80% was removed with CO_2 exposure, as opposed to 60% without CO_2, with recovery less than 10% for experiments with CO_2 and between 10 and 20% for those without.
- In the case of experiments using As (III), As (V), and DMA model species, approximately 100% As removal was seen for all but DMA which had a maximum of 80% As removal.
- Of these three solutions, DMA demonstrated the highest recovery in the PAC eluent both with and without CO_2 treatment, between 20% and 60% respectively, while As (III) and As (V) recovery was 10% or less.
- These results demonstrate that further work is needed to recover all arsenic and antimony from BPW samples. The data strongly imply the possibility of As volatilization. Another mechanisms such as deposition of unreactive As solids or irreversible adsorption that is preventing arsenic liberation cannot be excluded and are to be investigated.

- The effectiveness of zero valence iron as a catalyst to promote the removal of varying forms of arsenic should be explored further with the goal of understanding of fundamental mechanisms governing the removal of As in Fe/C systems and to achieve greater removal of all arsenic species in the case of practical BPW treatment.

Arsine Detection Experiments

- The wavelength of maximum absorbance observed for AgDDC complexes with arsines formed as a result of borohydride reduction of the SR solutions most closely resembles that in case of DMA precursors that forms dimethylarsine, with absorbance maxima ~ 420 to 430 nm and a second shoulder peak at ~480 rather than the 525 nm repeatedly seen for arsenite and arsenate precursors. This strongly indicates that the arsenic present in the BPW samples is a methylated form, possibly mono-, di-, or trimethylated arsines.
- Stibine absorbance spectra and their maxima were different from those for the arsine, demonstrating a clear peak at 507 nm with the antimony ICP standard used as the precursor. This shift in absorbance maxima may help to identify whether methods found to successfully treat arsines also achieve stibine removal from the off-gas stream of ME.
- The unique broadening of the absorbance shoulder for SR12 at 500 nm is likely to indicate a different solution composition than the other SR solutions.
- The kinetic profiles of SR solutions, particularly SR8 and SR11, demonstrate a decrease in absorbance similar to that of the dimethylarsine profile. This reinforces the possibility that the SR arsenic source might be methylated.
- It is observed that nitrogen flux, as suggested in the standard method, did yield an increase in absorbance as compared to arsine generation experiments conducted without gas flow. While the increase may not be greatly significant, it confirms the suggestion

that nitrogen as opposed to the hydrogen produced by borohydride reduction improves transport of arsines to the AgDDC scrubber solution.

Future work

Future work needs to be carried out to provide more detailed answers and yet missing information that is necessary for further optimization of the ME treatment approach and its implementation, as well as further elucidation of fundamental mechanisms that affect As volatilization in the ME processes and in landfills:

- Additional measurements that utilize advanced highly sensitive analytical and structural methods, for instance SEM and EXAFS, need to be performed to determine the chemical nature of the non-mobilizable arsenic that may remain in the PAC/ZVI solids.
- Given that the mass balance of As was examined in the study for ME solids that have been in contact with As-containing solutions for 24 hours, it may be necessary to examine the effects of shorter contact times on the degree of As retention in the solid phase. The leaching of As backing into solution at shorter contact times is suggested to explain other results from the group which show As concentration increasing in the last few hours of the ME experiment.
- Volatilization of As during ME treatment must be studied further, as there is a significant difference between removal rates for samples with and without CO_2 flux. These experiments should use the AgDDC method, or, if needed, an alternative suitable method, to quantify the evolution of As volatiles as a function of carrier gas rate, pH and properties of BEW process water whose chemical composition can be highly variable.

- Relating to this last point, it is necessary to investigate the interaction of CO_2 (an acidic gas) with pyridine (a base) to understand whether this carrier gas flow which facilitates ME treatment will impede absorbance measurements with the AgDDC method.
- Further experiments need to be performed to determine the speciation of As volatiles formed in the ME treatment. The data obtained in this study indicate that these volatiles are dominated by methylated arsines, notably dimethylarsine with virtually no presence of the highly reactive and toxic AsH_3 but this observation needs to be confirmed further.
- It is suggested to expand the range of model As compounds that produce various arsines in sufficiently reductive conditions. For instance, it is beneficial to use monomethylarsonic acid and trimethylarsine oxide to generate monomethylarsine and trimethylarsine, respectively whose spectroscopic signatures in AgDDC measurements have not been measured in this study.
- Formation of sulfur-containing As volatiles may also take place in ME treatment. As their reactivity and volatility may be highly distinct from those of the methylated arsine, the elucidation of the presence of thiolated As volatiles is of high priority.
- Potential impact of formation of hydrogen sulfide and volatile organic compounds on the AgDDC method needs to be determined. This can be done using an efficient hydrogen sulfide interceptor (e.g., lead acetate) to capture this interference before gas flow reaches the scrubber solution. In fact this approach is recommended in the standard methods but it was not used due to the supply interruption and the necessity to examine the evolution of all possible types of As volatiles, including those that have As-S bonds.
- Further measurements of the removal of As volatiles species by oxidative methods (e.g., permanganate) and/or adsorption (e.g., impregnated GAC or silica gel) or by thermal

degradation need to be carried out. This is critical for the practical implementation of the ME method and can be appended to the column reactor setup currently being developed for larger-scale ME treatment

- The occurrence of a dark-colored product formed in the case of borohydride reduction merits further study. This can be achieved through analysis of dried solids from the arsine generation experiments and comparison of ionic content (through conductivity measurements) and carbon content (DOC or TOC) to explain different responses from the SR solutions.
- More detailed experiments using antimony are needed to determine the magnitude of stibine formation during ME experiments and whether the proposed arsine capture methods of oxidation, degradation, and adsorption will successfully remove stibine from the off-gas stream.

Acknowledgements

This study was funded by King County Solid Waste Division (project 6085198). I am deeply grateful for their support of my studies.

I would like to acknowledge Professor Gregory Korshin for his guidance throughout the project and for the opportunity to work on this research, as well as Professor Jessica Ray for serving on my thesis committee and providing feedback on my work.

The microelectrolysis and mass balance techniques were taught to me by Surbhi Malik, who helped perform many of the experiments described in this thesis. Po-An Chen and Chenyang Zhang contributed greatly to the arsine generation experiments discussed here.

I would also like to acknowledge my lab members Samuel Walters, Domenico Giaquinto, Ivette Pinochet Troncoso and Gabriel Rifkin for their help and collaboration on this project.

I am grateful to the entire King County and CHRLF team (Kris McArthur, Said Seddiqi, Glynda Steiner, Joan Kenton, Laura Belt, Sterling Bath) for their support, collaboration and advice.

References

Arora, T., Linde, N., Revil, A., & Castermant, J. **Non-intrusive characterization of the redox potential of landfill leachate plumes from self-potential data.** Journal of contaminant hydrology, 2007 *92* (3-4), 274-292.

Arsenic. *Thermo Fisher Scientific Inc.* https://xpssimplified.com/elements/arsenic.php (accessed 2021-05-26).

Budensinsky, B. W. **Arsenic Colorimetry with Silver Diethyldithiocarbamate**. Microchemical Journal 1979 *24* (80-87). DOI: 10.1016/0026-265X(79)90041-9.

Cross, J. B. **Determination of stibine in air with pyridine-silver diethyldithiocarbamate scrubber and flameless absorption spectrometry.** Analytical Chemistry 1979 *51* (12), 2033-2035. DOI: 10.1021/ac50048a031.

Feldmann, Jörg. **Chapter 10: Volatilizatino of Metals from a Landfill Site (Generation and Immobilization of Volatile Species of Tin, Antimony, Bismuth, Mercury, Arsenic, and Tellurium on a Municipal Waste Deposit in Delta, British Columbia.** Biogeochemistry of Environmentally Important Trace Elements ACS Symposium Series 2003, 128-140.

Fu, Qiang., Lian Li, Connie H. Li, Michael J. Begarney, Daniel C. Law, and Robert F. Hicks. **Mechanism of Arsine Adsorption on the Gallium-Rich GaAs(001)−(4 × 2) Surface.** The Journal of Physical Chemistry B 2000 *104* (23), 5595-5602. DOI: 10.1021/jp0005827.

Guo, Fangyuan., Yu Liu, Jun Hu, Honglai Liu, and Ying Hu. **Screening of Porous Materials for Toxic Gas Adsorption: Classical Density Functional Approach.** Industrial & Engineering Chemistry Research 2020 *59* (32), 14364-14373. DOI: 10.1021/acs.iecr.0c02659.

Hussam, A., M. Alauddin, A. H. Khan, S. B. Rasul, and A. K. M. Munir. **Evaluation of Arsine Generation in Arsenic Field Kit.** Environmental Science & Technology 1999 *33* (20), 3686-3688. DOI: 10.1021/es9901462.

Kopp, J. F. **L-Ephedrine in chloroform as a solvent for silver diethyldithiocarbamate in the determination of arsenic**. Analytical Chemistry 1973 *45* (9), 1786-1787. DOI:10.1021/ac60331a042.

Korshin, G.V., Malik, S. and Liu, S. **Examination of Options to Remove Arsenic from Cedar Hill Regional Landfill Facility Leachates and Gas Condensates.** Results of Phase I. 2019 University of Washington.

Korshin, G.V., S.Malik, G.Rifkin, S.Liu. **Tests of methods to remove As from BEW process water. As leaching from landfill gas treatment solids. Nature of As species in BEW process water.** Phase II Results. Project 6085198. 2020 Report to King County Solid Waste Division.

Korshin, G.V., A. Cheney-Irgens, S. Malik, G.Rifkin.. **Characterization of BEW process water. Removal of As from BEW process water and As mass balance in microelectrolysis treatment. As leaching from landfill gas treatment solids.** Phase II Results. Project 6085198. 2021 Report to King County Solid Waste Division.

Korshin G. V. **Arsenic in the environment, redox effects**. CEE 445 lecture notes 2021.

Korshin, G. V. **Arsenic occurrence and sources.** CEE 445 lecture notes 2021.

Korshin G. V. **Redox transitions. pe, pH predominance diagrams for Fe^{3+}/Fe^{2+} and As^{5+}/As^{3+} transitions.** CEWA 543 lecture notes 2022.

Kovalskiy, A. et al. **Structural origin of surface transformations in arsenic sulfide thin films upon UV-irradiation**. Applied Surface Science 2017 *394*, 604-612.

Kumar, C. P. **Status and mitigation of arsenic contamination in groundwater in India.** Int J Earth Environ Sci 2015 *1* (1), 1-10.

Levy, Ivana K., Martín Mizrahi, Gustavo Ruano, Guillermo Zampieri, Félix G. Requejo, and Marta I. Litter. **TiO_2-Photocatalytic Reduction of Pentavalent and Trivalent Arsenic: Production of Elemental Arsenic and Arsine.** Environmental Science & Technology 2012 *46* (4), 2299-2308. DOI: 10.1021/es202638c.

Lim, S. et al. **Organic Arsenic Adsorption onto a Magnetic Sorbent**. Langmuir 2009 *25* (9), 4973-4978.

Lin, Yilong., Xueqian Wang, Jiming Hao, Ping Ning, Guangfei Qu, Yixing Ma, and Langlang Wang. **Improved Arsine Removal Efficiency Over MnOx Supported Molecular Sieves Catalysts via Micro-Oxygen Oxidation.** Energy & Fuels 2017 *31* (9), 9752-9759. DOI: 10.1021/acs.energyfuels.7b01477.

Liu, Siqi., Kuznetsov, M., Han, Weiqing., Masliy, Alexei N., Korshin, Gregory V. **Removal of Dimethylarsinic Acid (DMA) in the Fe/C system: Roles of Fe (II) Release, DMA/Fe(II) and DMA/Fe(III) Complexation.** Water Research 2022 118093.

Lu, Peng., Zhu, Chen. **Arsenic Eh-pH diagrams at 25°C and 1 bar.** Eviron. Earth Sci 2011 *61*, 1673-1683. DOI: 10.1007/s12665-010-0652-x.

Mestrot, Adrien., Joerg Feldmann, Eva M. Krupp, Mahmud S. Hossain, Gabrieal Roman-Ross, and Andrew A. Meharg. **Field Fluxes and Speciation of Arsines Emanating from Soils.** Environmental Science and Technology 2011 *45*, 1798-1804. DOI: 10.1021/es103463d.

Naudet, V., Revil, A., Rizzo, E., Bottero, J. Y., & Bégassat, P. **Groundwater redox conditions and conductivity in a contaminant plume from geoelectrical investigations.** Hydrology and Earth System Sciences 2004 (1), 8-22.

Quinn, Robert., Thomas A. Dahl, Barry W. Diamond, and Bernard A. Toseland. **Removal of Arsine from Synthesis Gas Using a Copper on Carbon Adsorbent**. Industrial & Engineering Chemistry Research 2006 *45* (18), 6272-6278. DOI: 10.1021/ie060176v.

Sahoo, P. K., & Kim, K. **A review of the arsenic concentration in paddy rice from the perspective of geoscience.** Geosciences Journal 2013 *1* (1), 107-122.

Sandhu, Shingara S., and Peter Nelson. **Ionic interference in the determination of arsenic in water by the silver diethyldithiocarbamate method**. Analytical Chemistry 1978 *50* (2), 322-325. DOI: 10.1021/ac50024a038.

Sengupta, Mrinal K., Maather F. Sawalha, Shin-Ichi Ohira, Ademola D. Idowu, and Purnendu K. Dasgupta. **Green Analyzer for the Measurement of Total Arsenic in Drinking Water: Electrochemical Reduction of Arsenate to Arsine and Gas Phase Chemiluminescence with Ozone.** Analytical Chemistry 2010 *82* (9), 3467-3473. DOI: 10.1021/ac100604y.

Sengupta, Mrinal K., and Purnendu K. Dasgupta. **Oxidation State-Differentiated Measurement of Aqueous Inorganic Arsenic by Continuous Flow Electrochemical Arsine Generation Coupled to Gas-Phase Chemiluminescence Detection.** Analytical Chemistry 2011 *83* (24), 9378-9383. DOI: 10.1021/ac201972m.

Seredych, Mykola., John Mahle, Gregory Peterson, and Teresa J. Bandosz. **Interactions of Arsine with Nanoporous Carbons: Role of Heteroatoms in the Oxidation Process at Ambient Conditions.** The Journal of Physical Chemistry C 2010 *114* (14), 6527-6533. DOI: 10.1021/jp911890c.

Shaikh, Ali U., and Dennis E. Tallman. **Determination of sub-microgram per liter quantities of arsenic in water by arsine generation followed by graphite furnace atomic absorption spectrometry.** Analytical Chemistry 1977 *49* (8), 1093-1096. DOI: 10.1021/ac50016a010.

Shen, Hong., and Purnendu K. Dasgupta. **Electrochemical Arsine Generators for Arsenic Determination.** Analytical Chemistry 2014 *86* (15), 7705-7711. DOI: 10.1021/ac501636u.

Sparks, Donald L., **Chapter 5 – Sorption Phenomena on Soils, Environmental Soil Chemistry (Second Edition)**. Academic Press 2003, 133-186. DOI: 10.1016/B978-012656446-4/50005-0.

Sulfur. *Thermo Fisher Scientific Inc.* https://xpssimplified.com/elements/sulfur.php (accessed 2021-05-26).

Tesfalidet, Solomon., and Knut Irgum. **Polymer-bound tetrahydroborate for arsine generation in a flow-injection system.** Analytical Chemistry 1989 *61* (18), 2079-2082. DOI: 10.1021/ac00193a015.

Uthus, Eric O., Michael E. Collings, W. E. Cornatzer, and Forrest H. Nielsen. **Determination of total arsenic in biological samples by arsine generation and atomic absorption spectrometry.** Analytical Chemistry 1981 *53* (14), 2221-2224. DOI: 10.1021/ac00237a017.

Virji, Shabnam., Robert Kojima, Jesse D. Fowler, Richard B. Kaner, and Bruce H. Weiller. **Polyaniline Nanofiber−Metal Salt Composite Materials for Arsine Detection.** Chemistry of Materials 2009 *21* (14), 3056-3061. DOI: 10.1021/cm802397j.

Wang, Xueqian., Hongqi Huang, Qiqi Zhou, Ping Ning, Jinhuan Cheng, Yilong Lin, Langlang Wang, and Yibing Xie. **High-Performance Arsine Removal Using CuOx/TiO2 Sorbents under Low-Temperature Conditions.** Energy & Fuels 2018 *32* (6), 7035-7045. DOI: 10.1021/acs.energyfuels.8b00448.

Wang, Peipei., Guoxin Sun, Yan Jia, Andrew A Meharg, and Yongguan Zhu. **A review on completing arsenic biogeochemical cycle: Microbial volatilization of arsines in environment.** Journal of Environmental Sciences 2014 *26*, 371-381. DOI: 10.1016/S1001-0742(13)60432-5.

Weithmann, Nicolas., Stanislava Mlinar, Frank Hilbrig, Samer Bachmaf, Julia Arndt, Britta Planer-Friedrich, Alfons R. Weig, and Ruth Freitag. **Arsenic metabolism in technical biogas plants: possible consequences for resident microbiota and downstream units.** AMB Express 2019 *9* (190), 1-16. DOI: 10.1186/s13568-019-0902-6.

Yao, L. et al. **Hydrothermal Treatment of Arsenic Sulfide Residues from Arsenic-Bearing Acid Wastewater.** Int. J. Environ. Res. Public Health 2018 *5*, 1863.

Zhang, Yingjie., Ping Ning, Xueqian Wang, Langlang Wang, Yibing Xie, Qiang Ma, Rui Cao, and Hang Zhang. **Simultaneous Removal of Elemental Mercury and Arsine from a Reducing Atmosphere Using Chloride and Cerium Modified Activated Carbon.** Industrial & Engineering Chemistry Research 2019 *58* (51), 23529-23539 DOI: 10.1021/acs.iecr.9b04999.

Appendix

Arsenic and Iron Environmental Mobility

Arsenic mobility is briefly discussed in the introduction section and is further explained here for the purpose of comparison with iron mobility. Figure 69 demonstrates a Pourbaix diagram for arsenic, demonstrating the forms of arsenic that will dominate at varying pE and pH conditions.

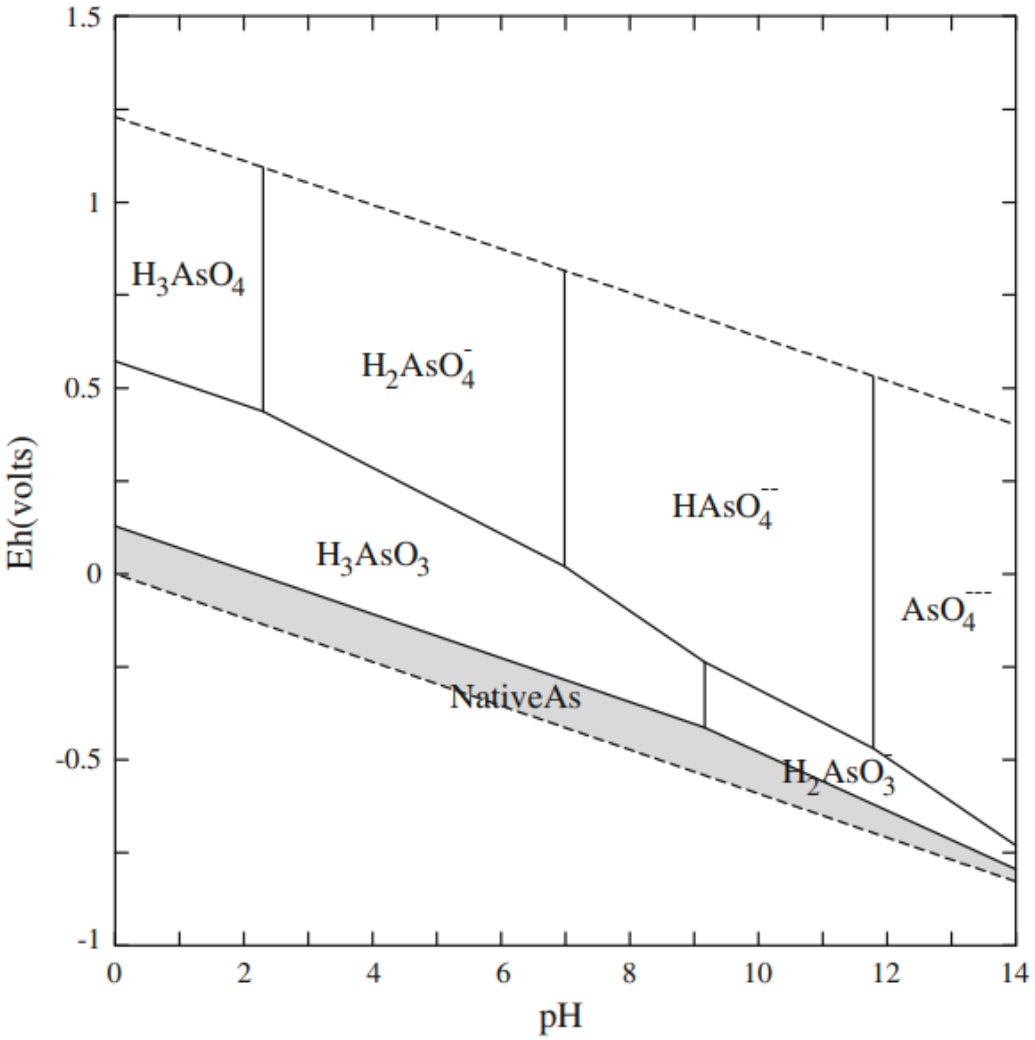

Figure 69. Pourbaix diagram of arsenic, reproduced from Figure 1 of Lu et al. (2011).

Iron is also found in significant concentrations in the BPW, with a similarly variable but often much larger value than arsenic. Figure 70 illustrates the likeness of the arsenic and iron Pourbaix diagrams, indicating that a similar relationship exists between pH and mobility for both metals. This allows for a greater range of indicators of pE and pH conditions in the landfill environment of study.

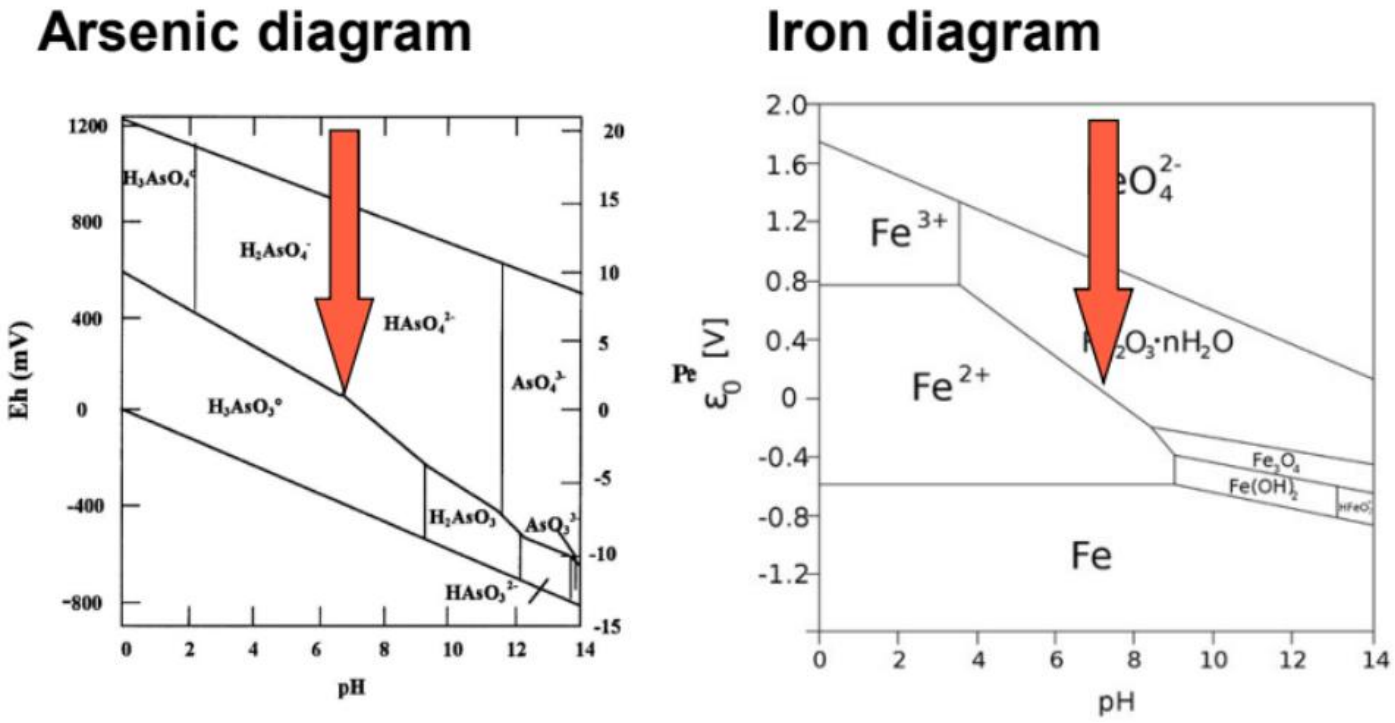

Figure 70. Pourbaix diagrams of arsenic and iron environmental mobility. Reproduced from Korshin (2022) Redox transitions. pe, pH predominance diagrams for Fe^{3+}/Fe^{2+} and As^{5+}/As^{3+} transitions, CEWA 543 lecture notes.

Standard Curves

Preliminary data with the Perkin Elmer Lambda 18 Spectrometer and Shimadzu UV-2700 UV-Vis Spectrometer included standard curves with a range of concentrations from 50 to 2000 ug/L as arsenic (50, 100, 200, 500, 1000, 2000 ug/L). Solution pH was adjusted to 1 or 2. Sodium borohydride (98+%, powder, Acros Organics) solutions with either 1% or 5% w/v were used as a reducing agent, as opposed to only 1% used in the previously described experiments.

The scrubber tube contained a volume of 4 mL of a silver diethyldithiocarbamate (ACS grade, Alfa Aesar) solution in either chloroform (Mallinckrodt Hach, ACS grade) or pyridine (Fisher).

In the case of the chloroform solvent, the absorbance of AgDDC solutions was measured in a Shimadzu UV-2700 UV-Vis Spectrometer. In the case of the pyridine solvent, a Perkin Elmer Lambda 18 Spectrometer was used and measurements were taken in a hood. Standard curves and absorbance spectra were generated for known concentrations of arsenite, arsenate, and DMA to demonstrate the formation of arsines from inorganic and organic (DMA) precursors. However, later measurements using the fiber-optic Perkin Elmer Lambda 465 system showed that ex situ measurements using the Lambda 18 and UV-2700 instruments were insufficiently precise, in the sense that in some important cases (e.g., the formation of dimethylarsine from DMA), the absorbance spectra of AgDDC/arsine systems faded before and during the ex situ measurements, and the system may have also been affected by its contact with atmospheric oxygen. In addition, measurements using AgDDC chloroform solutions were found to be less sensitive and stable compared with those for AgDDC solutions in pyridine. Still, some of the data of the ex situ measurements are shown in this appendix to demonstrate the appearance of AgDDC solutions interacting with arsines, general calibration results and some other data.

In the case of arsenite, the calibration data show that the use of a 1% w/v $NaBH_4$ solution was much more effective than a 5% w/v solution in yielding a greater range of absorbance values (Figures 71-73). Subsequent experiments utilized the 1% w/v $NaBH_4$ solution, as recommended by the standard methods. Experiments were also carried out without the use of the acetate buffer to determine whether the resistance to pH change would impact arsine generation throughout the experiment. In the case of arsenate, there was considerable scatter in the standard curve data, particularly at lower concentrations, with the resultant decrease of the R^2 values for these calibration curves (Figures 74, 75).

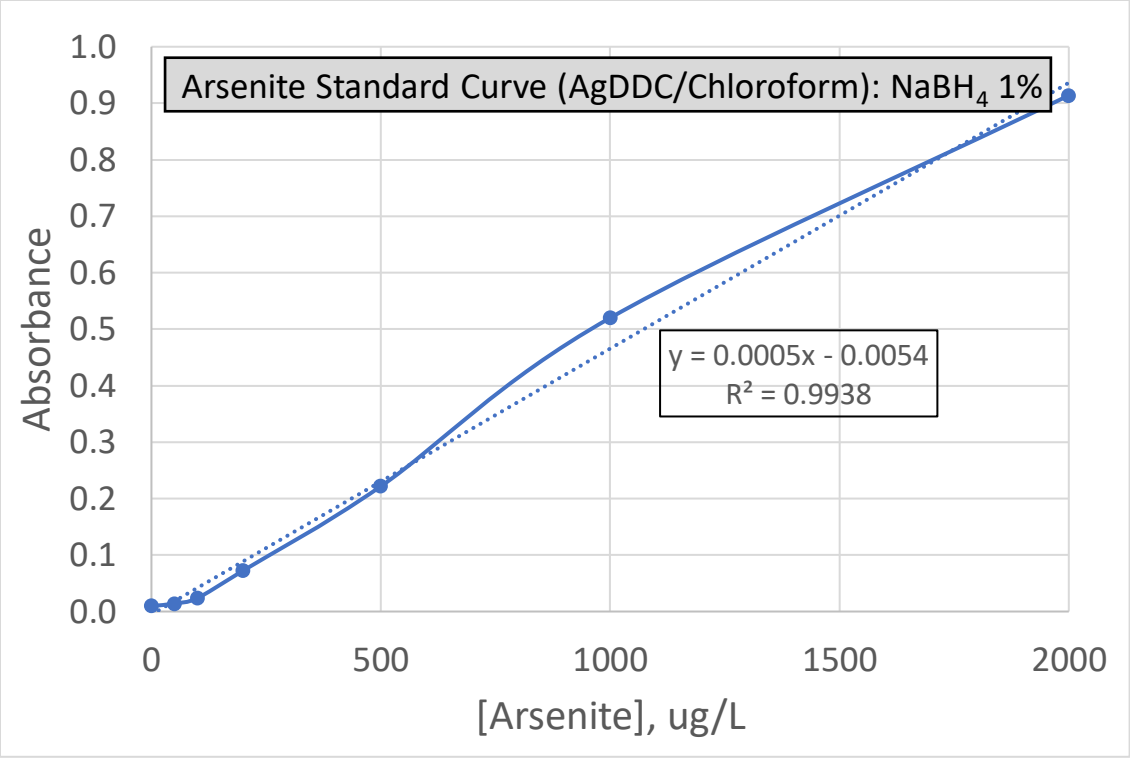

Figure 71. Arsenite standard curve at 520 nm, AgDDC/chloroform. (NaBH4 1%, Acetate Buffer, pH 2). 8/12/21. Absorbance > 0.9 at 2000 ug/L [arsenite].

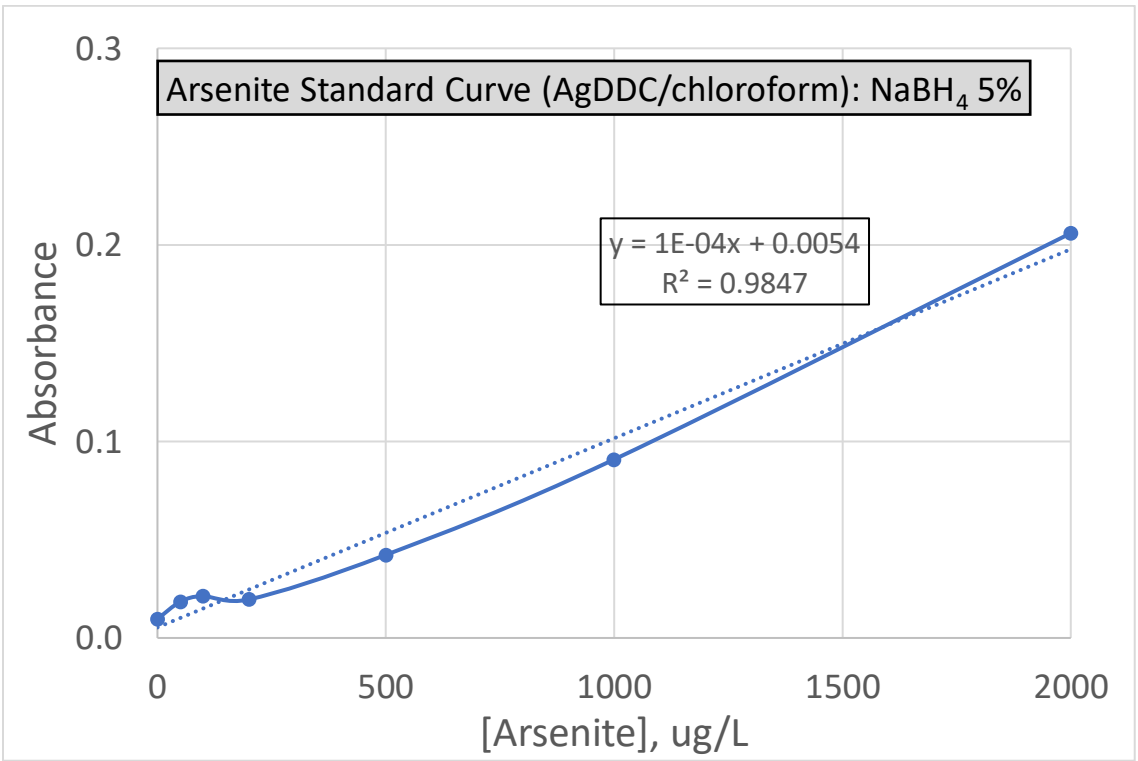

Figure 72. Arsenite standard curve at 520 nm, AgDDC/chloroform. (NaBH4 5%, No acetate buffer, pH 1). 8/19/21. Absorbance > 0.2 at 2000 ug/L [arsenite], only 20% of absorbance with NaBH4 1%.

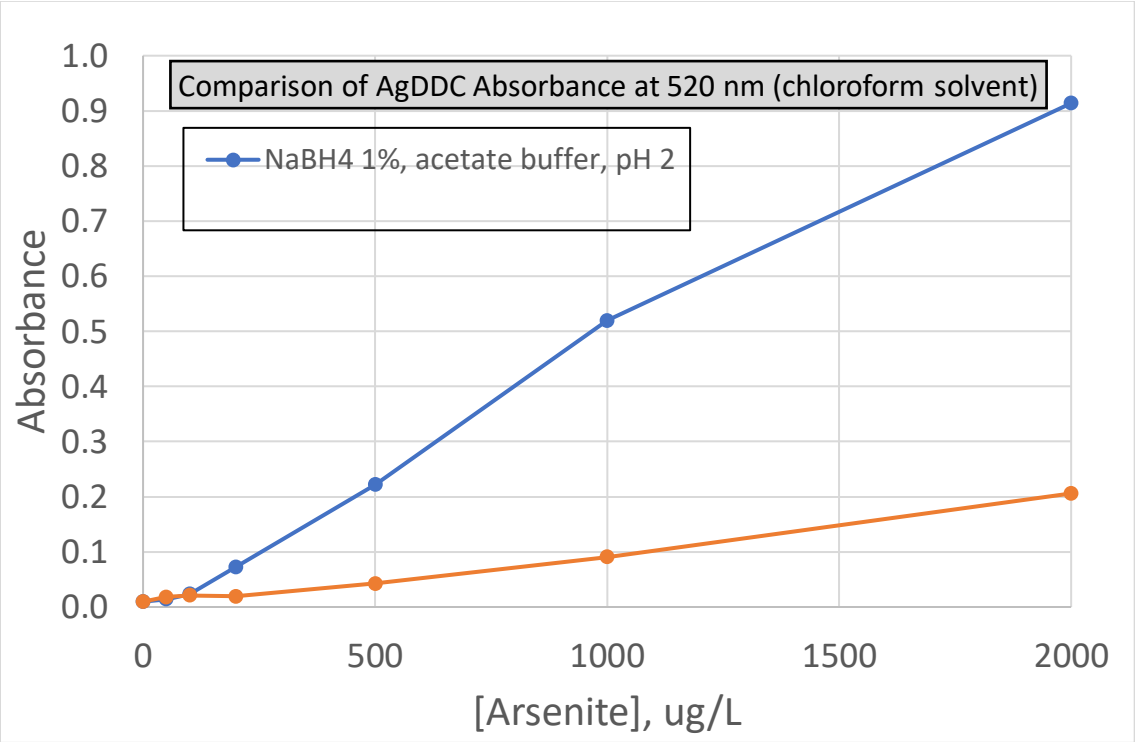

Figure 73. Comparison of Arsenite absorbance (1% vs 5% NaBH4). Absorbance differs by 80% at 2000 ug/L.

In an effort to improve the quality of AgDDC calibration data, the chloroform solvent was replaced with pyridine, as recommended in some of the versions of the AgDDC method (Cross (1979), Kopp (1973), Budesinsky (1979), Sandhu and Nelson (1978), Shaikh and Tallman (1977)). In the case of both arsenite and arsenate, this noticeably improved the R^2 values of the calibration curves (Figures 74, 75). This was particularly evident for arsenate, as the R^2 value increased from 0.9746 to 0.9896.

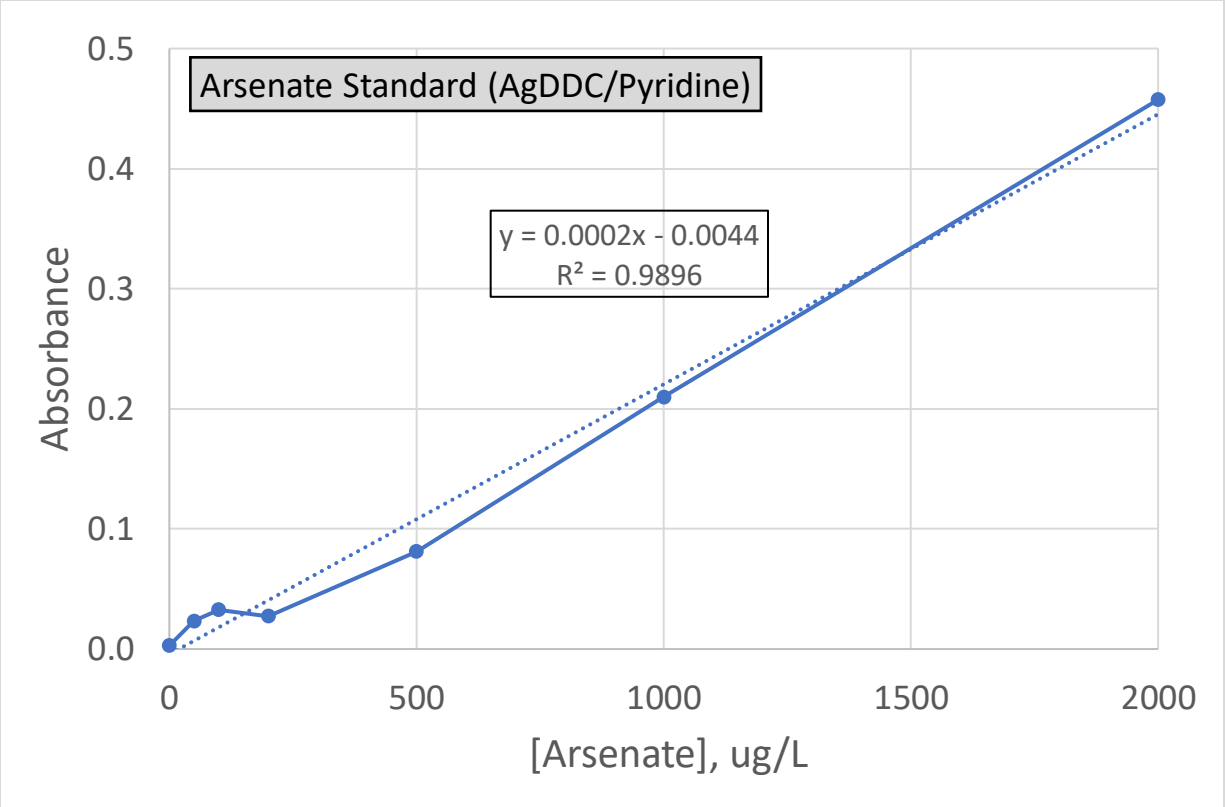

Figure 74. Arsenate Standard Curve at 520 nm, AgDDC/pyridine. (NaBH4 1%, No acetate buffer, pH <1), Shimadzu. 9/7/21.

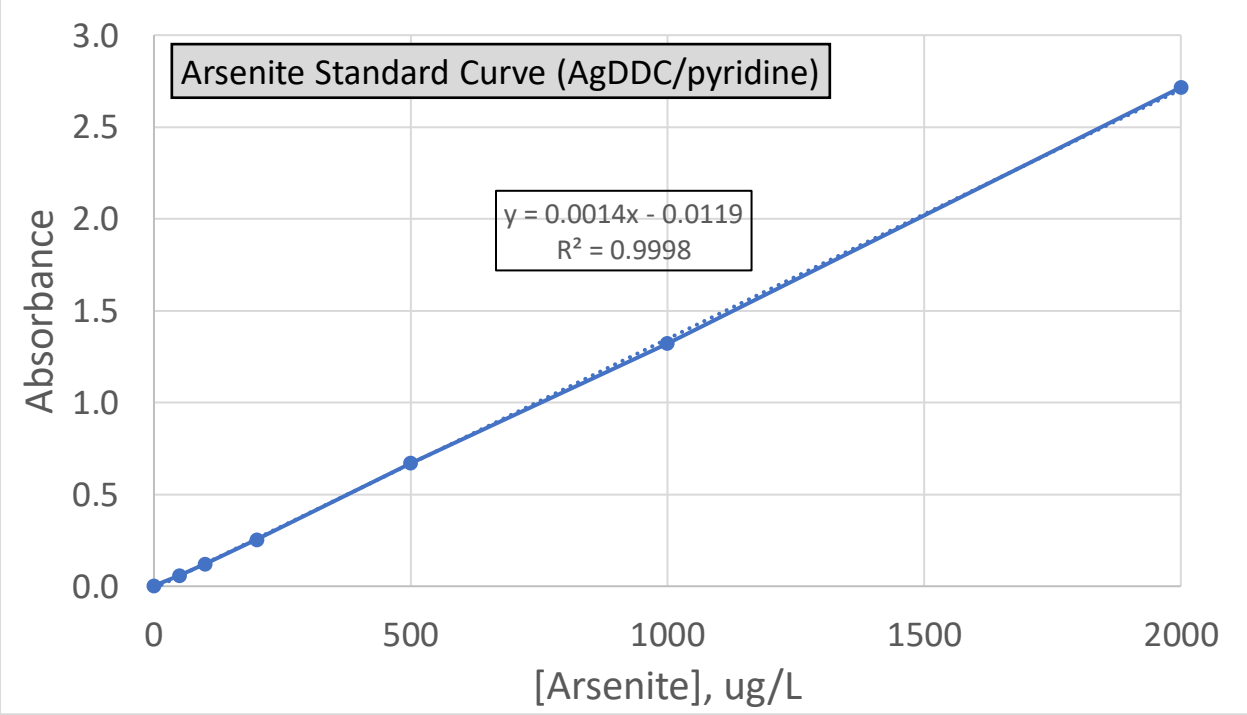

Figure 75. Arsenite Standard Curve at 520 nm, AgDDC/pyridine. (NaBH4 1%, No acetate buffer, pH 1), Perkin Elmer. 9/3/21.

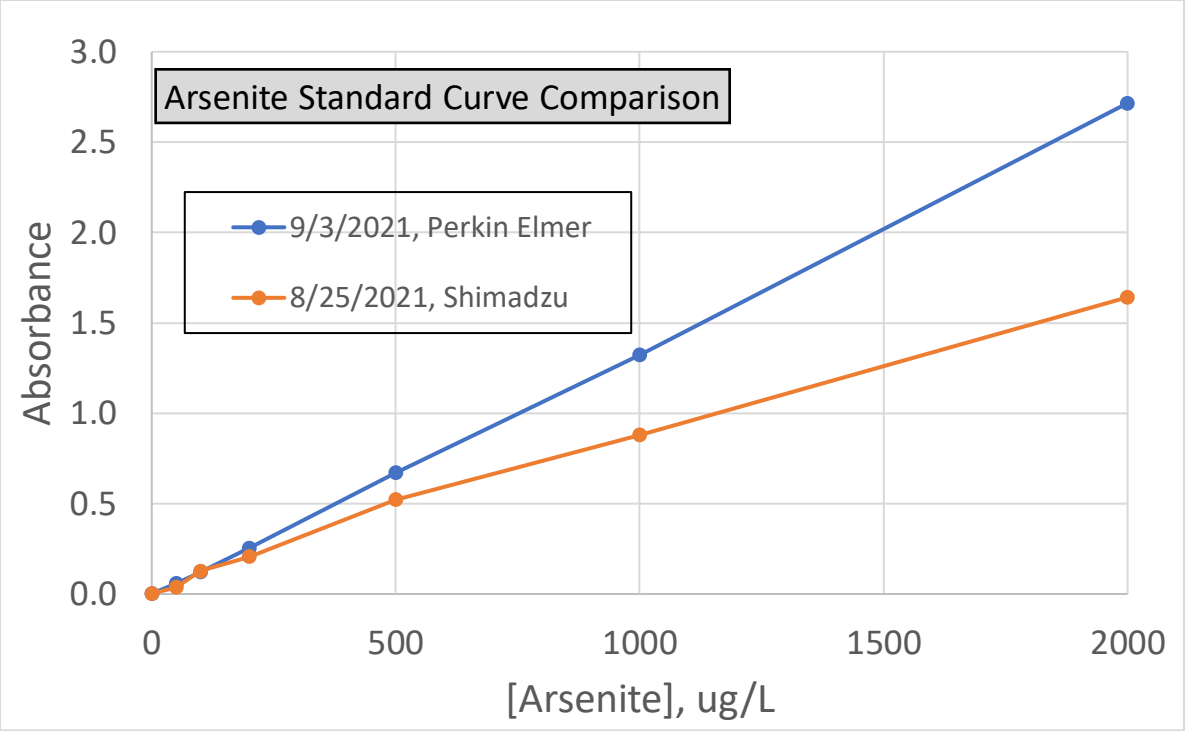

Figure 76. Comparison of Arsenite Standard Curves Generated using Shimadzu and Perkin Elmer spectrophotometers (AgDDC/pyridine). Absorbance measurements at 520 nm, 1 cm optical cell.

The intensity of the color of AgDDC solutions was also notably higher in pyridine than in chloroform. This encouraged the use of pyridine solvent for the remainder of experiments (Figures 77, 78).

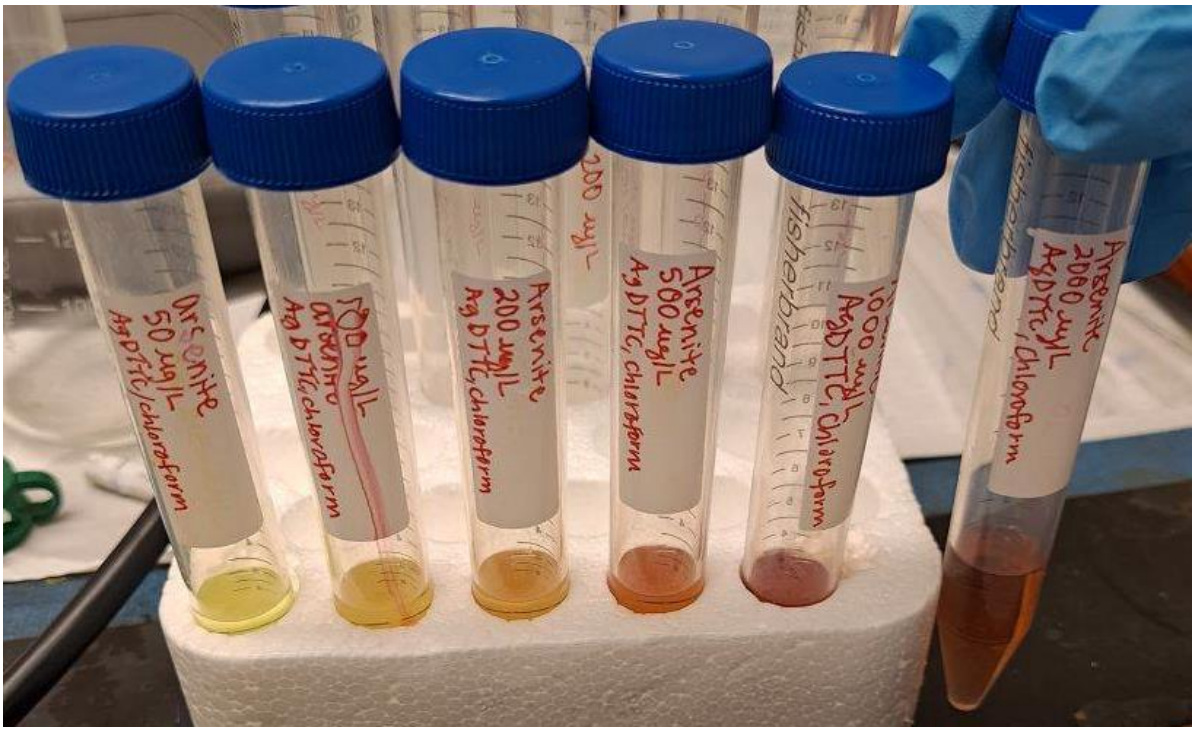

Figure 77. Arsenite color development in AgDDC/chloroform is concentration-dependent for 50-2000 ug/L.

Figure 78. Arsenite color development in AgDDC/pyridine. Noticeably improved color distinction from 0-2000 ug/L As.

For experiments with the DMA arsine precursor and pyridine solvent, color fading is demonstrated.

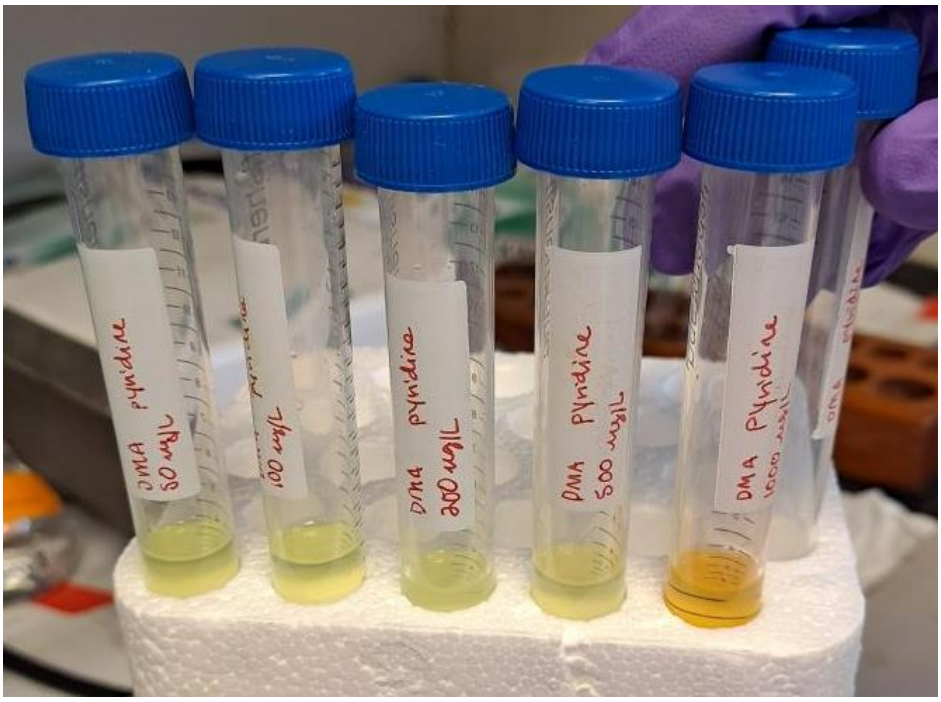

Figure 79. DMA in AgDDC/pyridine. (1000 ug/L at 0 minutes from experiment end).

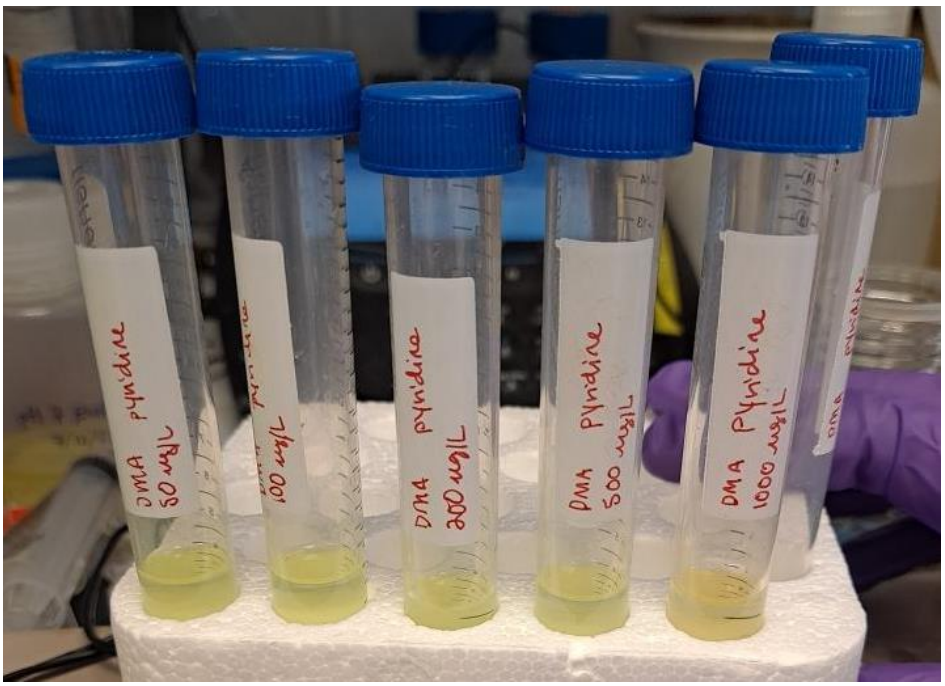

Figure 80. DMA in AgDDC/pyridine. (1000 ug/L at 15 minutes from experiment end).

SR Results

In experiments examining arsine generation and capture from SR samples, it was seen that the solution of SR8 and hydrochloric acid immediately turned very dark when the 1% $NaBH_4$ was added (Figure 81). This did not occur with the SR10 samples but it did sometimes with SR9 samples. This is likely to be a result of considerable differences in chemical properties between the three samples. For instance, the formation of black particulates shown in Figure 81 may be caused by the borohydride-driven reduction of iron and sulfur compounds in SR8 sample and attendant precipitation of iron sulfides. The occurrence of such reactions and their significance for BPW treatment in general arsine generation in particular is to be explored further. It is also important to note that the positions of the absorbance maxima of AgDDC/arsine complexes formed for SR9 and SR10 BPW samples do not match the position of the maximum at 520 nm, as stated in the standard methods for arsine determination by the AgDDC method This position of the absorbance maxima is likely to indicate the formation of an organic arsine or a combination of arsines such as dimethyl or trimethyl arsine which, when reacted with AgDDC, produced a complex with an absorbance peak distinct from that for the standard AgDDC/AsH_3 system.

Figure 81. SR9 color change a few minutes after $NaBH_4$ addition.